Journal of Cardiovascular Magnetic Resonance®, 4(1), 1–61 (2002)

Oral Abstracts*

101. Prediction of Contractile Improvement in Chronic Heart Failure Patients Treated with Beta-Blocker Therapy

David Bello,[1] Francis Klocke,[2] John Vargas,[2] Michelle Parker,[2] Robert Bonow,[2] Robert Judd,[2] Mihai Gheorghiade,[1] Raymond Kim.[2] [1]*Northwestern University 244 E Pearson, #1006, Chicago, IL USA;* [2]*Northwestern University, Northwestern University Medical School, Chicago, Illinois, United States*

Introduction: Contrast-enhanced MRI (ceMRI) can visualize both transmural and subendocardial myocardial infarction and predict left ventricular contractile improvement in patients (pts) with coronary artery disease (CAD) following revascularization.

Purpose: We hypothesized that ceMRI may also predict contractile improvement in chronic heart failure pts after 6 months of beta-blocker therapy (BBT).

Methods: Cine and ceMRI was performed before and after 6 months of BBT in 34 pts (21 CAD +, 13 CAD−) with ventricular dysfunction (LVEF 27 ± 11) who were not candidates for revascularization. Wall motion and the transmural extent of hyperenhancement (HE) representing prior infarction was scored by two blinded observers using a 72 segment model.

Results: HE was observed in all 21 CAD + pts and in 3 of 13 CAD− pts before BBT. For CAD− pts, 630 segments (77%) were dysfunctional and 63% of these improved after BBT. For CAD+ pts, 1177 segments (84%) were dysfunctional and 27% of these improved, a rate which was lower ($P < 0.001$) than for CAD − pts. However the likelihood for contractile improvement increased progressively as the transmural extent of HE decreased ($P < 0.001$) and approached the rate for CAD − pts in whom 94% of segments had no HE. For CAD+ pts the degree of improvement in the global mean wall-motion score ($P < 0.01$) and the ejection fraction ($P < 0.02$) after BBT was strongly related to the percentage of the left ventricle that was both dysfunctional and viable (no HE) before BBT.

Conclusion: For heart failure pts, the likelihood of improvement with BBT is inversely related to the transmural extent of HE. CeMRI can identify CAD+ pts who are unlikely to improve contractile function with BBT.

102. Real Time MRI Superior to Echocardiography in the Evaluation of Patients with Congestive Heart Failure

Erasmo De La Pena-Almaguer,[1] Michael D. Hope,[1] Masahiro Terashima,[1] Roger A. Wagner,[1] Phillip C. Yang,[1] David H. Liang,[1] Michael V. Mcconnell,[1] Bob S. Husfu. [1]*Stanford University, Cardiovascular Medicine, Stanford, California United States*

Introduction: The serial evaluation of patients with CHF is very important in their management. Magnetic Resonace Imaging has been shown to be more consistent in the assessment of ventricular function in patients with CHF. Real-time CVMR is

Table 1

Comparison of Echo vs. Real-Time MRI in the Assesment of Volumes and Ejection Fraction

	R2 Echo	R2 RTMRI	Slope Echo	Slope RTMRI	p Echo	p RTMRI
EDV	67	78	0.75	1.07	0.0003	<0.001
ESV	77	82	0.82	1.06	<0.001	<0.001
EF	24	73	0.61	0.77	0.08	0.0001

*For some abstracts, original art was not available.

a faster and more versatile method for the assessment of ventricular mass and function since no breathholding or cardiac gating is needed. However, poor ventricular function may adversely affect blood-myocardium contrast. We compared real-time CVMR with echocardiography using conventional Cine-MRI as the gold standard.

Purpose: To assess the value of real-time MRI in the evaluation of patients with congestive heart failure.

Methods: Fourteen patients with CHF were recruited from the stanford heart failure clinic and echocardiography laboratory. All patients were studied with echocardiography, Real-Time CVMR and conventional MR (Cine CMR). The studies were performed within 1 month of each other. Study duration, ventricular segmental visibility, LVESV, LVEDV, and EF were calculated.

Results: Real-time CVMR and echo measurements of LV volume and EF were both correlated with cine MR. However, RT MRI was less biased (RT mean error −1.2 c/w Echo mean error 2.8) and less variable (RTMRI variance 48 vs Echo variance 124) than echocardiography in calculating EF. Furthermore, image quality was more consistent with rt-MR (222/224 segments acceptable in MR vs 196/224 segments in echo) RT MR Studies were also acquired in a shorter period of time than either echo or conventional MR (Real Time MRI 6 ± 5 minutes vs Echo 25 ± 11 Minutes).

Conclusion: Real-Time CVMR is superior to echo in the assesment of ventricular function in patients with CHF, resulting in shorter and more accurate studies

103. Magnetic Resonance Imaging Protocol for Assessment of RV Morphology and Function in Patients with Right Ventricular Arrhythmias

Sven Plein,[1] Timothy Bloomer,[1] Chris Pepper,[1] John Ridgwa,[2] Campbell Cowan,[1] Mohan Sivananthan.[1] [1]*Leeds General Infirmary, Gt. George Street, Leeds, West Yorkshire, United Kingdom;* [2]*Leeds Teaching Hospitals, Department Of Medical Physics, Leeds, West Yorkshire, United Kingdom*

Introduction: Magnetic Resonance Imaging (MRI) is an excellent imaging tool for assessment of right ventricular (RV) morphology. In addition MRI can provide quantitative data of RV function. Both morphological and functional abnormalities of the RV have been described separately in patients with RV arrhythmias. With modem fast acquisition techniques, data for a combined morphological and functional assessment of the RV can be acquired in one imaging session. This may provide complimentary information in the assessment of patients with RV arrhythmias.

Purpose: To assess a combined MRI protocol for morphological and functional assessment of the RV in normal controls and patients with RV arrythmias.

Methods: 104 subjects were studied: 34 controls, 18 patients meeting the diagnostic criteria for Arrhythmogenic Right Ventricular Cardiomyopathy (ARVC), 41 with RV outflow tract tachycardia (RVOT) and 11 relatives of patients with ARVC. MRI scanning was performed in the prone position on a 1.5T Philips Gyroscan NT system (Philips, Best, The Netherlands) with a 5-element cardiac synergy coil. The MRI protocol combines sequences for morphological imaging with quantitative assessment of global and regional RV function and includes:

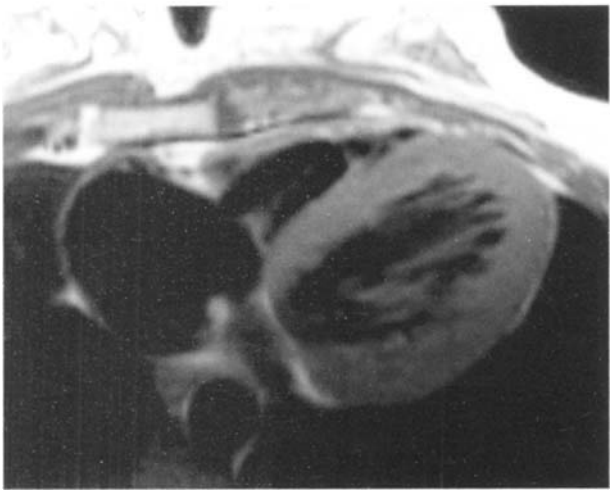

Figure 1. ARVC.

—breath-hold axial gradient echo (GRE) cines (TR 7.8ms, TE 4.6ms, flip angle 30°)
—breath-hold axial GRE cines with antero-posterior line tagging
—velocity-encoded imaging perpendicular to the tricuspid valve (retrospective gating, free breathing, TR 18ms, TE 3.4ms, flip angle 40°)
—axial T1-weighted spin echo (SE) imaging of the RV (TR = 1 heart beat, TE = 15ms)
—weighted SE imaging with frequency-selective fat suppression
—axial T2-weighted SE imaging (TR = 2 heart beats, effective TE = 100-120ms, dual inversion preparation scheme to suppress the signal from flowing blood).

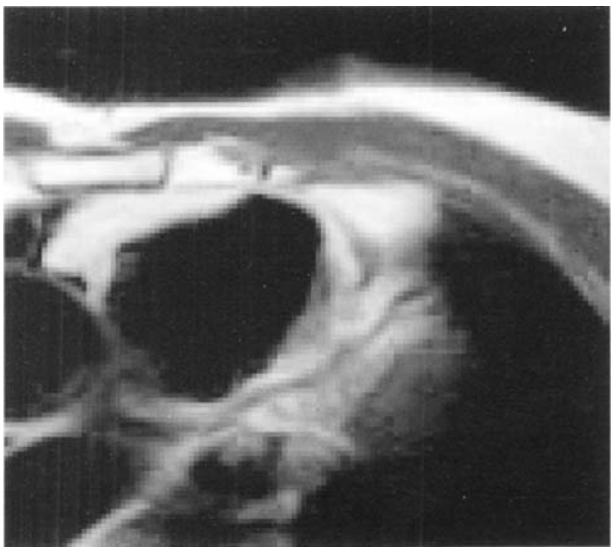

Figure 2. RVOT

Table 1

	Fat	Dyskinesia	Thinning	Outpouching	Dilatation	EF	%FS	E/A
Normals	1	0	10	0	4	59.9	26.1	1.41
Relatives	0	3	0	1	0	61.7	30.4	1.32
ARVC	7	15	7	6	13	50.7*	21.8*	1.03*
RVOT	3	23	10	2	14	59.9	27.9	1.10*

* = $p < 0.05$ compared with normals, EF=ejection fraction, %FS=percentage fractional shortening, E/A = E/A ratio of tricuspid flow

Morphological analysis assessed the presence of intramyocardial fat, wall thinning, aneurysms or outpouchings, dilatation and dyskinesia (from SE scans). Functional analysis included the calculation of RV volumes and ejection fraction (from GRE cines), the percentage fractional shortening (%FS) of 6 segments of the RV (from tagged GRE cines) and the E/A ratio of tricuspid flow (velocity encoded imaging).

Results: Results for morphological analysis and functional measurements are listed in Table 1. Morphological results in the table list the total number of abnormalities reported for the groups. ARVC patients showed significantly more morphological abnormalities than the other groups (mean 2.8/patient), see Table 1. In addition, the ARVC group significant differences in the functional parameters compared with the group of normals with reduced EF, lower fractional shortening and abnormal E/A ratios of tricuspid flow. In RVOT patients, morphological abnormalities were also found (mean 1.5/patient), most of which were limited to the RV outflow tract, but some extending into the RV. Quantitative measurements in the RVOT group were normal apart from a significantly lower E/A-ratio compared with the normal group, suggesting impaired RV diastolic function. Unexpectedly, some morphological abnormalities were reported in the normal group, mainly areas of thinning near the moderator band. A few minor abnormalities were seen in relatives of ARVC patients, but functional parameters were normal. Figure 1 gives an example of morphological abnormalities in a patient with ARVC (thinning and fatty infiltration). Figure 2 shows a dilated and serrated outflow tract in a patient with RVOT.

Conclusion: In conclusion, a combined assessment of RV morphology and function with MRI is feasible and provides complimentary information. Both morphological and functional abnormalities are found in patients with ARVC and RVOT, with abnormalities more severe in ARVC. As the diagnosis of ARVC is frequently difficult, this comprehensive imaging approach may enhance the diagnostic accuracy of MRI for this indication. Some abnormalities reported in the control group may represent normal variants.

104. Visualization of Myocardial Scarring in Hypertrophic Cardiomyopathy by Contrast Enhanced MRI

Lubna Choudhury,[1] Heiko Mahrholdt,[2] Anja Wagner,[2]Kelly Choi,[1] Michael Elliott,[1] John Vargas,[2] Robert Bonow,[1] Robert Judd,[2] Raymond Kim,[2] [1]*Northwestern University, 201 East Huron Street, Gaiter-10-240, Chicago, IL USA;* [2]*Duke University Medical Center, P.O. Box 3934, Durham, NC, USA*

Introduction: Myocardial scarring is postulated to be part of the arrhythmogenic substrate in hypertrophic cardiomyopathy, a primary cardiac disease associated with a risk of sudden death. Necropsy studies report myocardial scarring in highly selected patients with HCM. Whether scarring occurs in an unselected, non-referral population with HCM is unknown. Gadolinium-enhanced MRI is a new technique to visualize both transmural and subendocardial scarring.

Purpose: The aim of the present study was to determine whether myocardial scarring is present in patients with hypertrophic cardiomyopathy who are representative of the majority of community patients with this disease.

Methods: Cine and gadolinium-enhanced MRI was performed in 21 HCM patients who were predominantly asymptomatic. The extent of myocardial scar, represented by gadolinium hyperenhancement, was compared to left ventricular (LV) wall thickness and thickening on a regional basis, (using a 36 segment model per short axis slice of the left ventricle) and to maximum wall thickness, LV mass, and LV ejection fraction on a per patient basis.

Results: Scarring was present in 17 patients (81%). Scarring occurred only in hypertrophied regions ($^{*}10$ mm), was patchy, with multiple foci, and predominantly involved the middle third of the ventricular wall. All 17 patients had scarring at the junction of the interventricular septum and the right ventricular (RV) free wall. On a regional basis, extent of scarring was positively correlated with wall

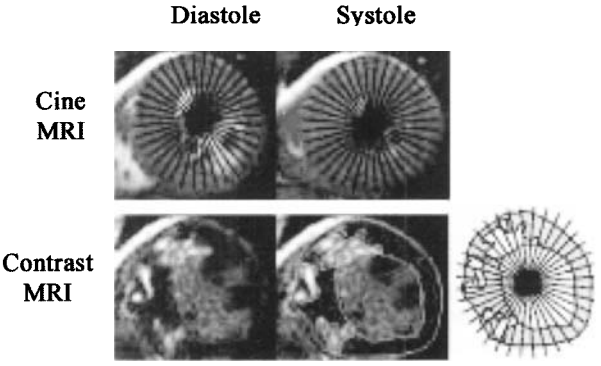

Figure 1.

thickening (3639 segments, $r = -0.21$, $P < 0.0001$). On a per patient basis, extent of scarring (mean, 9 ± 9% of LV mass) was minimally related to maximum wall thickness ($r = 0.3$ 9, $P = 0.08$) and LV mass ($r = 0.32$, $P = 0.15$), and was inversely correlated ($r = -0.45$, $P = 0.04$) with ejection fraction.

Conclusion: Myocardial scarring is common in minimally symptomatic HCM patients. When present, scarring occurs in hypertrophied regions, is consistently localized to the junctions of the septum and the RV free wall, and correlates positively with regional hypertrophy and inversely with regional contraction.

105. Quantification of Myocardial Injury After Percutaneous Transluminal Septal Myocardial Ablation in Hypertrophic Obstructive Cardiomyopathy

Willem Van Dockum,[1] Folkert Ten Cate,[2] Jurrien Ten Berg,[3] Aernout Beek,[1] Albert Van Rossum.[1] [1]*Vu University Medical Center, Boelelaan 1117, Amsterdam, Noord-Holland, The Netherlands;* [2]*Thoraxcenter Academic Hospital Dijkzigt, Dr. Molewaterplein 40, Rotterdam, Zuid-Holland, The Netherlands;* [3]*St. Antonius Hospital, Nieuwegein, Koekoekslaan 1, Nieuwegein, Utrecht, The Netherlands*

Introduction: Percutaneous transluminal septal myocardial ablation (PTSMA) is a nonsurgical therapeutic procedure for reducing left ventricular outflow tract obstruction symptomatic patients with hypertrophic obstructive cardiomyopathy (HOCM).

Purpose: The aim of this study was to evaluate septal myocardial injury size after PTSMA using delayed contrast-enhanced (DCE) magnetic resonance imaging (MRI).

Methods: 12 patients (mean age 52 ± 15 years, 7 males) underwent MRI before and 4 weeks after PTSMA; volume of ethanol injected during procedure was 1 to 5 mL. Images were acquired on a 1.5 T scanner (Vision/Sonata, Siemens, Erlangen, Germany). Cine gradient-echo MRI was performed for assessment of global left ventricular function at baseline and follow-up. Inversion-recovery turbo-FLASH images (TE 3.4 ms, TR 7.6 ms, TI 250-300 ms) were acquired at follow-up, 20 to 30 minutes after i.v. administration of 0.2 mmol/kg gadolinium-DTPA. Left ventricular function parameters, myocardial mass, and hyperenhanced area's (including central dark zones of hypoenhancement) were quantified using the MASS software package (Leiden University Medical Center, the Netherlands).

Results: Left ventricular mass values before and after PTSMA were 235.6 ± 70.7 g vs. 225.2 ± 71.7 g ($p = 0.001$), respectively. Septal myocardial mass pre- and post PTSMA was 79.2 ± 29.4 g vs. 72.7 ± 26.2, resp. In all patients the injured myocardium was well visualized. The hyperenhanced septal myocardial mass ranged from 3.6 to 24.9 g [mean: 12.8 ± 7.8 g], involving 5.0 % ± 4.0 of the post-ablational total LV mass and 21.2 % ± 16.0 of the septal myocardial mass. Myocardial injury size did not correlate with the volume of ethanol administered.

Conclusion: The extent of myocardial injury after PTSMA can be determined using DCE-MRI and did not correlate with the volume of ethanol administered. The method may serve as control and feedback for the interventional procedure.

106. Non-invasive Early Detection of Rejection for Transplanted Hearts with Multi-Dimensional Cardiac MRI

Yi-Jen Lin Wu,[1] Shinichi Kanno,[1] Chien Ho.[1] [1]*Pittsburgh Nmr Center For Biomedical Research, Carnegie Mellon University, Pittsburgh, Pennsylvania, United States*

Introduction: Organ transplantation is becoming the therapeutic treatment for patients with end-state organ failure. The current "gold standard" for detecting or confirming organ rejection requires biopsy, which is an invasive procedure with an associated risk and also prone to sampling errors. A sensitive and non-invasive method to detect graft rejection is needed for proper management of transplant patients.

Purpose: Non-invasive imaging modalities have been used to detect global systolic dysfunction. However, this stage with global systolic dysfunction is usually too late for medical intervention to save the rejected grafts. Our purpose of this study is to focus on whether multi-dimensional functional cardiac MRI is suitable for detecting rejection at an earlier stage (grade II or lower). A modified working heart and lung transplantation model in rats is established for this study.

Methods: 1. Animal model: A novel heterotopic working heart and lung model in the inguinal region with DA to BN rat pair is established. The transplanted hearts preserve natural blood flow, pre-loads, SV, EF, and pressures in all 4 chambers. At post-operational day (POD) 6-7, allogeneic grafts developed moderate to severe rejection (grade III and higher); whereas at POD 3-5, the rejection was mild to moderate (grade II or less). The rejection grade for each heart was determined by pathology after MRI. Total 72 transplanted animals studied include 14 DA-DA isografts, 16 BN-BN isografts, and 42 DA-BN allografts (10 mild, 19 moderate, 13 severe rejection).

2. MRI protocols: Density-weighted spin-echo images were used to cover the whole 3D volume of the heart at 8 to 12 time points in a cardiac cycle. Cardiac tagging was achieved by modified DANTE sequence. All MRI scans were performed on Bruker AVANCE DRX 4.7-T system.

Results: Global systolic functions are evaluated with ejection fraction (EF) and wall thickening (Fig. 1). Wall thickening is defined as the ratio of wall thickness between the end-diastole (ED) and the end-systole (ES). Our data showed that EF and wall thickening declined for severe rejection, but no significant reduction in EF or wall thickening found for mild and moderate rejection.

We have explored the volume-time relationships in the working heart transplantation model with the following parameters: maximum volume (Vmax), time to max (Tmax), and the time constants for diastolic phase (τ_D) and systolic phase (τ_s). Both LV blood volume (LVV) and the LV wall (LVW) volume were analyzed. Vmax is the maximum change in volume occurred in a cardiac cycle. Tmax is the time in percent cardiac cycle needed to reach the Vmax. Time constants (τ_D and τ_S) for dynamic volume changes are defined by $V = V_0 e^{-t/\tau}$. The data from only the mildly to moderately rejected hearts are summarized in Fig. 2, without severely rejected cases. For the mildly to moderately rejected hearts, no significant changes in Tmax or Vmax were observed. However, some time constants for LVV and LVW showed significant changes. The diastolic constants (τ_D) altered more than the

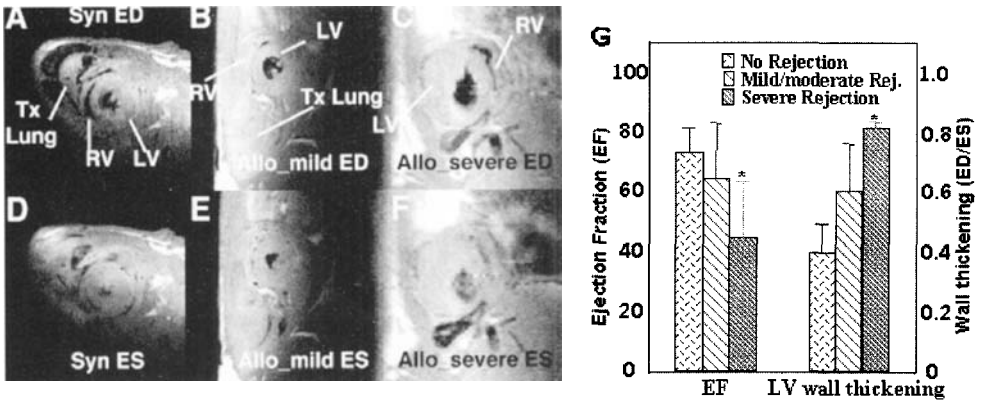

Figure 1. A-F: Spin-echo for the transplanted heart and lung (Tx Lung). G: mean data for all hearts.

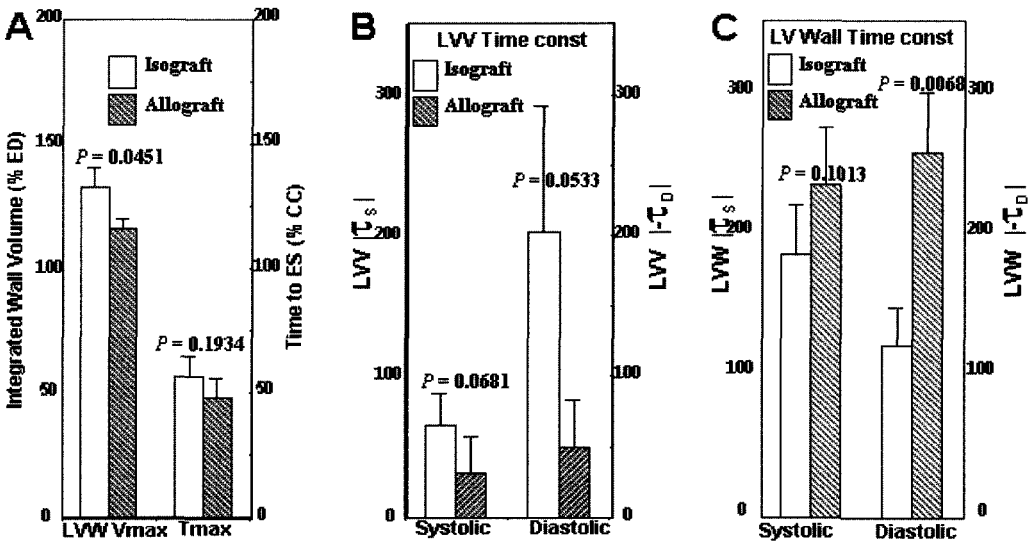

Figure 2. Dynamic measurements for the mildly to moderately rejected hearts. Severely rejected allografts are not included.

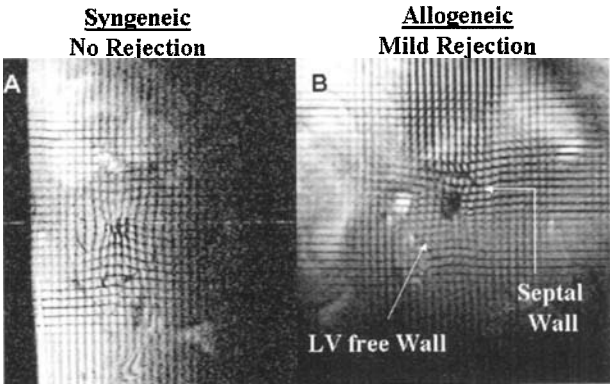

Figure 3. Cardiac tagging for transplanted hearts at ES.

systolic time constants (τ_S). In addition, changes in LV wall are more profound than that of LVV. Among all, the diastolic time constant τ_D for LV wall showed the most significant differences between moderately rejected allografts and the controls. Our preliminary data suggested that time-dependent dynamic properties can be sensitive enough for detecting early rejection, and the diastolic dysfunction occurs earlier than the systolic dysfunction.

Cardiac tagging images at ES (Fig. 3) showed that impaired contractility is not homogeneous at the early rejection. The septal wall of the heart preserved the majority of the contractility, whereas the LV free wall has lost most of its contractility. At this stage, the global systolic function is largely preserved. This is indicative that at the early stages of rejection, functional loss for contractility is regional, presumably localized to the infiltrated foci.

Conclusion: Our data showed that the diastolic functions deteriorate earlier than the systolic functions during the rejection process, and the diastolic dysfunction can be detected by the volume-based hemodynamic parameter (τ_D) of the LV wall, which cannot be detected by the conventional global systolic function parameters EF and wall thickening. Cardiac tagging revealed impaired regional contractility in early rejection. Multi-parameter MRI measurements makes correct and non-invasive diagnosis of early rejection possible.

107. An Integrated MRI Protocol for Assessment of Myocardial Function, Perfusion, Viability and Coronary Artery Morphology—Initial Results

Sven Plein,[1] John Ridgway,[2] Tim Jones,[1] Mohan Sivananthan.[1]
[1]*Leeds General Infirmary, Gt. George Street, Leeds, West Yorkshire, United Kingdom;* [2]*Leeds Teaching Hospitals, Department of Medical Physics, Leeds, West Yorkshire, United Kingdom*

Introduction: Magnetic Resonance Imaging (MRI) can provide diagnostic information about ventricular function, myocardial perfusion and viability as well as coronary artery morphology. A combined assessment of all these parameters may be a highly sensitive screening test for patients with coronary artery disease (CAD) and a comprehensive tool for their risk-stratification. However, with conventional MRI acquisition methods, an integrated evaluation of these parameters in a single imaging session would require unacceptably long examination times. Recent developments in MRI hardware and software have resulted in improved ECG triggering, better gradient performance and faster acquisition sequences. This may now allow the combination of several MRI component scans for the assessment of CAD in a single study.

Purpose: To develop and evaluate a MRI protocol, which combines the assessment of global and regional left ventricular function, myocardial perfusion at rest and stress, myocardial viability and coronary artery morphology in a single integrated study.

Methods: 10 patients (5 with previous myocardial infarction, 5 with angina) who were listed for coronary x-ray angiography were studied. MRI scanning was performed on a Philips 1.5T Intera CV system (Philips Medical Systems, Best, The Netherlands) with vectorcardiographic ECG-triggering and a 5 element cardiac synergy coil. The imaging protocol included: Localizers; Short-axis, two-chamber and four-chamber cine images (Steady State Free Precession = SSFP, TR 2.8 ms, TE 1.4 ms, flip angle 55°, 1 slice/breath-hold); Resting perfusion (T1 Turbo Gradient Echo = TGE with SENSE, TR 3.1 ms, TE 1.6 ms, flip angle 15°, SENSE factor 2, 4 short axis slices acquired every heart beat, 0.05 mmol/kg Gadolinium injected during breath holding); SENSE reference scan; Multi-slice cines of the LV in short axis (SSFP, 2 slices/breath hold); Scout-scan for localization of the coronary arteries; High-resolution MRI of the right coronary artery (3D TGE, T1 preparation, TR 7 ms, TE 2.1 ms, flip angle 40°, free breathing, prospective navigator gating, resolution $1.04 \times 0.78 \times 1.5$ mm, 16 slices, nominal scan time 1.40 to 2.20 min); Stress perfusion with Adenosine (140 mcg/kg/min for 5 minutes, sequence as above); High resolution MRA of the left coronary system (sequence as above); Viability imaging (delayed Gadolinium enhancement = deMRI, T1 TFE with 180° prepulse, 6–8 short axis slices, 1 slice/breath hold).

For analysis short axis slices were divided into four segments and correlated to coronary artery territories (anterior and septal = LAD, inferior = RCA, lateral = LCX). Segmental wall motion (WM) was scored on a scale from 1–4 (normal to akinetic) and perfusion graded qualitatively as normal, fixed defect or inducible defect. From deMRi images, the presence and extent of delayed hyperenhancement in each segment was recorded. Coronary MRA analysis assessed presence of stenoses >70%. The sensitivity and specificity to detect stenosis of >70% in individual vessels on x-ray angiography was assessed for each MRI component separately and for all components combined.

Results: All patients completed the examination and no complications occurred. The mean scan time was 61 (±6) minutes. Two coronary arteries could not be analysed due to poor image quality. All 5 patients with previous MI showed matching areas of abnormal WM and hyperenhancement on deMRI. The sensitivities and specificities of the MRI component scans are listed in Table 1. The combined analysis yielded a sensitivity and a negative predictive value of 100% with a specificity of 72.7% to detect significant CAD in individual coronary vessels. Figure 1 gives imaging examples from a patient with abnormal inferior WM (systolic phase shown) and hyperenhancement, compatible with previous inferior MI. In addition, stress perfusion shows inducible inferior and anterior perfusion defects. Figure 2 shows the MRAs and x-ray angiograms from the same patient, with the

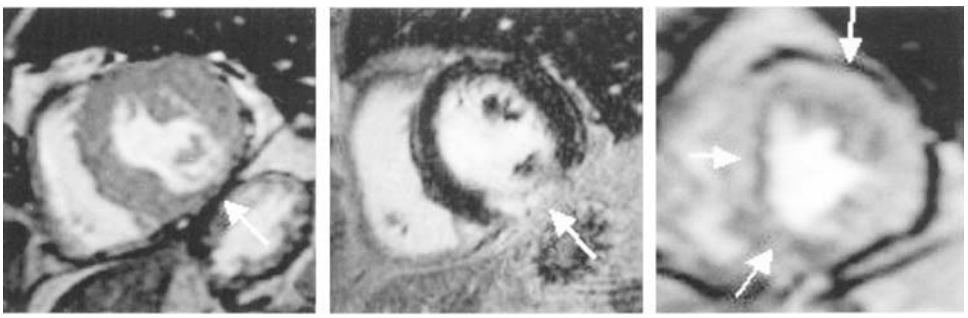

Figure 1.

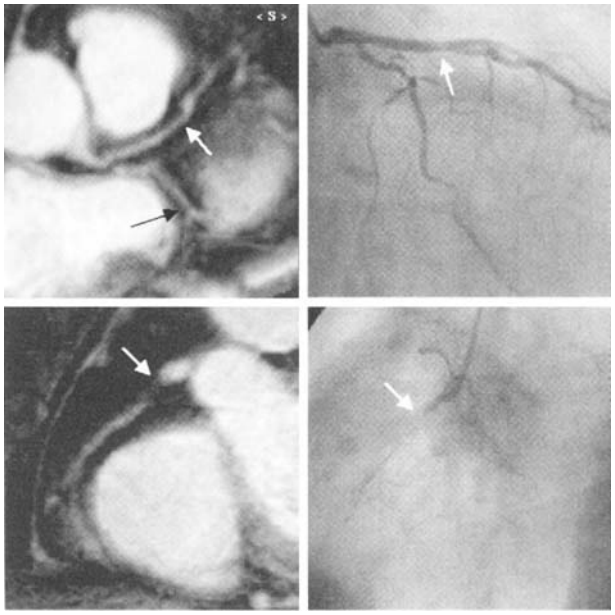

Figure 2.

Table 1

	Sensitivity	Specificity	PPV	NPV
Coronary MRA	72.1	88.9	92.8	61.5
Perfusion	75.1	90	93.8	64.3
deMRI	38.3	88.9	88.9	38.1
Wall motion	40.3	90	88.9	42.9
Combined	100	72.7	86.4	100

arrows indicating a proximal occlusion of the RCA and a significant stenosis in the mid LAD.

Conclusion: The protocol presented allows a comprehensive assessment of CAD, combining evaluation of wall motion, perfusion, viability and coronary artery morphology in a single imaging session of one hour. The combined analysis yields high sensitivity and NPV for detection of significant CAD and allows localization of disease to individual coronary vessels. The protocol now warrants evaluation in a wider patient population.

108. Single Breath-Hold Volumetric Mapping of the 3D Wall Motion in the Human Heart

Han Wen,[1] Eric Bennett,[1] Vinay Pai.[1] [1]*National Institutes Of Health, Lce/Nhlbi, Bethesda, Maryland, United States*

Introduction: The three-dimensional displacement field of the left ventricular wall is measured over 5 transverse slices that covers 60 cm length of the LV, in a breath-hold of 15

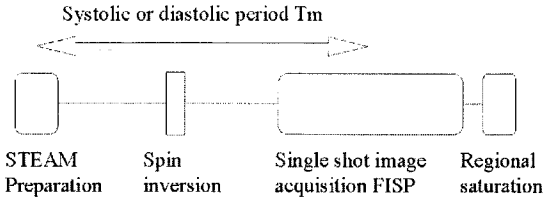

Figure 1.

heartbeats. The true resolution is $2 \times 3 \times 8\,mm^3$. The method is based on phase-contrast displacement encoding with stimulated-echo acquisition (DENSE) (1, 2).

Purpose: The purpose is to quantitatively assess the function of the myocardial wall in the human heart in vivo. This requires 3D measurements of the wall motion over the volume of the left ventricle, at high spatial resolution. The imaging time is limited to a practical breath-hold.

Methods: The scans were performed on a 1.5T Siemens Sonata system. A block diagram of the pulse sequence is shown in Fig. 1.

Motion encoding gradients are applied during STEAM preparation after EKG trigger and the proper delay. After a period of ventricular contraction or dilation, the phase distribution is re-acquired with a single-shot FISP like readout scheme. By computing the difference between the initial and end phase distributions, the 3D displacement vector of each voxel is measured. STEAM image acquisition preserves the spin coherence over a period comparable to T_1. The STEAM preparation is localized to the volume of interest, which allows limited FOV imaging without aliasing. Un-encoded signals from T_1 relaxation during the contraction or dialation period

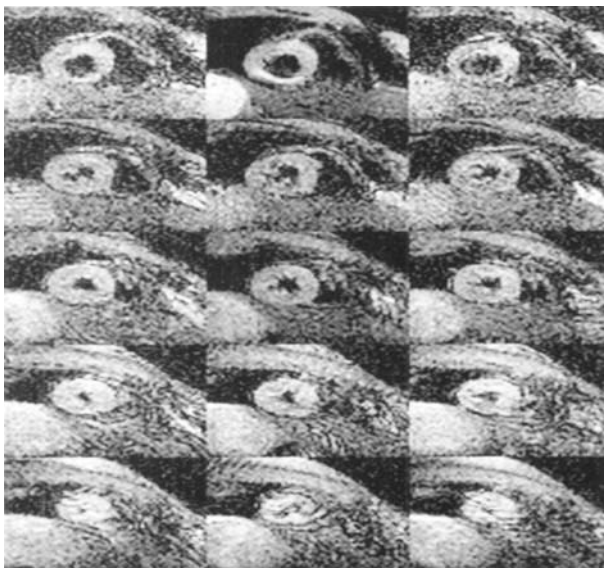

Figure 2. A five-slice data set acquired at end systole. The 3D motion over the systolic period is encoded.

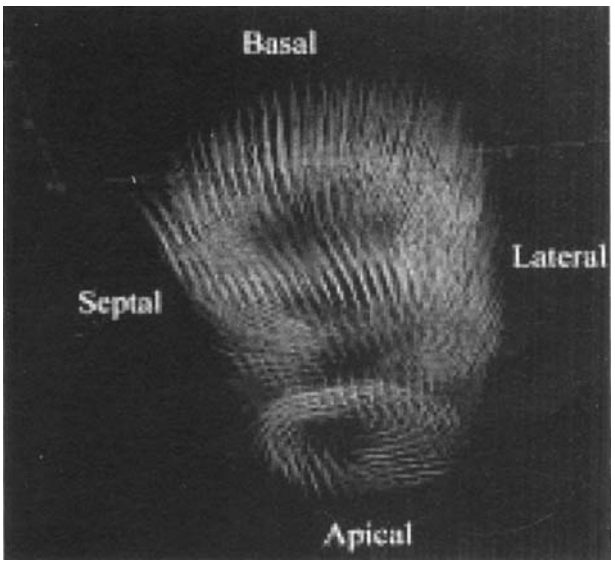

Figure 3. Three-dimensional displacement of each voxel is shown with a line connecting the end-diastolic position with the end-systolic position. Five slices are shown in alternating color schemes.

(FID) is suppressed with the combination of two measures used in the past, through-slice encoding gradients (2) and a spin inversion near the mid-point of the Tm period (3). Extraneous phase errors from B0 field variation are removed with a refocusing pulse in the STEAM preparation.

Results: A complete data set of a 32 year old male normal subject is shown in Fig. 2. The true resolution of the images is $2 \times 3 \times 8\,mm^3$. Each slice contains three images that encode the movement in the three Cartesian coordinates respectively. The three dimensional wall motion of the LV is plotted in Fig. 3. Each line connects the initial and end positions of a voxel over the systolic period. Odd and even slices are depicted with different color scales. Bulk motion subtraction is not applied. Some obvious features are that the base of the heart moves toward the apex during contraction, and The twist of the apical portion is evident.

Conclusion: With a STEAM based phase-contrast technique, a volumetric measurement of the 3D motion of the LV is acquired in 15 heartbeats at image resolution. From this measurement various 3D strain and wall thickness parameters are then derived with automated routines. As a tool for assessing wall motion of the human heart, it improves the speed and accuracy over standard multiple breath-hold 2D measurements.

References

1. Callaghan PT. Principles of nuclear magnetic resonance microscopy. Oxford: Clarendon Press; 1991. 430 p.
2. Aletras AH, Ding S, Balaban RS, Wen H. J Magn Reson Med 1998; 39:482–490.
3. Aletras AH, Wen H. Magn Reson Med 2001; 46: 523–534.

109. Blood Flow Based Navigation for Cardiac Tracking

Vinay Pai,[1] Han Wen.[1] [1]*National Institutes of Health, Bldg. 10, Room B1d-416, Msc 1061, Bethesda, Maryland, United States*

Introduction: Navigating, a non-breathhold technique for reducing respiratory motion artifacts, has certain advantages as compared to breath-hold techniques since the available imaging time is extended, and issues of needing significant patient cooperation do not arise [1]. A commonly used navigator applies pencil-beam excitation to the diaphragm, and the motion of the diaphragm tracked by this approach is then correlated to cardiac motion. However, it has been shown that respiratory motion patterns can be very patient-specific, needing development of patient-specific correlations for the motion [2].

Purpose: This paper presents an approach for determining the cardiac position by using a blood flow based complex-difference "double-shot" scheme. This approach tracks the fast moving blood during systole as a marker for the heart position, while stationary or slow-moving spins are suppressed. By this approach, the position of the heart can be determined directly, without needing fractional correlation with the diaphragm motion.

Methods: In the double-shot (DS) scheme, a pair of alternating bipolar flow encoding gradients, constituting a single shot, are repeated twice, as shown in figure 1a. The complex-difference (CD) operation is performed for each of the two shots, and a final CD is performed between the resulting CD images to yield the navigator image. The double-shot approach effectively cancels out the chest wall motion, and yields the motion primarily of the heart. The navigator DSs were immediately followed by an imaging sequence over the given R–R interval, as shown in figure 1b. The heart motion as tracked by the imaging sequence can then be compared to the motion predicted by the navigation scheme.

The scans were performed on a Siemens Sonata 1.5-T whole-body scanner (Siemens Medical Systems, Erlangen, Germany) with gradients of 45 mT/m and maximum slew rate of 300 mT/m-ms. The ECG-triggered navigator sequence was a spoiled-FLASH sequence with spoiling in the slice-select direction and bipolar gradient for flow encoding, and its implementation included a TR/TE of 10/3.2 ms, RF flip angle of 4° and slice thickness of 20 mm. The imaging sequence was a FISP sequence with TR/TE of 3.2/1.6 ms, RF flip angle of 15° and slice thickness of 8 mm. Both the sequences had base and phase resolutions of 128 × 120 pixels. The breathhold case used a FOV of 340 mm, while the normal breathing case used a FOV of 395 mm, yielding pixel resolutions of 2.66 and 3.09 mm/pixel respectively in the readout direction for the navigators. The ADC bandwidth was 1 kHz/pixel. Navigator scans were done in early- to mid-systole, and the imaging scans from mid-systole. After the navigator scans were obtained, the complex difference data was obtained by $CD = |(M2 - M1) - (M4 - M3)|$, where Mi represents the magnetization signal after the i^{th} bipolar in the DS scheme. The CD values for the first R–R interval were used as a reference to set up a floating kernel for the remaining CD data to determine the locations of maximal motion. The imaging scan for the first R–R interval was used as the reference imaging scan to which imaging scans for subsequent R–R intervals were correlated with a motion registration algorithm.

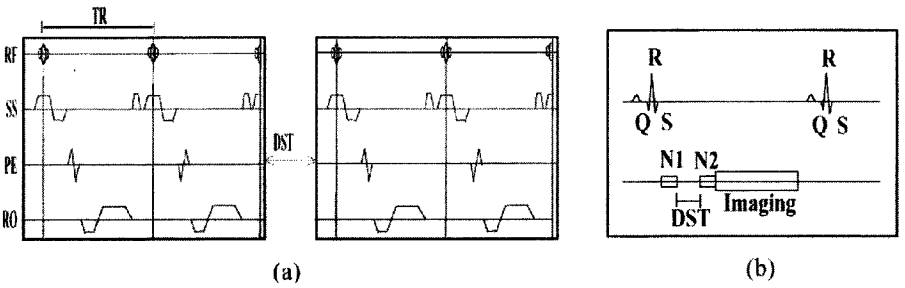

Figure 1. Double-shot navigation. (a). Two spoiled-FLASH single-shots separated by double-shot time (DST); each single shot is comprised of a pair of alternating bipolar gradients, (b). Location of the navigators and imaging sequence in a R–R interval, with N1 and N2 representing the two single-shots.

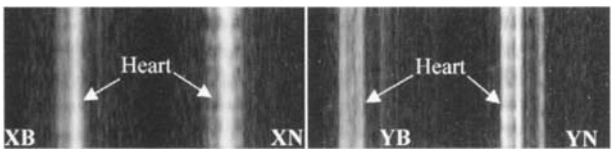

Figure 2. Navigator echoes for a sagittal slice through the heart under breathhold (XB,YB) & normal breathing (XN,YN). X: H–F; Y: A–P directions.

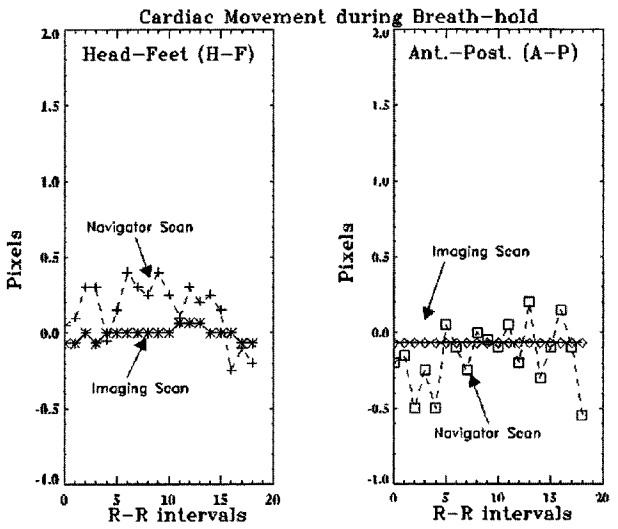

Figure 3. Cardiac Motion under Breath-hold Condition.

Results: Figure 2 shows the navigator echoes obtained. Both plots show the variation in the echo signal due to the motion of the chest for normal breathing conditions. There is some mild signal intensity variation during the breath-hold conditions which might be an indication of surface coil loading changes with breathing.

Figures 3 and 4 show the comparison between the cardiac motion calculated from the navigator and the imaging scans for breathhold and normal breathing cases. The imaging plots show

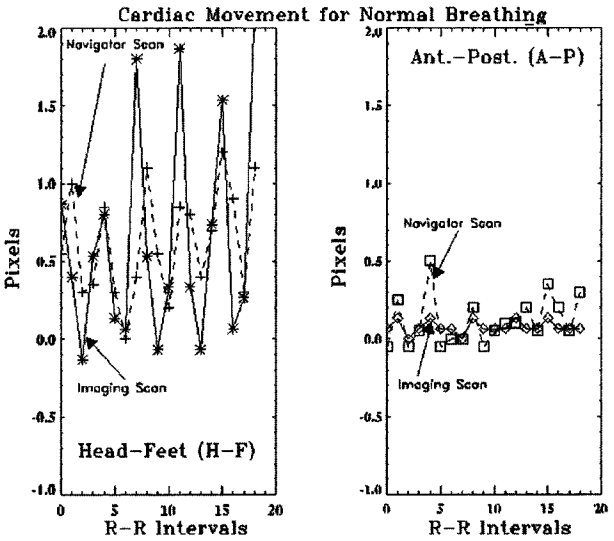

Figure 4. Cardiac Motion for Normal Breathing.

negligible heart motion during breath-hold condition. However, the navigator sequence erroneously predicts cardiac motion of the order of 0.4 pixels (equivalent to 1 mm). The standard deviations for the navigator echo plots in the H–F and A–P directions were 0.19 and 0.21 respectively. For the normal breathing case, there is a close match between the navigator and the imaging sequence plots for the A–P and the H–F directions.

Conclusion: The blood flow based CD approach to tracking cardiac motion appears capable of monitoring heart bulk movement greater than one mm. This technique obviates the need to obtain correlative factors as needed in diaphragm-based navigation techniques.

110. Human Cardiac Motion Measurements with Dense and Myocardial Tagging

Anthony Aletras,[1] Gauri Tilak,[2] Kwabena Agyeman,[1] Andrew Arai.[1] [1]*National Institutes Of Health, Building 10, Room B1d-*

416, Bethesda, Maryland, United States; [2]New Jersey Medical School, 467 Valley Street, Maplewood, New Jersey, United States

Introduction: Assessment of global and regional left ventricular (LV) function is central to evaluating coronary artery disease. Although echocardiography and MRI provide high quality diagnostic assessment of regional LV function, the interpretation is considered the most difficult part of such studies. An objective or quantitative measure of regional LV function could help considerably in this task. While MRI tagging methods have been highly accurate, the burden of post-processing time has minimized clinical applicability. A promising technique for measuring regional function is Displacement Encoding with Stimulated Echoes (DENSE). This phase-based method allows for automatic and rapid image processing and it provides quantitative results of both myocardial motion and myocardial strain. DENSE functional images summarize the displacement of cardiac tissue over the entire systole in a single high-resolution image.

Purpose: In this work, we compare myocardial displacement measurements acquired with DENSE to those obtained with tagging, which has been the gold standard for MRI myocardial displacement. In addition, the reproducibility of DENSE displacement measurements is also evaluated.

Methods: Multi-slice DENSE and tagged short-axis images were acquired from 6 normal volunteers on a GE Cv/i 1.5T system. Image preparation (i.e. tag placement and DENSE position encoding) was prescribed so as to occur at the same cardiac phase for both methods albeit during separate breath-holds. Imaging was performed in a single-phase mode for both techniques always at end-systole, which was approximately 300 ms from the peak of the R-wave. In order to capture motion' over various time intervals during systole, image preparation was progressively shifted closer to end-systole in 6 steps. As such, displacement over the following intervals was recorded: 300, 250, 200, 150, 100 and 50 ms. Grid tag spacing was 7 mm and DENSE encoding strength was 2 mm/π. For tagging, 8 lines of k-space were acquired per RR interval while for DENSE the corresponding value was 24. The spatial resolution for displacement measurements was 7 mm for tagging and 2.8 mm for DENSE.

Images were processed with in-house software written in IDL (Boulder, CO). Tag displacement along both the X and Y-axes was measured via manual tag-grid identification. Processing time was 4.5 hours per multi-slice dataset for all 6 cardiac phases recorded. DENSE displacement along both the X and Y-axes was measured directly from the phase of each pixel. Processing time was 1.5 minutes accordingly. Displacement values along both the X and Y-axes were compared via Bland–Altman analysis. Repeated DENSE measurements with DENSE were also similarly compared.

Results: Figure 1 presents typical tag vs. DENSE comparison Bland–Altman plots for X (top) and Y (bottom) displacements. These plots show displacement comparison data obtained 250 ms after the onset of systole at the mid-ventricular level. The horizontal axis depicts the average displacement measured by the two methods while the vertical axis shows the difference of the two measurements. The bias for X and Y is 0.6 and 0.1 mm respectively. The corresponding standard deviations are 1.4 and 1.6 mm.

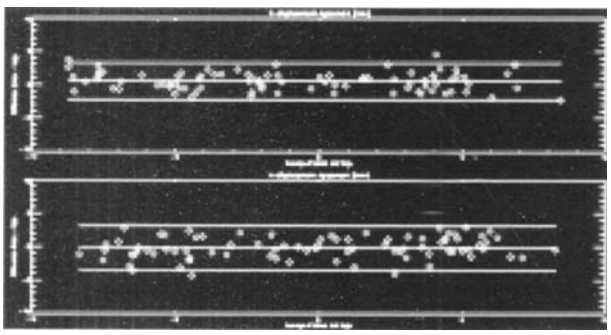

Figure 1.

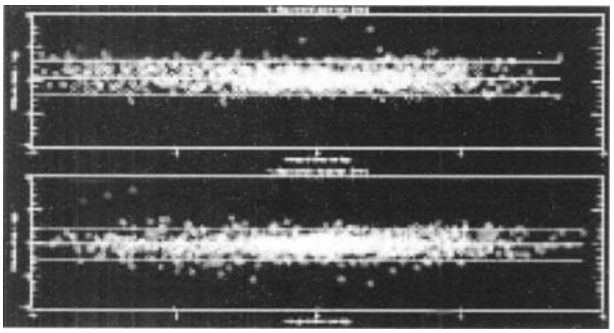

Figure 2.

Summary comparison data for all slices (apical, mid-ventricular and basal) and all 6 time intervals imaged are shown in Figure 2. The bias for X and Y is 0.5 and 0.2 mm respectively. The standard deviation is 1.2 mm for both plots.

Bland–Altman reproducibility comparison data for the entire systolic interval acquired with DENSE, acquired from a mid-ventricular slice, showed zero biases for both X and Y-axes. The corresponding standard deviations are 0.2 and 0.3 mm. (plots not shown due to space limitation).

Conclusion: With minimal data processing effort (1 sec/-slice for strain maps), DENSE yields both quantitative displacement and strain functional data at high spatial resolution (2.8 mm in-plane). To validate DENSE against tagging, displacement was preferred over strain for two reasons. First, even in normal volunteers, displacement measurements along the X and Y-axes span over a wide range of values (approximately ± 8 mm of displacement) thus simplifying the logistics of these lengthy comparative experiments. In addition, by comparing displacement, the extra processing step of calculating tagging strain via parametric fitting was eliminated. This process, which averages and interpolates over space and time, could have complicated things further. The comparison of displacement measurements was chosen to be the most direct method available. Overall, tagging and DENSE are in good agreement despite that the data were acquired with the two methods approximately 30 minutes apart. In addition, the data suggest that DENSE is highly reproducible. This reveals new potential for quantitative clinical applications in the future.

With high resolution and on-the-fly processing, DENSE promises to be a valuable tool for evaluating LV regional wall motion even in cases where rapid feedback is desired.

111. High-Resolution Spiral CSPAMM MR Myocardial Tagging

Salome Ryf,[1] Kraig Kissinger,[2] Peter Börnert,[3] Warren Manning,[2] Peter Boesiger,[1] Matthias Stuber.[2] [1]*University And Eth Zurich, Gloriastrasse 35, Zurich, Switzerland;* [2]*Beth Israel Deaconess Medical Center, Cardiovascular Division, Boston, MA, United States;* [3]*Philips Research Laboratories, Technical Systems, Hamburg, Germany*

Introduction: Myocardial tagging techniques, such as SPAMM (1) and CSPAMM (2), have shown to be most useful for the assessment of myocardial motion. However, one limitation of conventional tagging methods includes the relatively low resolution of the tagging grid (typically 8 mm).

Recently, a new technique has been introduced by Urayama et al. (3) to apply a high-resolution tagging grid. Because of the rapid fading the tags, the grid has to be applied four times during the cardiac cycle.

Spiral MRI offers a time-efficient sampling pattern for the acquisition of data in k-space while the small number of RF-excitations leads to a good conservation of the tagged information. The combination of the CSPAMM tagging technique together with a spiral-readout allows the acquisition of isotropic high-resolution tagging images with a tag-distance as low as 4 mm within one breath-hold. Alternatively, with a lower spatial resolution, the spiral readout permits a high temporal resolution with 77 frames/s.

Purpose: To investigate the use of a spiral readout for the acquisition of CSPAMM images with a high spatial or temporal resolution.

Methods: CSPAMM is based on the subtraction of two images with a complementary tagging modulation, while fading of the tags is suppressed throughout the entire cardiac cycle. Two 90°-block pulses, interspersed by a dephasing gradient, produce a sinusoidal modulation of the magnetization, and thus, a line shaped tag pattern. To generate a tagging grid, the modulation is applied in both spatial directions prior to the imaging sequence. To acquire images with a high spatial resolution, lines or a grid with a tag-distance of 4 mm were applied. For images obtained with a high temporal resolution, a grid with a tag-distance of 8 mm was used.

Examination Protocol:

After tagging preparation, cine imaging was accomplished with a spiral imaging sequence. A ramped spectral spatial excitation was applied for fat suppression (4) and constant tagging contrast, which lead to a TE of 3.6 ms. All measurements were performed on a commercial 1.5 T whole body scanner (Gyroscan ACS-NT, Philips Medical Systems). The measurements were achieved in 5 healthy adult subjects. Basal, mid-myocardial and apical short-axis views and four-chamber views were acquired.

High spatial resolution:

A field of view of 320 mm × 320 mm was imaged with a spatial resolution of 1.25 mm × 1.25 mm. Sixteen frames were imaged per RR-interval with a temporal resolution of 35 ms.

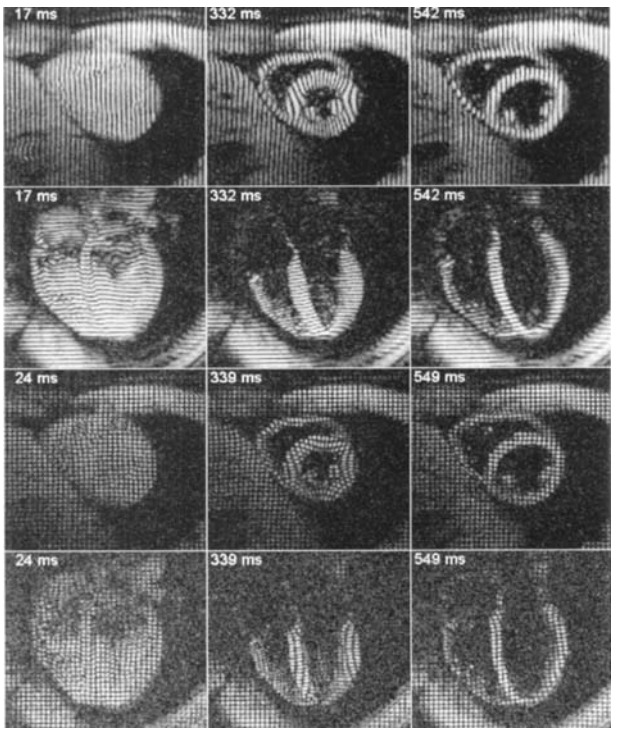

Figure 1. Mid-myocardial short-axis and four-chamber view of a line and a grid-tagged myocardium, tagline-distance 4 mm.

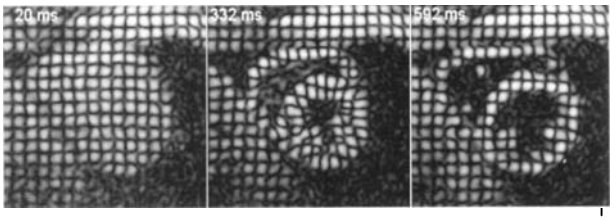

Figure 2. Short-axis view of a grid-tagged myocardium. Temporal resolution of the cine-sequence: 77frames/s.

Ten segmented spiral interleaves were acquired each with a sampling window of 23 ms per cine frame. The breath-hold duration was 22 R–R intervals.

High temporal resolution:

A field of view of 256 mm × 256 mm was imaged with a spatial resolution of 2 mm × 2 mm. Forty-five heart phases were acquired with a temporal resolution of 13 ms. Twelve spiral interleaves were performed each with a sampling window of 5 ms, leading to a breath-hold duration of 26 R–R intervals.

Results: Figure 1 shows a mid-myocardial short-axis view and a four-chamber view of a line-tagged and a grid-tagged myocardium acquired in the same subject. The tag-line distance is 4 mm and three out of 16 heart-phases are displayed at 17 ms, 332 ms and 542 ms after the R-wave for the line-tagged images

and at 24 ms, 339 ms and 549 ms for the grid-tagged images. On the short-axis view of the grid-tagged images approximately fifty tagline-intersections are observed on the myocardium. In Figure 2, three out of 45 heart-phases are displayed at 20 ms, 319 ms and 592 ms after the R-wave. With the grid-distance of 8 mm, about 22 tagline-intersections appear on the myocardium. For all acquisitions the tag-contrast remained constant throughout the entire cardiac cycle.

Conclusion: It has been shown that tagging images with a high spatial or temporal resolution can be acquired. Hereby, high image quality can be obtained and fading of the tags can be suppressed. Because of the efficient k-space sampling associated with spiral imaging, only a small number of RF-excitations are required with subsequent preservation of the magnetization. The short echo-time enables the application of a spatial spectral pulse for fat suppression and the spiral read-out is less susceptible to flow-artifacts. The high isotropic spatial resolution of the spiral-images enables the application of a dense tagging pattern with a line-distance as low as 4 mm. The increased amount of taglines on the myocardium may lead to a more accurate registration of the myocardial function and a better distinction between adjacent segments of the myocardium. The high temporal resolution of the images may lead to a more detailed description of myocardial motion. The technique now remains to be investigated in specific patient collectives.

112. Infarct Imaging in a Single Heart Beat

Yiu-Cho Chung,[1] John Vargas,[2] Orlando Simonetti,[1] Raymond Kim,[2] Robert Judd.[2] [1]*Siemens Medical Solutions, Cardiovascular Mr Research, Chicago, IL, USA;* [2]*Northwestern University, Feinberg Cardiovascular Research Institute, Chicago, IL, USA*

Introduction: Imaging of myocardial infraction is very important in cardiac disease management. Identification of viable myocardium is useful in predicting if a patient may have improved heart function after revascularization. Previous studies have found that contrast enhanced MRI can distinguish between viable and non-viable myocardium. Inversion recovery, segmented TurboFLASH (IR-TFL) has been found very useful in differentiating infarct and viable myocardium. The method takes about 8–10 heart beats. Hence image quality of the technique is prone to heart beat irregularity (irregular RR interval affects magnetization recovery and thus the image quality) and the patient's breath-holding ability. Single shot imaging techniques are highly desirable.

Purpose: To design a single shot, inversion recovery trueFISP sequence (IR-trueFISP) on a clinical MRI scanner equipped with high performance, state of the art gradient systems and apply it to infarct imaging.

Methods: *The sequence*

It has been found magnetization recovery of IR-trueFISP follows the T1 relaxation curve for flip angles between 10°–50°. A single shot 2D IR-trueFISP sequence kernel was designed. It consists of an $\alpha/2$ pulse, 20 dummy cycles, the actual acquisition cycles and lastly an $-\alpha/2$ flipback pulse. Linear reordering is used. The IR pulse precedes the sequence kernel. The inversion time (TI) is defined as the time between

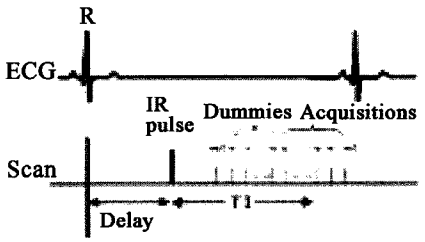

Figure 1. The single shot IR trueFISP sequence.

the IR pulse and the k-space center line. Fig. 1 shows the sequence. Asymmetric echo is used to reduce TR and get higher echo signal.

Both IR-trueFISP and IR-TFL were implemented on a MAGNETOM Sonata (Siemens, Erlangen, Germany, max gradient = 40 mT/m, min slew rate = 200 mT/m/ms).

Patient imaging

Four patients with known infarcts were imaged using the two sequences. The study followed the IRB approved protocol. In the study, the short axis, long axis and 4-chamber views of the heart were first found. Cine images were then acquired for these views to document the heart function. After that, IV injection of Gd-based contrast agent (~0.1 mmol/kg) was performed to the patient. Images was acquired for these views 5–10 min after contrast injection. IR-TFL sequence was applied first, immediately followed by IR-trueFISP. Multiple slices were acquired to cover the whole heart along the short axis. Parameters used in the sequences are:

TFL: ECG trig, 124 lines, 25 segments, FOV = ~270 mm × 360 mm, slice = 6 mm, flip angle = 30°, TE/TR = 4.3 ms/11 ms, TI = 300–400 ms, bandwidth/pixel = 140 Hz, gradient refocused, matrix = 256^2. Lines acquired every other beat. Scan time = 10 beats.

TrueFISP: ECG trig, ~100 lines, single shot, FOV = ~270 mm × 360 mm, slice = 6–8 mm, flip angle = 30°, TE/TR = 1.2 ms./2.7 ms, TI = 350–450 ms, bandwidth/pixel = 980 Hz, matrix = 256^2.

Nonselective IR pulses were used in both cases to avoid flow artifact. Acquisitions were timed to occur at the diastolic phase of a cardiac cycle. Acquisition window was kept to about 275 ms. While high flip angle in trueFISP usually gives images with higher SNR, a flip angle of 30° was chosen for IR-trueFISP to get magnetization recovery characteristics close to the T1 relaxation curve.

Results:

Fig. 2 shows the typical appearance of infarcted myocardium (bright) obtained using IR-TFL and IR-trueFISP in one patient. The infarct showed up very clearly in both cases. The image obtained using IR-TFL was sharper than those obtained from IR-trueFISP. This is because ~100 lines/image were collected in IR-trueFISP while 124 lines/image were collected in IR-TFL. Similar results were obtained in the other three patients.

The robustness of IR-trueFISP could be seen in another patient whose heart beat was irregular. IR-TFL (Fig 3b) failed

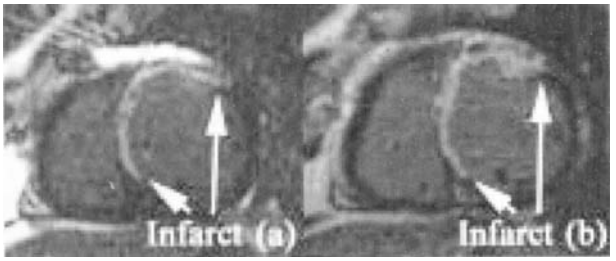

Figure 2. The SA images obtained in one patient. (a) IR-trueFISP. (b) IR-TFL. The latter image was taken about 15 min before (a). The slight difference in the infarct size may be caused by patient movement.

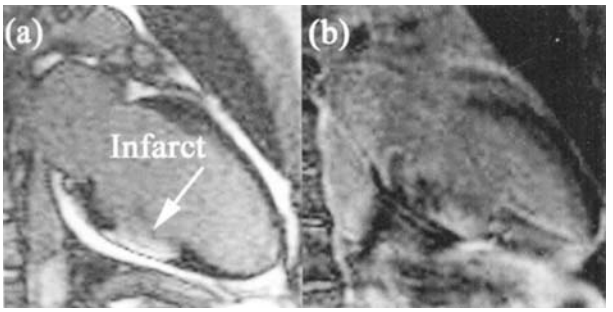

Figure 3. The 2-chamber images obtained from another patient. (a) IR-trueFISP. (b) IR-TFL. The image quality from IR-trueFISP is much less sensitive to heart beat irregularity or patient motion.

to give an image of diagnostic quality. IR-trueFISP acquired a respectable image for diagnosis with no difficulty (Fig 3a).

Conclusion: The study shows that IR-trueFISP is a robust technque for infarct imaging. The sequence produces images with quality immune to heart rate variability. The images are comparable to those obtained using IR-TFL. During the design of IR-trueFISP, the exploitation of high performance gradients and the use of asymmetric echo collection help reduce the TR in trueFISP and allows more lines to be collected. This helps improve image quality and reduce blurring in the images. The technique of IR-trueFISP can be extended to segmented acquisition, which may give improved image resolution while keeping imaging time short.

113. MRI Evaluation of Right Ventricular Function Before and After Pulmonary Valve Replacement in Repaired Fallot Patients

Alexander Van Straten,[1] Hubert Vliegen,[1] Mark Hazekamp,[1] Arno Roest,[1] Albert De Roos.[1] [1]*Leiden University Medical Center, The Netherlands, PO Box 9600, Leiden, Zuid-Holland, The Netherlands*

Introduction: Severe pulmonary regurgitation (PR) late after total correction for tetralogy of Fallot leads to progressive right ventricular (RV) dilatation and an increased incidence of severe arrhythmias and sudden death.

Purpose: MRI was used to assess the effect of pulmonary valve replacement (PVR) on RV function and PR.

Methods: 26 Adult patients who underwent PVR in our institution between 1998 and 2001 were studied. Mean age at initial repair was 5.5 ± 3.6 years and mean duration of follow-up was 30.0 ± 8.9 years. Cardiac MRI was performed 6.2 ± 3.7 months before and 7.7 ± 2.3 months after PVR. Pulmonary regurgitation (PR), RV end-diastolic volume (RVEDV), Right ventricular end-systolic (RVESV) and RV ejection fraction (RVEF) were measured.

Results: Preoperative PR was 45% (range from 25 to 64%). After PVR, 20 out of 26 patients (77%) showed no residual PR. RVEDV decreased from 305 ml ± 87 ml to 210 ml ± 62 ml ($p < 0.01$) and RVESV decreased from 181 ± 67ml to 121 ± 58ml ($p < 0.01$). No significant change was found in RVEF (42 vs. 43%).

Conclusion: Adult patients with severe PR, late after total correction for tetralogy of Fallot, show remarkable hemodynamical improvement after PVR. Most patients show no signs of residual PR and both RVEDV and RVESV decrease dramatically, although no improvement in RVEF is found. Reduced RV volume may lead to a lower risk for RV failure and severe arrhythmias.

114. T1-Relaxation Kinetics of Gd-Dpta After Bolus Injection in Patients with Chronic Ischemic Heart Failure

Christoph Klein,[1] Stephan Nekolla,[2] Bernhard Schnackenburg,[3] Thomas Balbach,[1] Markus Schwaiger.[1] [1]*Nuklearmedizinische Klinik, Technische Universität München, Ismaningerstr. 22, München, Bayern, Germany;* [2]*Nuklearmedizinische Klinik Der Tu, München, Klinikum Rechts Der Isar, München, Bayern, Germany;* [3]*Philips Medical Systems, Augustenburger Platz 1, Berlin, Bayern, Germany*

Introduction: Several studies indicate that contrast enhanced magnetic resonance imaging after a bolus injection of an extracellular contrast agent can distinguish between viable and non-viable (scar) myocardium in acute and chronic myocardial infarction. Scar tissue is defined as increased signal intensity compared to viable myocardium. By determining T1-relaxation times, animal studies suggested, (using an acute occlusion and reperfusion model) that an equilibrium distribution of an inert extracellular contrast agents over time exists both in normal and scared myocardium. Thus the partition coefficient can be calculated.

Purpose: The aim of the present study was 1) to determine T1 relaxation kinetics of blood, normal and scared myocardium, 2) investigate if an equilibrium distribution in normal and scared myocardium exists and 3) calculate the optimal point of time for contrast enhanced imaging in patients with chronic ischemic heart failure after bolus injection of Gd-DPTA.

Methods: 14 patients with coronary artery disease (x-ray angiography) and heart failure (EF < 35%) were examined

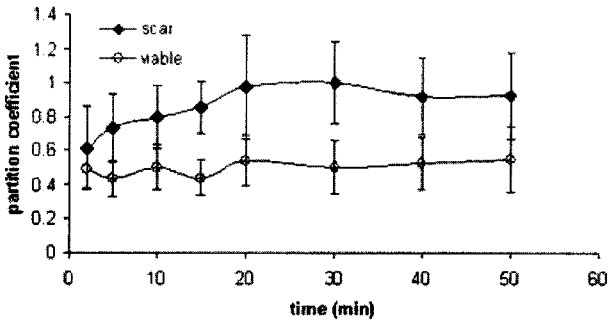

Figure 1. Partition coefficient of Gd-DPTA in normal and scared myocardium

with an 1.5 Tesla scanner (ACS NT, Philips Medical Systems, Best, Netherlands using a dedicated cardiac phase array coil. With a breath hold technique (12 sec), T1 relaxation times(in sec) using a modified Look–Locker sequence (TR/TE 8.9/4.8 ms, flip angle 10°, EPI factor 5, spatial resolution $2.7 \times 2.7 \times 8\ mm^3$, temporal resolution 34 ms), imaging 3 short axis views (apical, medial, basal) were acquired before and 2, 5, 10, 15, 20, 30, 40 and 50 min after a bolus injection of 0.2 mmol/kg body weight Gd-DPTA. A total of 85 images covering several heartbeats after the inversion pulse were acquired. Twenty minutes after the bolus, a 3D inversion recovery fast hybrid technique (TE/TR 3.3/5.4 ms, EPI factor 11, slice thickness 5 mm, spatial resolution 1.2 × 1.2 mm2, flip angle 15°, acquisition time 284 ms, prepulse delay 225–300 ms) was applied. The left ventricle was divided into 18 segments using a representative apical (6 segments), equatorial (6 segments) and basal (6 segments) short axis view, yielding a total of 252 segments in 14 patients. In each segment non-viable tissue (scar) was defined as increased signal intensity in the inversion recovery sequence. The extent of hyperenhancement was divided into transmural and subendocardial. Look–Locker images were analysed using a specially designed software at our institution ("Munich Heart") by defining the endo- and epicardial border in each cardiac phase. Signal intensity time curves were generated for each segment and the blood pool. To determine T1, the curves were fit to the predicted longitudinal magnetization curves. Assuming that equilibrium state of distribution can be achieved a few minutes after the administration of an inert extracellular contrast agent the relative quantities in tissue over blood constitute the partition coefficients (λ). Therefore λ was calculated by the equations: R1 = 1/T1 (1), ΔR1 = R1postcontrast − R1precontrast (2), ? = ΔR1myocardium/ΔR1blood (3). T1 values and λ were calculated only for segments which showed no or transmural enhancement only.

Results: Of the 252 segments 47 showed transmural and 175 no enhancement. T1 relaxation rates over time for normal and enhanced myocardium and the blood are shown in Table 1. There was no significant difference in T1 relaxation values between normal and scared myocardium before contrast application. However, significant differences between normal and enhanced myocardium are already evident 2 min after contrast application and continue to up to 50 minutes ($p < 0.0001$). Significant differences between blood and enhanced myocardium did not exist 10–15 min after contrast ($p > 0.05$), therefore making the delineation of the endocardial border difficult which may be important for quantification of infarct size. Values for the partition coefficient are shown in figure 1. As there is equilibrium distribution of Gd-DPTA in normal myocardium, enhanced segments show an altered pattern.

Conclusion: This study suggest that in patients with ischemic heart failure 1) significant differences in T1 relaxation times between viable and scar tissue exist as early as 2 min after contrast application and last up to 50 min, 2) the optimal time point for data acquisition with the enhancement technique starts at 20 minutes and stays as long as 50 min and 3) there is no equilibrium distribution of Gd-DPTA in scar compared to normal tissue before 20 min after bolus, probably due to reduced blood flow.

115. Gene–Environment Interactions in the Human Left Ventricular Growth Response: Elucidation with CMR

Saul Myerson,[1] David Brull,[2] Suki Dhamrait,[2] Vera Regitz-Zagrosek,[3] Michael World,[4] Steve Humphries,[2] Dudley Pennell,[5] Hugh Montgomery.[2] [1]*Royal Brompton Hospital, Sydney Street, London, England, UK;* [2]*University College London, Centre For Cardiovascular Genetics, London, England, UK;* [3]*Humboldt University, Berlin, Germany;* [4]*Royal Defence Medical College, Gosport, Hampshire, UK;* [5]*Royal Brompton And Harefield Nhs Trust, Sydney Street, London, England, UK*

Introduction: Left ventricular hypertrophy is an important cause of mortality and morbidity. Many factors influence the growth process and are likely to include genetic determinants, though the detection of modest genetic influences on left ventricular (LV) mass is difficult and requires precise LV mass

Table 1

Kinetics of T1 Values (sec) for Blood, Normal, and Transmurally Enhanced Myocardium After Bolus Injection

	Baseline	2 min	5 min	10 min	15 min	20 min	30 min	40 min	50 min
Blood	1.23 ± 0.15	0.17 ± 0.04	0.21 ± 0.02	0.25 ± 0.04	0.28 ± 0.03	0.29 ± 0.04	0.33 ± 0.04	0.36 ± 0.07	0.38 ± 0.06
Normal	0.77 ± 0.12	0.26 ± 0.04	0.33 ± 0.05	0.35 ± 0.06	0.39 ± 0.04	0.36 ± 0.04	0.40 ± 0.05	0.43 ± 0.08	0.43 ± 0.06
Trans	0.73 ± 0.18	0.22 ± 0.05	0.23 ± 0.03	0.24 ± 0.03	0.28 ± 0.02	0.26 ± 0.04	0.30 ± 0.05	0.29 ± 0.04	0.32 ± 0.05

measurement. Cardiovascular magnetic resonance is suitable for this purpose.

Purpose: Angiotensin-converting-enzyme (ACE) activity influences human LV hypertrophy and the deletion ('D'), rather than the insertion ('I') polymorphic variant of the ACE gene is associated with both greater LV ACE activity and growth response. This effect might be mediated through the increased synthesis of the growth factor angiotensin II and/or degradation of growth-inhibitory kinins. The absence (−) rather than the presence (+) of a 9 base-pair deletion in the bradykinin-2 receptor gene (B2BKR) is associated with higher receptor mRNA expression. If ACE does regulate cardiac growth through kinin modulation, then LV growth to a prospective environmental stimulus should be influenced by both ACE and B2BKR genotypes. We have explored this hypothesis.

Methods: Caucasian male military recruits were selected for ACE I/D homozygosity and the LV growth response to a 10-week physical training programme was determined using cardiac magnetic resonance imaging. 141 recruits (79 DD, 62 II) completed training, for whom DNA stock was available in 109 and B2BKR genotype was determined in these. Data were compared between genotype groups using unpaired t-tests, and across genotypes using linear trend analysis. In addition, further evidence of biological interaction between genotypes sought by separate analysis of BK2 influence on LV growth amongst each ACE genotype.

Results: LV growth amongst recruits was ACE genotype dependent (II vs. DD +4.3g vs. +11.6g, from the original cohort, $p = 0.002$: and 6.9g vs. 11.2g, $p = 0.09$ amongst the smaller sample reported here). B2BKR genotype was also strongly associated with LV growth response (a gain of 4.6g vs. 8.3g vs. 13.7g for the 16, 60 and 33 individuals of −9/−9, −9/+9 and +9/+9 genotypes respectively: $p < 0.01$ for linear trend). ACE and B2BKR genotypes interacted additively, with growth being greatest amongst those of DD/+9+9 genotype (lowest kinin and BK receptor activity), and least amongst those of II/−9−9 genotype (highest kinin and BK receptors levels): 15.7g vs. −1.4g respectively: $p = 0.009$ for comparison of homozygotes, $p = 0.003$ for trend across all genotypes). Percentage growth responses differed by a factor of 25, being −0.4% vs. 9.5% respectively: $p = 0.001$ (see figure). Evidence of biological interaction is further provided when the influence of B2BKR is examined separately amongst those of II and DD genotype. Amongst those of II genotype, LV growth rises by −1.4g, 6.2g and 11.5g for those of BK2BR −9/−9, −9/+9 and +9/+9 genotype respectively ($p = 0.02$). However, such a gradient is far less clear (9.3g, 9.6g and 15.7g) amongst those of DD genotype, and fails to reach statistical significance ($p = 0.18$). Even when only those taking placebo are studied, B2BKR genotype-associated differences in LV growth persist (1.3g vs. 8.7g vs. 13.8g for −9/−9 vs. −9/+9 vs. +9/+9 genotypes: p for linear trend = 0.03).

Conclusion: Our data demonstrate a role for both the ACE and B2KBR genotypes in determining the human LV growth response, and suggest that alterations in kinin levels (marked by the ACE genotype) and kinin receptor transcription (marked by BK2BR genotype) interact biologically in an additive way. These data thus support a role for bradykinin in the regulation of human LV growth, and suggest that—at least in part—the effects of ACE may be mediated through alterations in kinin levels. Nonetheless, care must be taken in the extrapolation of these findings to the genesis of pathological hypertrophy, in which the magnitude of the role of kinins may differ.

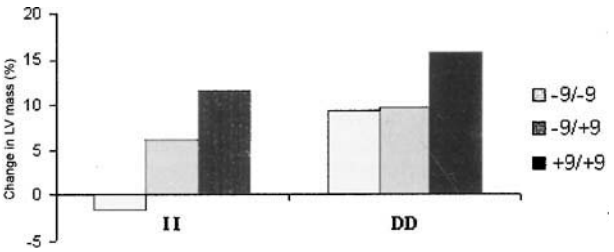

Figure 1. Percentage change in LV mass over a 10-week training period, amongst those of ACE 'II' and 'DD' genotype. Subjects are subdivided by genotype for the BDKRB2 gene.

This study demonstrates the usefulness of CMR in elucidating these modest differences in gene–environment interactions. The data may have implications for the treatment of those patients with pathological LVH. In particular, they suggest potential roles for new combined neutral endopeptidase/ACE inhibitors in the manipulation of LV mass.

116. The Effects of Blood Pressure and Anaemia on Functional Abnormalities in the Uraemic Heart, Measured Using Cardiovascular Magnetic Resonance Imaging

Nicola Johnston,[1] Alan Jardine,[1] Graham Stewart,[1] Henry Dargie.[1] [1]*University of Glasgow, Clinical Research Initiative, Glasgow, Scotland, United Kingdom*

Introduction: Premature cardiovascular disease (CVD)is the principal cause of morbidity and mortality in patients with chronic renal failure (CRF)including those who have undergone successful renal transplantation.Compared to the general population, the age and sex adjusted mortality rate for CVD is 10–20 fold greater in patients with CRF and over 40% of deaths in this population are attributed to cardiovascular causes. Left ventricular (LV) abnormalities such as left ventricular hypertrophy (LVH) and left ventricular systolic dysfunction (LVSD), collectively known as uraemic cardiomyopathy, are strong independent risk factors of cardiovascular outcome in these patients and are common findings in patients on haemodialysis (HD) programmes with around 80% patients with echocardiographic evidence of LVH and 37% with evidence of LVSD. Given the prognostic importance of LVH and LV dysfunction in this population it is essential to find an accurate, reproducible method of measurement of these abnormalities, to define targets for treatment and to power interventional trials. Hypertension has been shown to be the strongest determinent of LV abnomalities in this population with anaemia also a factor. Studies have shown that echocardiography is inaccurate in the measurement of LV mass and function in patients with abnormal LV geometry. There are no studies using cardiovascular magnetic resonance (CMR) in renal patients.

Purpose: The aim of this study was to assess the use of CMR as the method of measurement of LV abnormalities in patients

with end stage renal failure and to clarify the determinants of blood pressure (BP) and effect of anaemia using this method.

Methods: Fifty haemodialysis patients and ten controls were recruited. CMR and echocardiography were performed on the morning following dialysis less than three hours apart.CMR was performed on a Siemens Impact Expert (Siemens UK) operating at 1 Telsa with ECG triggering. Long-axis, pilot scans were obtained through the apex of the left ventricle, aligning it with the centre of the mitral valve and then 8 mm short-axis images were obtained using a breath-hold fast low angle shot (FLASH) cine sequence to acquire approximately six images per slice at different phases of the cardiac cycle. The images were analysed by a single trained observer (MC), who manually traced LV area at each slice in end systole and end diastole. The area multiplied by the depth of each slice gave myocardial volume and chamber volume; LV mass was calculated by multiplying myocardial volume by myocardial density (1.05). A proportion of the CMR scans were examined by a second observer to calculate inter-observer variability. All patients underwent ambulatory blood pressure monitoring in the twenty-four hours following CMR as well as resting BP and phlebotomy for haemoglobin. Cardiac output (CO) was calculated by multiplying stroke volume (SV) by the heart rate. SV was calculated by subtracting end-diastolic volume (EDV) from end-systolic volume (ESV). Systemic vascular resistance (SVR) was estimated from the CO and mean arterial pressure (MAP) immediately prior to the procedure.

Results: 56 patients completed the study. Four were unable to tolerate CMR secondary to claustrophibia. The results in the control group using CMR as the method of measurement and the inter-observer variabliity corresponded well with published normal ranges for CMR values. LVMI ($p < 0.001$), ESV ($p < 0.001$), SVR ($p = 0.050$) and heart rate ($p = 0.032$) were all significantly higher in the dialysis group compared to controls. LV ejection fraction ($p = 0.001$) and SV ($p = 0.038$) were significantly lower compared to controls. Comparing CMR to echocardiography 24.5% of renal patients had an ejection fraction below the normal range compared to 45.2% using echocardiography. 43.5% patients had LVH measured using CMR compared to 68.1% using echocardiography. BP correlated significantly with CO ($p = 0.001$ $r = 0.512$) and EDV ($p < 0.001$ $r = 0.565$) in the dialysis group but there was no correlation between BP and SVR ($p = 0.158$ $r = 0.201$). Haemoglobin was found to have a negative correlation with both CO ($p = 0.002$ $r = -0.460$) and EDV ($p = 0.014$ $r = -0.375$) and a positive correlation with SVR ($p = 0.035$ $r = 0.352$) in the dialysis group. No correlation was found between haemoglobin and BP ($p = 0.279$ $r = 0.158$).

Conclusion: The dialysis patients had a significantly higher LVMI and lower LVEF than the control group measured using CMR. 24.5% of renal patients had LVSD and 43.5% had LVH. The corresponding values measured using echocardiography significantly over-estimated the proportion of renal patients with LVH and LVSD. This result supports the finding of previous studies that when the LV is abnormal in shape or size, echo becomes inaccurate.

The relationship of BP (and LVMI) with CO and EDV and not SVR, supports the theory that in this population, the major determinant of BP is intravascular volume on which CO depends. It would follow that better control of intravascular volume during dialysis programmes would significantly improve BP control. Anaemia also increases intravascular volume in this population and reversal of anaemia may further improve the control of BP in this population.

CMR has the potential in patients with CRF to redefine uraemic cardiomyopathy and identify future targets for intervention, thereby improving cardiovascular outcome in these patients.

117. MRI Tagging Demonstrates Non-uniform Intramural Changes of Regional Systolic Twist and Shortening after Myocardial Infarction in Rats

Wei Liu, Junjie Chen, Stacy Allen, Mark Mclean, Samuel Wickline, Xin Yu. *Cardiovascular MR Laboratories, Washington University in St. Louis, Box 8086 660S. Euclid Ave, St. Louis, MO, USA*

Introduction: Although rodent models have assumed a prominent role in elucidating molecular and cellular mechanisms associated with post-infarct remodeling, few studies have addressed the regional heterogeneity of myocardial function after myocardial infarction. While MRI tagging provides a valuable tool for noninvasive assessment of regional myocardial wall motion and kinematics, its application on small animals has been limited due to the requirements for high-resolution tagging. To date, most of the cardiac tagging studies were performed on either human subjects or large animals such as dogs and pigs.

Purpose: The purpose of this study was to quantify regional transmural alterations in ventricular twist and shortening in remodeled rat hearts with the use of high-resolution MRI tagging.

Methods: MRI tagging was performed on 20-month old Fischer 344 rats 4 weeks after infarction. Infarction was created by ligation of the left coranary artery descending branch ($n = 4$). Sham operated rats of the same age were used as control group. MR imaging was performed on a Varian 4.7T scanner with a birdcage RF coil. The rats were sedated with 1% isofluorine by a nose cone. Tagged images of three short-axis slices were acquired at basal, midventricular, and apical levels. Imaging sequence was a SPAMM1331 sequence, applied immediately after ECG trigger in two perpendicular directions, followed by gradient-echo cine sequence. Imaging parameters were: TR/TE,14.7 ms/3 ms; field-of-view, 6.5 cm × 6.5 cm; matrix size, 256 × 256; tagging resolution, 0.9 mm; slice thickness 1.5 mm. A total of 15 frames

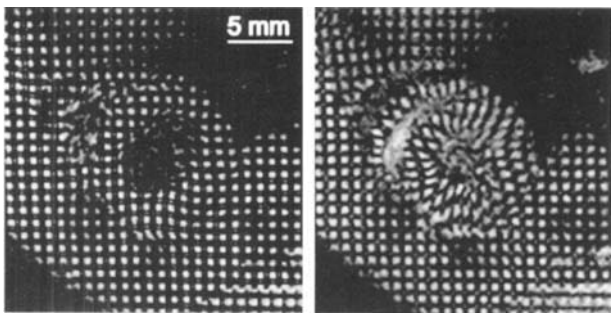

Figure 1. Tagged short-axis images at diastole and systole.

Table 1

*Anterior Twist (Degrees, * $p < 0.05$ compared to control)*

	Subepi Infarct	Control	Subendo Infarct	Control
Base	2.8 ± 1.1	4.9 ± 2.3	4.7 ± 1.4	8.2 ± 4.8
Mid	2.5 ± 1.1*	7.1 ± 1.7	3.3 ± 0.6*	9.0 ± 2.3
Apex	2.6 ± 0.3*	9.0 ± 1.0	4.2 ± 1.9*	9.9 ± 2.7

Table 2

*Septum Shortening (mm, * $p < 0.05$ compared to control)*

	Subepi Infarct	Control	Subendo Infarct	Control
Base	0 ± 0.20*	−0.5 ± 0.13	0.1 ± 0.20*	−0.4 ± 0.08
Mid	0.3 ± 0.06*	0.04 ± 0.04	0.5 ± 0.04*	0.2 ± 0.1
Apex	0.6 ± 0.09*	0.3 ± 0.02	0.7 ± 0.05*	0.4 ± 0.02

were acquired during one cardiac cycle. Following MRI studies, hearts were excised for histological analysis.

Images were analyzed with MATLAB based softwares developed in our laboratory. Epicardial and endocardial boders, intersecting tag points were traced interactively. Ventricular twist and radial shortening were computed relative to the center of ventricular cavity using 2D homogenous finite element analysis. Positive twist value indicated clockwise twist viewed from base. Positive radial shortening indicated inward motion. The left ventricle was segmented into anterior, lateral, inferior, and spetal regions. Subendocardial and subepicardial twist and shortening in these four regions were thus calculated.

Results: Shown in Figure 1 are examples of tagged images of a rat heart. In infarct group, transmural infarction was present in anterolateral region at apical to midventricular level from histological analysis. As a result, anterior region underwent the greatest reduction in twist (58 ~ 71%, Table 1) while lateral region demonstrated significant loss in radial shortening (44 ~ 86%, Figure 2). Contrary to the loss of twist and shortening in anterior and lateral regions, septum shortening increased significantly in infarct group at apical and midventricular levels (Table 2). At base, septum manifested a reversal of wall motion from lengthening to shortening. In addition, there was also a trend of increased septal twist.

Conclusion: Increased septal shortening and twist were observed in rats 4 weeks after infarction, possibly to compensate for the loss of shortening and twist in anterolateral regions where infarction occured. These data illustrate for the first time the regional and transmural changes of myocardial

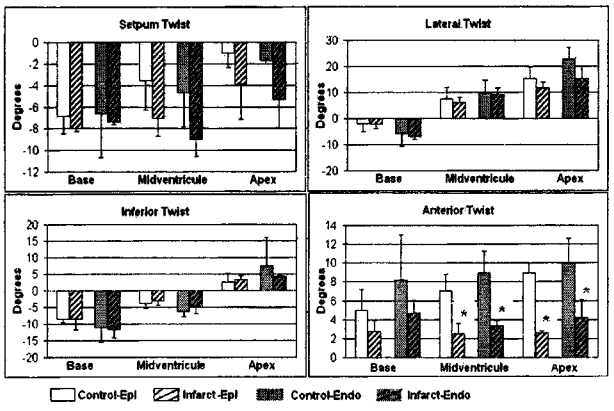

Figure 2. Net twist of infarct rat vs control (* $p < 0.05$).

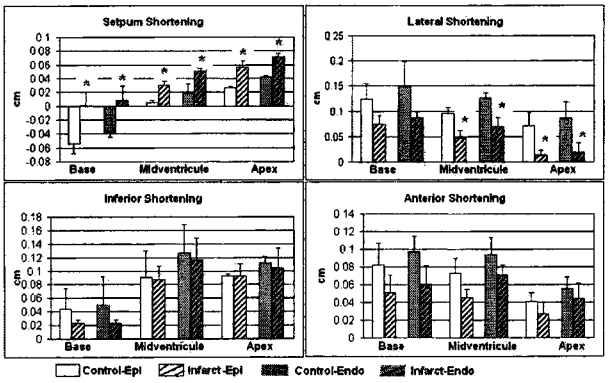

Figure 3. Net shortening of infarct rat vs control (*$p < 0.05$).

twist and shortening as a consequence of remodeling after infarction in rodents. Future work will include structural and molecular analysis in conjunction with MRI tagging to elucidate the mechanism of mechanical compensation.

118. Cardiac MRI Provides Evidence that Inflammatory Activation Contributes to Contractile Dysfunction in the Remote, Non-infarcted Left Ventricle Early After Myocardial Infarction

Zequan Yang, Frederick H. Epstein, Stuart S. Berr, Wesley D. Gilson, Joel Linden, Brent A. French. [1]*University of Virginia, Departments of Biomedical Engineering, Radiology and Medicine, Charlottesville, Virginia, United States*

Introduction: Contractile dysfunction in the remote, non-infarcted left ventricle (LV) contributes to early mortality after large, anterior myocardial infarction (MI). Recent work in the field of cardiac MR supports the long-standing contention that contractile dysfunction in the remote zone early after MI is due to the increased systolic longitudinal wall stress brought on by infarct expansion, which might occur without a loss of intrinsic contractility in the remote regions (1). However, pro-inflammatory genes are known to become activated after MI (2) and pharmacologic data suggests that inflammatory activation may indeed contribute to remote zone dysfunction early after MI (3).

Purpose: The purpose of this study was to assess the potential role of inflammatory activation in remote zone dysfunction using a potent and highly-selective agonist of the A2A adenosine receptor (ATL146e, Adenosine Therapeutics, Charlottesville, VA). This compound exhibits a broad spectrum of anti-inflammatory properties (4). The possibility that inflammatory activation may contribute to contractile dysfunction early after MI was explored by using cardiac MRI to examine the effects of this potent A2A adenosine receptor agonist on contractile function in the remote LV one day post-MI.

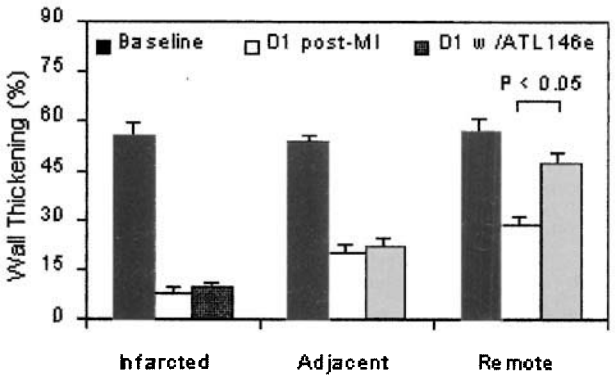

Figure 1. A potent anti-inflammatory agent restores contractile function in the remote LV on Day 1 post-MI. Baseline wall thickening was determined by cardiac MRI 3 d before MI. A 1 hr coronary occulusion was imposed on Day 0, and vehicle or ATL146e was injected IP at 1, 4 and 8 hr after reperfusion. Compared with vehicle control, ATL146e improved reginal LV wall thickening (W Th) by 65% in the remote LV on Day 1 post-MI. But not in the infarcted or adiacentzones.

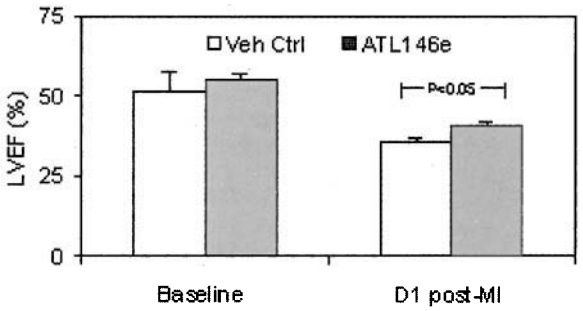

Figure 2. A potent anti-inflammatory agent improves global LV function on Day 1 post-MI. Baseline left ventricular ejection fraction (LVEF) was determined by cardiac MR1 3 d before MI. A 1 hr coronary occulsion was imposed on Day 0, and vehicle or ATL146e was injected IP at 1, 4 and 8 hr after reperfusion. The results indicate that the improvement in remote zone function attributable to ATL146e was adequate to yield a small but significant increase in LVEF ($P < 0.05$).

Methods: ECG-triggered, cardiac MRI was performed using a birdcage quadrature coil (RF Design Consulting, Newberry, FL) on a Varian INOVA 4.7T scanner equipped with Magnex gradients. Ten C57BL/6 mice were imaged at baseline before MI, then again 24 hr after a reperfused, 1 hr occlusion of the left anterior descending coronary artery. In 5 of these mice, 3 low-dose injections of ATL146e (each 2.4 μg/kg, IP) were made 1, 4 and 8 hr after MI. Injection of ATL146e at this very low dose did not significantly effect either blood pressure or heart rate. One day post-MI, Gd–DTPA was infused and hearts were imaged in 1 mm-thick, short-axis slices after a 20 min delay. Cine FLASH imaging used a TE of 3.9 ms and a flip angle of 60° to increase T1 weighting for infarct size determination (6). During each imaging session, the entire LV was assessed using 7 to 8 contiguous short-axis slices. The images from each session were scaled and converted to the appropriate format for image analysis using ARGUS (Siemens Medical Systems) to yield left ventricular end-systolic volume (LVESV), end-diastolic volume (LVEDV) and ejection fraction (LVEF). ARGUS was also used to determine wall thickening (WTh) in 2 adjacent, mid-ventricular, short-axis slices from each heart using 8 sectors/slice. Sectors within Gd-enhanced regions were defined as Infarct, sectors bordering Infarct sectors were defined as Adjacent and the remaining sectors were defined as Remote.

Results: As shown in Fig. 1, mean WTh ± SEM for all slices at baseline was 56 ± 3%. One day post-MI, WTh in the remote zones of mice treated with ATL146e (47 ± 4%) was markedly improved over control (28 ± 3%, $P < 0.05$). While there was no difference in infarct size between groups, Fig. 2 shows that mice treated with ATL146e had significantly improved LVEF (41 ± 1%, mean ± SEM) in comparison with control mice (36 ± 2%, $P < 0.05$).

Conclusion: Remote zone LV function and LVEF 24 hr after large MI can be significantly improved by a potent anti-inflammatory agent (ATL146e), indicating that inflammatory activation plays an important role in remote zone LV dysfunction early after MI. The concept that inflammatory activation may contribute to remote zone LV dysfunction early after MI is important because this problem is amenable to pharmacologic intervention, whereas treatment options would be severely limited if the mechanisms underlying remote zone LV dysfunction were purely mechanical in nature.

119. Contrast Washout by MRI Identifies Stunned Myocardium in Patients After Reperfused Myocardial Infarction

C. Joon Choi,[1] Shahriar Haji-Momenian,[1] Joseph Dimaria,[1] John Christopher,[1] Jennifer Hunter,[1] Christina Bove,[1] Frederick Epstein,[1] Christopher Kramer.[1] [1]*University of Virginia, Cardiovascular Division and Department of Radiology, Charlottesville, Virginia, United States*

Introduction: In patients after reperfused myocardial infarction (MI), the extent of hyperenhancement (HE) on delayed post-contrast MRI relates to infarct size. The transmurality of HE correlates inversely to functional recovery and may have better prognostic value than ejection fraction (EF) (1). Due to contrast washout kinetics, the timing of delayed imaging after contrast infusion may be important in the assessment of infarct size and transmurality. A recent study in a rat MI model demonstrated that imaging prior to 15 minutes after contrast caused overestimatation of infarct size (2).

Purpose: We hypothesized that the size of the HE region in humans post-MI may change over time after contrast infusion. This timing parameter may be important for predicting myocardial functional recovery.

Methods: Imaging

Eighteen patients (14 male, mean age ± S.D. 53 ± 8) were studied on day 4 ± 2 (Wk1) and week 8 ± 1 (Wk8) after reperfused first MI defined by troponin and/or CK-MB elevation, typical chest pain >30 mins., and ECG changes. The patients were imaged on a Siemens Vision 1.5 T magnet using a phased-array surface coil. Seven patients had anterior and 8 inferior ST elevation and 3 had a non-ST elevation MI. Nine patients received primary stenting, 6 thrombolytics, 2 of whom required rescue stenting, and 3 reperfused spontaneously and received delayed stenting. Average peak CPK was 1628 ± 1470 U/L and troponin-I 42 ± 32 μg/L. Breath-hold short axis gradient echo cine imaging (TR, 100 ms with view sharing, 50 ms temporal resolution; TE, 4.8 ms; flip angle, 20°; slice thickness, 7 mm; FOV 30 cm; matrix, 126 × 256, 15 heartbeats) was performed from apex to base. Breath-hold tagged gradient echo cine imaging (TR, 90 ms with view sharing; 45 ms temporal resolution; TE, 4 ms; 8 mm tag line separations; 128 × 256 matrix interpolated to 256 × 256; FOV 30 cm) was performed in 3 short-axis slices 10 mm apart within the region of maximal dysfunction seen on cine imaging. After 0.1 mmol/kg Gd-DTPA infusion, a breath-hold segmented inversion recovery TurboFLASH sequence was performed in the same 3 slices used for tagged images beginning at 3–4 minutes post-contrast and every 2 minutes up to 20 minutes post-contrast (TR 1400 ms, TE 3.4 ms, inversion time 175–250 ms adjusted for optimal myocardial nulling, delay time 300 ms, FOV 300 mm, matrix 165 × 256). At Wk8, the same MR techniques were repeated in the same 3 slices matched by location. An additional 7 patients with persistent hypoenhancement at Wk1 were excluded from analysis.

Data Analysis

Signal intensity (SI) was measured in regions of interest from visually HE regions and remote (RM) regions by an observer using ImageJ for PC software (NIH). HE regions, defined as SI >200% of RM at minute 3–4, were planimetered from each slice at each time point during Wk 1 imaging. Regions of contrast washout (WO) were defined as those that normalized SI by 20 minutes post-contrast and identified as subendocardial or subepicardial. Percent circumferential intramyocardial shortening (%S) from tagged images was measured by a 2nd observer using the VIDA software package (©,, Univ. of Iowa) in subendocardial and subepicardial segments within HE (n = 74), WO (n = 43), and RM (n = 64) and compared by region and time using ANOVA with subtesting. End-diastolic and end-systolic volumes (EDV,ESV) and EF at Wk 1 and Wk 8 were measured from cine images using Argus (Siemens, Princeton, NJ).

Results: The area of HE at Wk1 declined over time (see Table 1, ANOVA $p < 0.001$) and was lower than the area at 3–4 minutes by 11–12 minutes post-contrast ($p < 0.05$). By 20 minutes post-contrast, the area of HE was 50% of the area at 3–4 minutes ($p < 0.001$) (Table 1 and Fig. 1). However, SI in the center of hyperenhanced regions relative to remote did not change over the 20 minutes after contrast infusion (243 ± 58% at min 3–4 to 228 ± 42% at min 19–20, p = NS). Ten of the 18 patients demonstrated WO. 43 segments (4.3 ± 3.4 segments per patient, 22 subendocardial and 21 subepicardial) demonstrated WO. Changes in regional %S over time are shown in Table 2. The improvement in %S from week 1 to week 8 was greater in WO than HE segments (10.7 ± 8.2% vs. 6.8 ± 7.0%, $p < 0.04$). In the 18 patients, EDV increased from 96.7 ± 19.2 ml at Wk1 to 107.1 ± 21.0 ml at Wk8, p = 0.01, without a change in ESV. EF improved from 60.6 ± 6.5% to 65.4 ± 5.5%, p = 0.002.

Table 1

Time Course of HE Area at Wk 1 After Gd-DTPA Infusion

	Area (%)	p Value vs. min 3–4
Min. 3–4	100 ± 0	NS
Min. 5–6	93.6 ± 8.5	NS
Min. 7–8	82.4 ± 13.2	NS
Min. 9–10	75.9 ± 11.7	NS
Min. 11–12	71.9 ± 19.3	0.045
Min. 13–14	71.1 ± 40.3	0.034
Min. 15–16	55.6 ± 15.2	<0.001
Min. 17–18	58.7 ± 22.9	<0.001
Min. 19–20	50.3 ± 16.7	<0.001

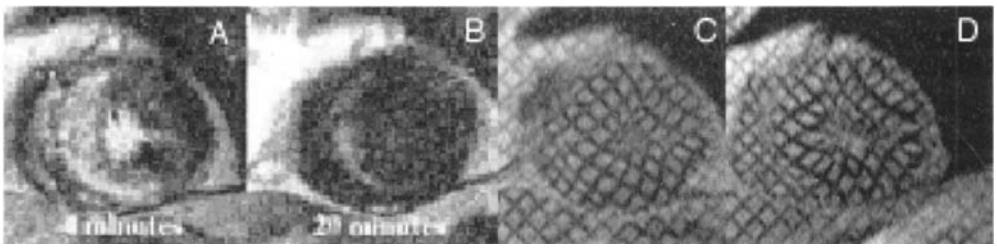

Figure 1. The area of HE decreases from min. 4 (A) to min. 20 (B) post-contrast at Wk1. Markedly decreased septal motion represented by lack of tag deformation at Wk1 (C) improved significantly by Wk8 (D).

Table 2

Changes in %S Between Wk1 and Wk8 in HE, WO, and RM

	HE (n = 74)	WO (n = 43)	RM (n = 64)	ANOVA p
Wk1 (%)	6.6 ± 7.5	7.0 ± 10.3	19.9 ± 6.9*†	<0.001
Wk8 (%)	13.8 ± 9.4	17.7 ± 11.6*	22.5 ± 7.6*†	<0.001
P	<0.001	<0.001	0.04	
	*p < 0.03 vs HE	†p < 0.03 vs WO		

Conclusion: In patients with first reperfused MI, as much as half of the area of contrast hyperenhancement washes out between minute 3 and minute 20 after Gd infusion. There is global improvement in intramyocardial function between week 1 and week 8 post-MI. However, both endocardial and epicardial segments with contrast washout by 20 minutes demonstrate greater contractile function at Wk 8 and greater functional recovery between Wk 1 and 8 than those with persistent hyperenhancement. Thus, the timing of imaging is critical to the assessment of the extent of hyperenhancement and extent of recovery of intramural contractile function.

120. Contrast-Enhanced MRI and Positron Emission Tomography Yield Similar Results for the Assessment of Myocardial Viability in Patients with Chronic Ischemic Heart Disease

Harald P. Kühl,[1] Aernout M. Beek,[1] Arno P. Van Der Weerdt,[1] Frans C. Visser,[1] Albert C. Van Rossum.[1] [1]*Vu University Medical Center, De Boelelaan 1117, Amsterdam, The Netherlands*

Introduction: Contrast-enhanced (CE) MRI has been shown to predict recovery of function after revascularization in patients with chronic coronary artery disease. However, the value of the technique in comparison to the in-vivo standard for viability assessment, Positron emission tomograhy (PET), is unknown.

Purpose: We compared CE-MRI to PET and Tetrofosmin-SPECT (SPECT) in 23 patients with ischemic heart disease and left ventricular dysfunction referred for myocardial viability assessment.

Methods: For CE-MRI an inversion-recovery gradient-echo sequence (TE/TR 4.4/9.6 ms, FA 25°, typical TI 250–300 ms, resolution 1.6 × 1.3 × 5 mm) was used on a 1.5 T MR scanner (Sonata, Siemens, Erlangen, Germany) 20 minutes after 0.2 mmol/kg Gadolinium-DTPA. Data acquisition was performed in short-axis views covering the whole left ventricle and in selected long-axis views. PET was performed under hyperinsulinemic euglycemic clamp using 18-Fluorodeoxyglucose (ECAT EXACT HR + , Siemens, CTI). Resting perfusion was assessed using SPECT. For data analysis we used a 17-segment model including 6 basal, 6 midventricular, 4 distal segments and the apex. Analysis of PET and SPECT data was done by visual interpretation using a four point score with a score of 1 indicating normal perfusion/metabolism and a score of 4 indicating severly reduced perfusion/metabolism or scar. According to PET/SPECT findings segments were categorized as either viable or non-viable. Viable segments were further cathegorized as either normal or hybernating (flow-perfusion mismatch). In corresponding segments the percentage regional and transmural extent of hyperenhancement at CE-MRI was calculated.

Results: Mean ejection fraction was 31 ± 11%. A total of 391 segments were analyzed with both techniques. Viable segments by PET/SPECT showed significantly less regional and transmural hyperenhancement compared to non-viable segments (5.2 ± 10.9% and 7.6 ± 13.2% vs. 66.2 ± 28.4% and 71.1 ± 28.4%; $p < 0.001$). Moreover, the extent of hyperenhancement was significantly related to PET score ($r = 0.74$; $p < 0.001$). By ROC analysis the area under the curve was 0.94. Using a cutoff value of 33% the sensitivity, specificity and accuracy for identification of myocardial viability was 96%, 90% and 95%, respectively, with excellent

agreement (Kappa value >0.8). 90% of segments (25/28) with a flow-perfusion mismatch were also identified as viable by CE-MRI. In the 3 "false negative" segments by CE-MRI the regional extent of hypertenhacement was close to the cutoff value of 33% (range 35 to 41%).

Conclusion: CE-MRI yield similar results compared to PET as reference standard for the assessment of myocardial viability.

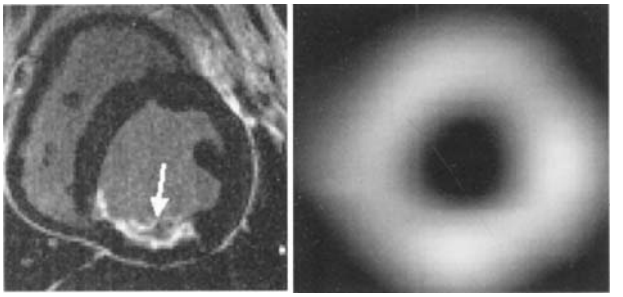

Figure 1.

121. MRI Detects Subendocardial Infarcts Which Are Missed by Spect

Anja Wagner,[1] Heiko Mahrholdt,[1] Thomas Holly,[2] Michael Elliot,[2] Kelly Choi,[1] Raymond Kim,[1] Robert Judd.[1] [1]*Duke Cardiovascular Magnetic Resonance Center, P.O. Box 3934, Durham, NC, USA;* [2]*Northwestern University, 12-723 Tarry Building, Chicago, IL, USA*

Introduction: Patients with subendocardial myocardial infarction (MI) are at increased risk for future infarction in the same territory.

Purpose: We hypothesized that SPECT will miss subendocardial MI's which could be assessed by contrast-enhanced MRI (ce MRI).

Methods: We studied 15 dogs and 32 patients. In dogs, ce MRI and 99 m Tc-sestamibi SPECT were performed 2 days after a 90 min coronary artery occlusion, followed by comparison to histology (TTC). In patients, ce MRI and a standard clinical SPECT stress/rest protocol were performed within 1 month. Animal data were analyzed quantitatively using a 30 segment model and patient data were read by experienced clinicians in a 14 segment model. With infarct size defined by TTC (dogs), both MRI and SPECT detected large infarcts but for subendocardial infarcts (Figure 1 above) MRI was three times more sensitive (Table 1 below). In patients, only 45% of subendocardial infarcts defined by MRI were detected by SPECT (Table 1).

Results: With infarct size defined by TTC (dogs), both MRI and SPECT detected large infarcts but for subendocardial infarcts (Figure) MRI was three times more sensitive (Table 1). In patients, only 45% of subendocardial infarcts defined by MRI were detected by SPECT (Table 1).

Conclusion: Ce MRI can be used to identify clinically-important subendocardial infarcts which are missed by routine clinical stress/rest SPECT protocols.

122. Late Recanalization of Infarct Related Artery Improves Circumferential Shortening of Infarct Related Left Ventricular Segment at 6 Months Follow-up

Carlos Rochitte,[1] João Silva,[1] Luiz Ávila,[1] José Parga,[1] Rosa Piva,[1] Claudio Castro,[1] Roberto Kalil Filho,[1] Giovanni Cerri,[1] José Nicolau,[1] José Ramires.[1] [1]*Heart Institute (InCor)-University of São Paulo Medical School, Rua Oscar Freire 1504, São Paulo, Brazil*

Introduction: Clinical benefits of infarct related artery recanalization later than 12 hours from symptoms onset after acute myocardial infarction (MI) still remain unclear.

Purpose: To test the open-artery hypothesis, we investigated whether late recanalization of infarct related artery would improve regional function over a period of 6 months

Methods: We studied 12 patients with anterior myocardial infarction with symptoms onset between 12 hours and 14 days prior to the enrollment, and with left anterior descending artery (LAD) occluded (TIMI 0 or 1) on the coronary angiography. Additionally, they needed to have no evidence of myocardial ischemia or significant viability on the left ventricle (LV) anterior wall by myocardial scintigraphy. They were randomized to either LAD recanalization by angioplasty (OPEN-6 pts) or no intervention (CLOSED-6 pts). Myocardial tissue tagging and delayed-enhanced MRI were performed at enrollment and 6 months later. We measured infarct size(IS), LV end diastolic(EDV)and systolic volumes(ESV),ejection fraction(EF), LV mass and myocardial circumferential shortening (%S) at midwall of infarcted related LV segment (ANTERIOR), adjacent and remote regions at enrollment and at follow-up cardiac MRI study.

Table 1

	Dogs	Dogs	Patients
Sensitivity	MRI vs TTC	SPECT vs TTC	SPECT vs MRI
Large MI (>75%tme)	100%	100%	100%
Medium MI (25–75% tme)	100%	57%	61%
Small MI (<25% tme)	88%	21%	45%
Specificity	98%	97%	81%

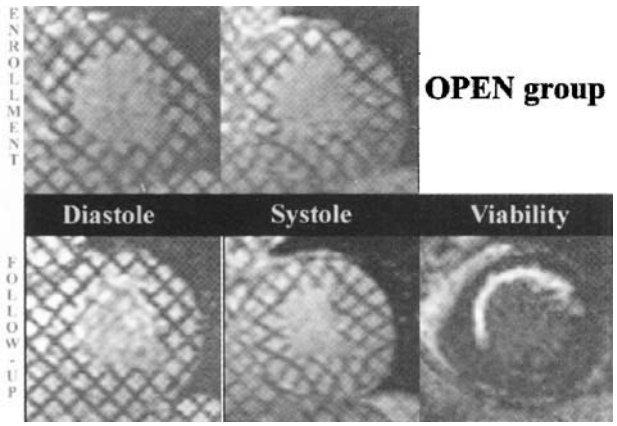

Figure 1. OPEN group: myocardial tagging and viability at enrollmnet and 6 month follow-up.

Results: Mean changes from enrollment to follow-up MRI studies in OPEN vs.CLOSED were: + 6.3 ± 14% vs. −14.9 ± 4.9% for IS, −2.1 ± 10.1% vs. −10.1 ± 13.1% for EDV, −19.7 ± 8.3% vs. −11.5 ± 13.9% for ESV, + 9.0 ± 4.2% vs. + 1.6 ± 4.8 for EF, −13.5 ± 9.7% vs. −16.6 ± 7.7% for LV Mass, respectively(p NS for all).

The magnitude of circumferential shortening (%S) at enrollment and follow-up in ANTERIOR were +2.4 ± 2.1% and −12.2 ± 2.1% ($p < 0.001$) in OPEN.

In CLOSED there was no significant changes on %S, that changes from +1.8 ± 1.6% at enrollment to +1.2 ± 1.3% at 6 month follow-up(p NS).

At follow-up OPEN had significantly better %S than CLOSED (−12.2 ± 2.1% vs. + 1.2 ± 1.3%, $p < 0.001$). Adjacent regions %S did not change significantly in OPEN (−22.6 ± 4.8% to −29.7 ± 3.5%, p NS), and improved significantly in CLOSED (−18.1 ± 2.8% to −31.8 ± 2.8%, $p < 0.01$). %S of remote regions did not change from baseline to follow-up in both OPEN and CLOSED groups(−31.4 ± 3.9% to −41.6 ± 4.2% and −38.3 ± 3.4% to −47.9 ± 4.1%, p NS, respectively).

Conclusion: We demonstrated that late recanalization of infarct related artery significantly improves the infarcted related LV segment circumferential shortening 6 months later. These findings support the open-artery hypothesis and may significantly impact clinical prognosis.

123. High-Dose Dobutamine Stress MRI for Follow-up After Coronary Revascularization Procedures in Patients with Wall Motion Abnormalities at Rest

Andreas Wahl,[1] Stefan Roethemeyer,[1] Ingo Paetsch,[1] Sonja Huehns,[1] Eckart Fleck,[1] Eike Nagel.[1] [1]*German Heart Institute Berlin, Augustenburger Platz 1, Berlin, Germany*

Introduction: In patients with known coronary artery disease (CAD) and prior coronary revascularization procedures, the diagnostic accuracy of noninvasive modalities is limited. This is most likely due to their complex coronary circulation with bypass grafts, coronary collaterals and diffuse minor vessel abnormalities, as well as to the high incidence of wall motion abnormalities at rest. While conventional intermediate- and fast high-dose dobutamine stress MRI (DSMR) have been shown feasible in patients with suspected or known CAD, patients with prior myocardial infarction or wall motion abnormalities at rest have been excluded from most previous studies.

Purpose: To determine the value of high-dose DSMR for diagnosis of ischemia in patients with known CAD, prior coronary revascularization procedures, and wall motion abnormalities at rest.

Methods: 160 consecutive patients (mean age 59 ± 8 years; prior myocardial infarction: 63%) with fully or partially revascularized CAD (prior PTCA: 90%; CABG: 28%) and wall motion abnormalities at rest, as determined by MRI, underwent DSMR (1.5 T; ACS NT, Philips, Best, The Netherlands) prior to clinically indicated invasive coronary angiography. Patients were requested to withhold beta-blockers on the day of the stress examination. Other anti-anginal medications were not discontinued. DSMR images were acquired at rest and during a standardized high-dose dobutamine-atropine protocol during short breath-holds in 3 short-axis views (apical, midventricular and basal), a 4-chamber and a 2-chamber view. A single-slice turbo gradient echo technique (TE/TR/flip angle 5.6/1.9/20; spatial resolution $\leq 1.5 \times 2.5 \times 8$ mm; temporal resolution <25 ms) was used. Dobutamine was infused intravenously during 3 minute stages at doses of 10, 20, 30, and 40 ug.kg − 1 min − 1, until ≥85% of age-predicted heart rate was reached, or continued and supplemented by 0.25 mg fractions of atropine (maximal dose 1 mg) if 85% of age-predicted heart rate was not achieved and the stress test was still negative. Stress testing was discontinued when ≥85% of age-predicted heart rate was reached, on patient request, termination of the infusion protocol, or when new or worsening wall motion abnormalities, progressive or severe angina, dyspnea, decrease in systolic blood pressure >40 mmHg, arterial hypertension (>240/120 mmHg), severe arrhythmias, or other serious adverse effects occurred. All digital MR images were displayed as continuous synchronized cineloops using a multiple screen format (MASS software package, version 4.2, Medis, Leiden, The Netherlands) to compare corresponding rest, increasing stress and peak stress levels. Regional wall motion was assessed off-line by consensus between 2 blinded observers using a 16 segment model. Segmental wall motion was semi-quantitatively graded by a four-point scoring system (1: normal; 2: hypokinetic; 3: akinetic and 4:dyskinetic). DSMR was defined as positive for ischemia in the presence of a new or worsening wall motion abnormality in ≥1 segment. In the absence of ischemia, failure to attain 85% of age-predicted maximal heart rate was identified as a nondiagnostic result. For comparison with invasive coronary angiography (QCA), segmental wall motion was related to the corresponding presumed coronary artery territories.

Results: 195 significant coronary artery stenoses (≥50% diameter stenoses by QCA) were found in 119 patients (74%). High-dose DSMR was successfully performed with diagnostic image quality in all patients. Target heart rate was not reached in 9 examinations (6%). This was due to end of protocol in negative submaximal examinations in 4 patients (3%), and

limiting side effects in 5 patients (3%), including ventricular extrasystoly (n = 2), severe chest pain (n = 1), nausea (n = 1) and asymptomatic decrease in blood pressure (n = 1). Other major side effects included a case (0.6%) of sustained ventricular tachycardia with hemodynamic compromise requiring external defibrillation at peak dobutamine dose in a 60 years old patient with three-vessel disease and a left ventricular ejection fraction of 35%, 2 cases (1.3%) of non-sustained ventricular tachycardia (4 QRS complexes), as well as one case (0.6%) of atrial fibrillation with rapid ventricular rate. Thus, diagnostic DSMR was achieved in 94% of patients. One hundred six (66%) showed a new or worsening wall motion abnormality, while 45 (28%) did not. The overall sensitivity and specificity of DSMR for the diagnosis of significant CAD were 89% and 85%, respectively. Diagnostic accuracy was 88%, positive and negative predictive value 94% and 73%, respectively. Sub-group analyses for patients with prior myocardial infarction or CABG yielded similar results. The overall sensitivity for detecting significant CAD in patients with one (n = 64), two (n = 34) or three (n = 21) diseased vessels was 87%, 91% and 100%, respectively. The localization of segments with an abnormal response to DSMR showed a good correlation with the presumed vascular territories of the coronary arteries. The correct identification of the site of the stenosis was possible in 87% of myocardial territories supplied by a stenosed coronary artery. In addition, most patients (78%) in whom a stenosis was not correctly recognized were nevertheless identified as having significant CAD, either because they had multi-vessel disease, and dobutamine-induced wall-motion abnormality in another territory, or simply because the observed wall motion abnormality had been erroneously attributed to the wrong coronary territory. In patients with one-vessel disease, the diagnostic accuracy of DSMR ranged from 79% for LAD territory stenoses to 89% for RCA territory stenoses.

Conclusion: High-dose DSMR is reasonably safe and feasible in patients with known CAD, and can be used for the follow-up after coronary revascularization procedures. Diagnostic accuracy is similar to MR data reported for patients with suspected CAD, and compares favorably with other established noninvasive techniques.

124. MRI Predicts Remodeling in Patients with Acute Revascularized Myocardial Infarction

Ingo Paetsch,[1] Andreas Wahl, [2] Albrecht Gollesch,[1] Sabine Hettwer,[1] Eckart Fleck,[1] Eike Nagel.[2] [1]*German Heart Institute of Berlin (DHZB), Augustenburger Platz 1, Berlin Germany;* [2]*German Heart Institute Berlin, Augustenburger Platz 1, Berlin, Germany*

Introduction: Microvascular obstruction (MO) in acute myocardial infarction (MI) is associated with a higher rate of cardiovascular complications.

Purpose: To determine whether quantitatively assessed infarct volume and presence of MO determine infarct expansion and ventricular remodeling.

Methods: 20 patients with first acute MI (57 ± 8 years; CKmax 912 ± 682 U/l) underwent primary PTCA (n = 12), or lysis (n = 4) or initial conservative management (n = 4) followed by elective PTCA. In addition, all patients received maximal medical treatment as defined by guidelines, and underwent invasive coronary angiography at 3 months follow-up to ensure patency of infarct related artery. Cardiac MRI was performed at baseline (<5 d after MI) and follow-up (1.5 T MR tomograph, ACS NT, Philips, The Netherlands). The complete heart was imaged with multiple cine short-axis views (balancedFFE-sequence, (TE/TR/flip 1.9/4.0/60)). 15 min after administration of Gd-DTPA (0.02 mmol/kg) a 3-D, navigator corrected inversion-recovery sequence (5.3/3.2/15, slice thickness 5 mm, PP-delay 225–250 ms) covering the complete heart was used for determination of hyperenhanced (HYPER) and hypoenhanced myocardium within the hyperenhancement (MO). Left ventricular volumes/mass, volume of HYPER and MO as well as transmural extent of MI were calculated. %Infarcted volume was defined as (HYPER + MO)/total myocardial volume.

Results: At initial MRI all patients presented with a regional hyperenhancement, 8 had MO. %Infarcted volume, but not transmural extent, correlated with CKmax (r = 0.85) and LVEF at follow-up (r = −0.82). In the absence of MO, LVEDV remained unchanged (138 ± 26 vs 136 ± 20 ml; p = ns), while LVEF increased at follow-up (40 ± 5 vs 49 ± 6 %; p < 0.05). If MO was present, LVEF did not improve (37 ± 11 vs. 37 ± 12 %; p = ns) and there was a trend towards increased LVEDV (150 ± 37 vs 168 ± 25 ml; p = 0.16).

Conclusion: Infarct volume 3 months after revascularization can be predicted using MR enhancement in the acute setting. The presence of MO predicts 1) an increase of LVEDV and 2) no improvement of LVEF. Maximal medical therapy prevents remodeling in patients with MI but without MO.

125. Asymptomatic Myocardial Infarction in Patients with Type 1 Diabetes Mellitus and Chronic Renal Failure

Michael Elliott,[1] Kelly Choi, [1] Michele Parker, [1] Dixon Kaufman, [1] John Vargas, [1] Robert Bonow, [1] Robert Judd,[1] Raymond Kim.[1] [1]*Northwestern University, Northwestern Medical Faculty Foundation, Chicago, Illinois, USA*

Introduction: An excess of cardiovascular disease and premature cardiac death is well-established in patients with type 1 diabetes mellitus (DM) and chronic renal failure. The 2-year major cardiac event (death, myocardial infarction (MI)) rate for patients with type 1 DM and diabetic nephropathy with unrevascularized coronary artery disease may exceed 50%, which underscores the importance of earlier diagnosis and preventive interventions for coronary artery disease and MI in this patient population. Contrast-enhanced MRI (ce-MRI) can accurately detect transmural and smaller, subclinical, subendocardial MI.

Purpose: To determine the prevalence of asymptomatic, subclinical MI in patients with type 1 DM and diabetic nephropathy by ce-MRI, and to assess relationships to left ventricular mass and other clinical variables.

Methods: We performed cine and ce-MRI on 41 consecutive patients (20 female, 21 male) with no prior clinical history of MI, who were under evaluation for kidney/pancreas transplantation, and 6 (3 female, 3 male, mean age 35 yrs) healthy controls.

Results: The mean age of the DM patients was 40 yrs (range, 22–52) and 24 (59%) were on dialysis. Asymptomatic MI by

ce-MRI was detected in 7 of the 41 (17%) DM patients without a prior history of MI, and in none of the controls. None of the 7 patients determined to have a MI by ce-MRI had electrocardiographic evidence of MI. The mean left ventricular mass (LVM) and left ventricular mass index (LVMI) for the control patients was 123 ± 13.0 g and 66 ± 5.2 g/m2, respectively. For the DM patients, the mean LVM was 191 ± 64.2 g, ($p < 0.0001$), and the mean LVMI was 104 ± 29.7 g/m2, ($p < 0.0001$). No significant correlation was found between MI on ce-MRI and LVMI, diabetes duration, dialysis status, hyperlipidemia, smoking, family history, or hypertension. Age was associated with MI ($p < 0.04$).

Conclusion: A high prevalence of asymptomatic MI is present in young DM patients with chronic renal failure. LVMI is not a predictor of the presence of asymptomatic myocardial infarction in this patient population. The detection of early, subclinical manifestations of ischemic heart disease by ce-MRI could lead to more effective preventive interventions for these high-risk patients with type 1 diabetes mellitus.

126. A Comparison of Strain and Torsion Immediately and One Year After Lad Infarct

Craig Scott,[1] Marc Gotte,[2] Susan Matulevicius,[1] Kevin Duffy,[1] Albert Van Rossum,[3] Victor Ferrari,[1] Leon Axel,[1] Martin St. John Sutton.[1] [1]*University of Pennsylvania, Cardiovascular Division, Philadelphia, Pennsylvania, United States;* [2]*Vrije Universiteit Medical Center al Amsterdam, DE Boelelaan 1117, Amsterdam, Noord Holland, Netherlands;* [3]*Vrije Universiteit Medical Center, Department of Cardiology, MB Amsterdam, Noord Holland, Netherlands*

Introduction: Infarction can affect both global and regional function initially after an infarct, and the infarcted heart may remodel with time. There are multiple fiber layers with different orientation in the left ventricle. An infarction may affect these fibers to different degrees in the same cardiac region or across regions. Therefore, infarction can affect global and regional wall thickening as well as LV torsion generation.

Purpose: The purpose of this study was to characterize LV principal strain and torsion immediately after infarction and determine if certain contraction parameters measured immediately after infarction predict remodeling.

Methods: We studied 12 normal volunteers and 12 patients with left anterior descending territory myocardial infarction using tagged MRI. The 12 patients were studied within days of infarction and one year post-infarction. The infarcts were limited to the mid to apical anterior septum, sparing the base. The patient group was divided into 6 patients whose global cardiac function decreased (remodeling) and 6 patients who had preserved function at one year. The tagged MRI data was analyzed using the SPAMMVU 2000 software from the University of Pennsylvania. Ejection fraction was measured using the MASS program from the Leiden University, the Netherlands.

Resting images were acquired at 3 short axis levels (base to apex) with an infarct and remote region defined on each level. We measured 2-dimensional end-systolic maximum and minimum principal strains E1 and E2, in-plane angular displacement (AD) of tag intersections, and torsion (T = differential AD relative to the basal segment) in patients and controls at frame rates greater

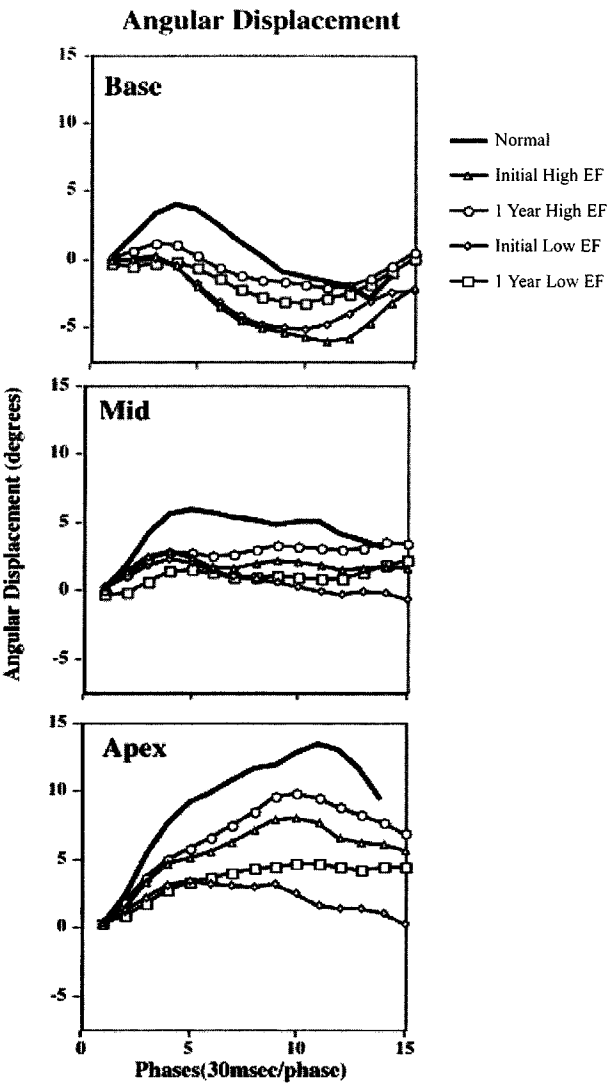

	Baseline		One Year	
	Normal EF	Low EF	Normal EF	Low EF
Strain				
E1 Infarct	0.16±0.08*	0.08±0.04*	0.29±0.09	0.13±0.07*
E1 Remote	0.52±0.15*‡	0.24±0.10#‡	0.43±0.04	0.29±0.07
E2 Infarct	-0.13±0.06*	-0.08±0.05*	-0.17±0.02	-0.15±0.03*†
E2 Remote	-0.22±0.03‡	-0.18±0.05‡	-0.22±0.03	-0.18±0.02
Torsion				
B-M Infarct	8.6±5.0	4.6±1.1	6.3±3.2	7.3±4.0
B-M Remote	9.8±4.4	9.5±3.0	8.0±1.8	4.4±4.3
B-A Infarct	11.7±8	5.2±3.3	15.7±3.6	8.7±2.9
B-A Remote	10.0±7.6*	12.7±2.0*	10.6±4.6*	9.0±5.0*
	*ANOVA P<0.05 vs Normal			
	†ANOVA p<0.05 vs same wall at baseline			
	#ANOVA p<0.05 vs same wall in normal EF			
	‡ANOVA p<0.05 vs same group/wall infarct			

Figure 1.

than 30 images per second. Counterclockwise rotation as viewed from the apex toward the base was defined as positive.

Results: Heart rate was similar between the control and patient groups. (Normal 70 ± 9/min vs. patients 63 ± 12, p = NS).

E1 was reduced compared to normals in the infarct region in both the low EF and normal EF group immediately after infarction (Table 1). E1 normalized in the normal EF group at one year, but remained depressed in the low EF group. E1 was supranormal in the normal EF remote region compared to both normal controls and the low EF group early after infarction, but returned to normal at one year. E1 was lower than normal in the remote region of the low EF group soon after infarction and did not increase at one year.

E2 in the infarct region had the same relation with normal controls as E1, with reduced (less negative) values for both low and normal EF patients at baseline, and an increase in the infarct E2 at one year in all patients. E2 was normal in the remote region for all patients early after infarct and at one year. The low EF patients had a lower mean E2 at each time point.

AD in the normal group shows an initial en block rotation of the entire LV before significant strain development (Fig. 1). This rotation pattern is lost in the low EF infarct group where apical slices immediately begin rotation in the opposite direction to the base. The normal EF group lost the pattern early after the infarct, but regained it at 1 year.

Base to mid-ventricular T is similar to normal in all patients. Base to apex T is reduced vs. normal in all infarct patients initially and at 1 year post-MI.

Conclusion: Regional strain within and remote to an infarction is depressed in patients who remodel both immediately after infarction and at 1 year. In patients who don't remodel, strain is decreased in the infarct zone and globally compared to controls due to decreased strain in the infarct, but there is recovery of global function at one year due to improvement in the infarct. A hyperdynamic remote segment predicted preservation of EF at one year.

AD and T are generated by the longitudinal fibers and are disturbed by infarction, but not in an intuitive way. In infarction, early basal systolic rotation is in the opposite direction compared to normal hearts. If the EF remains normal, the rotation pattern returns. T is usually higher in the lateral wall and increased toward the apex. This pattern is lost with infarction. T actually increased in some patients within an infarction due to tethering. T is also strongly affected by the degree of apical involvement, which can be variable in LAD infarction. Most importantly, unlike strain, torsion did not recover in the normal EF patients, suggesting a loss of apical twist that may affect diastolic filling and cause diastolic dysfunction despite normal systolic function.

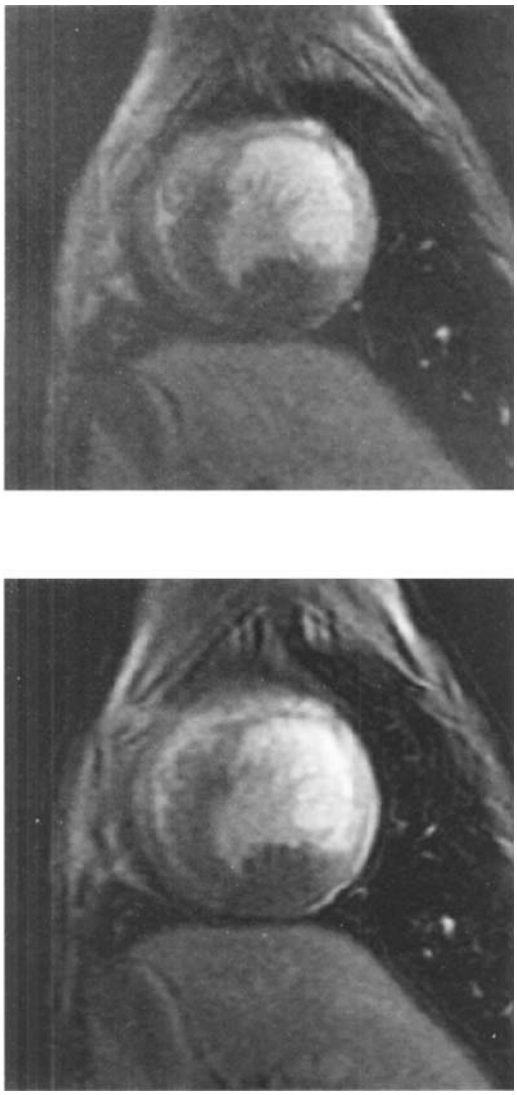

Figure 1. Comparison between a 2D (a) and 3D (b) IR-GRE short-axis images acquired in one mongrel dog. Note the identical visualization of the hyperenhancing region in the LAD territory obtained with the 3D scan compared to the 2D technique.

127. Myocardial Infarction Size Assessment with Single Breath-Hold Three-Dimensional Inversion-Recovery-Prepared MRI

Ernesto Castillo,[1] Luciano C Amado,[1] Bernhard L Gerber,[1] Atanas Kissiov,[1] Joao Ac. Lima,[1] David A. Bluemke,[1] Thomas Kf Foo,[2] Dara L. Kraitchman.[1] [1]*Johns Hopkins University, 600 N. Wolfe Street, Baltimore, MD, USA;* [2]*GE Medical Systems, 600 N. Wolfe Street, Baltimore, MD, USA*

Introduction: Breath-hold inversion-recovery gradient-echo (IR-GRE) 2D techniques are used currently to provide T1-weighted images for delayed contrast imaging of myocardial infarction. In order to cover the whole heart, multiple sections must be acquired, with each acquisition requiring a breath-hold of 10–16 s., and time for recovery between breath-holds. Thus, the total acquisition time may vary between 4–7 min.

Purpose: The purpose of our study was to evaluate a three-dimensional (3D) inversion-recovery gradient-echo acquisition to cover the entire left ventricular volume within a single breath-hold in a canine model of myocardial infarction (MI).

Methods: Seven adult mongrel dogs (20–25 kg) were anesthetized and underwent a 90-minute of closed-chest occlusion of the proximal left anterior descending (n = 6) and circumflex (n = 1) coronary arteries with an angioplasty balloon to produce MI. The animals were imaged within 24 hours of reperfusion in a 1.5 T MR System (Signa, GEMS) using a dedicated phased-array surface coil. After completion of first-pass perfusion imaging (0.2 mmol/kg Gd-DTPA i.v.), 2D and 3D IR-GRE sequences were acquired. The image acquisition parameters for the 2D-technique were: TR/TE/TI/FA:7.4 ms/3.3 ms/200–250 ms/25°; 31.25 kHz BW; 256 × 196 matrix; 8 mm slice thickness and 2 NEX. For the 3D-technique the following parameters were used: TR/TE/TI/FA:3.3 ms/1.3 ms/250 ms/25°; 125 kHz BW; 256 × 196 matrix; 4 mm slice thickness and 0.5 NEX. A 3D acquisition with variable sampling in time (VAST) was used. The volume of delayed hyperenhancing regions corresponding to the MI and scan times were compared between the 2D and 3D scans.

Results: The total scan time was 97.6 ± 26 s. (mean ± SD) for the 2D technique of 8–10 short-axis slices (without including rest periods between breath-holds). In comparison, the 3D acquisition with the slab also positioned along the short axis of the heart was acquired in 12.9 ± 3 s..Thus, the 3D acquisition was performed in 16.5 ± 5 % of the 2D scan time. The volume of the hyperenhanced regions was highly correlated between 2D and 3D techniques (r = 0.96).

Conclusion: Our results indicate that myocardial infarct size can be accurately assessed using a 3 D acquisition scheme. In addition, the 3D acquisition, which is performed in a single breath-hold, has the advantage of substantially reducing the total scan time for delayed myocardial enhancement imaging.

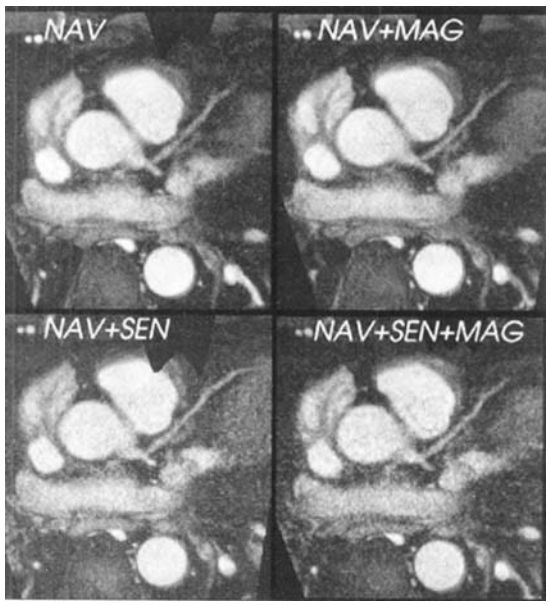

Figure 1.

128. Accelerated Acquisition of Free Breathing Navigator-Guided Coronary MR Angiography Using Sensitivity Encoding (SENSE) and Motion Adapted Gating (MAG)

Steve Hong,[1] Raja Muthupillai,[2] Jouke Smink,[3] Scott D. Flamm.[4] [1]*CVMRI Research Lab, St. Luke's Episcopal Hostpital, Houston, TX, USA;* [2]*Philips Medical Systems, St. Luke's Episcopal Hosp./Radiology/MRI, Houston, Texas, United States;* [3]*Philips Medical Systems, Bldg. QR, DA, Best, The Netherlands;* [4]*St. Luke's Episcopal Hospital, Director of CV MRI Research, Houston, Texas, United States*

Introduction: Coronary MR angiography (CMRA) is challenging because the coronary arteries are small and tortuous, and successful imaging requires both high spatial resolution and large coverage. In addition, data acquisition is time inefficient as it is limited to a small fraction of the cardiac cycle where vessel motion is minimal, and the coronary blood flow is maximal (i.e., mid-diastole). Meeting these stringent demands increases the scan duration to several hundreds of heartbeats, further necessitating a mechanism for compensating respiratory motion. Recently described navigator echo based methods have been shown to be effective in addressing respiratory motion. These prospective techniques monitor the respiratory position of the diaphragm or the heart using a pencil beam RF excitation during each heart beat immediately before collecting image data during diastole. When image acquisition occurs during a user prescribed acceptance window (e.g., 2 mm about the end expiratory phase as deduced from the navigator data) image data is accepted. If image data is outside this window the data is

Table 1

Quantitative Results

Method	NAV	NAV + MAG	NAV + SEN	NAV + SEN + Mag
Length (mm)	50.3 ± 9.5	51.6 ± 8.7	49.8 ± 11	50.5 ± 9.3
% Scan efficiency	51 ± 18	60 ± 18	50 ± 10	59 ± 17
Total heartbeats	912 ± 315	763 ± 267	449 ± 173	378 ± 113

discarded and reacquired. While these navigator based approaches have been effective in delineating the proximal to mid coronary arteries, the main drawback is the long acquisition time, which is typically on the order of 12–15 minutes per coronary arterial system.

Purpose: The purpose of this work was to quantitatively assess the relative merits of the following strategies to reduce acquisition time of the free breathing, navigator guided CMRA technique. The first approach was Motion Adapted Gating (MAG), wherein the acceptance window width is more stringent when acquiring low spatial frequencies (low Ky–Kz values), and is progressively relaxed for higher spatial frequencies, thus improving scan efficiency at the cost of accepting some motion-induced blurring. The second approach was to use SENSitivity Encoding (SENSE—a parallel acquisition technique) to cut down the acquisition time by roughly half, though at the cost of lowered SNR. The final approach was to assess the effect of combining both SENSE and MAG to improve scan efficiency.

Methods: The left anterior descending (LAD) coronary artery was imaged in volunteers (n = 17) using the four techniques, viz., the conventional prospective navigator technique (NAV), NAV with MAG, NAV with SENSE, and NAV with SENSE and MAG at 1.5 T. The following acquisition parameters were constant for all four 3D techniques: TR/TE/flip = 7.1/2.5/30°; FOV/matrix size/slice at thick = 360 − 400 × 270 − 300/512 × 384 (acquired)/10 at 3 mm (recon as 20 at 1.5 mm); phase-encoding steps/RR interval = 12; a composite RF pulse for muscle signal suppression, and a fat suppression pulse preceded data acquisition; a navigator echo was collected immediately before data acquisition; data acquisition was Vector-ECG gated and occurred in mid-diastole.

The acceptance window was progressively and smoothly increased from 4 mm (central 25%) to 8 mm (26–100%) for the two MAG acquisitions (with and without SENSE), and the number of in-plane phase encoding steps were reduced by a factor of 2 for the two SENSE acquisitions (with and without MAG). The order of the techniques used during data acquisition was randomized. The total number as well as the accepted RR intervals (heartbeats) were recorded for each technique. The performance of the four techniques were quantitatively evaluated using: (a) the length of the coronary artery visualized, (b) total acquisition time (in heartbeats), and (c) scan efficiency.

Results: The addition of MAG to the NAV technique reduces average acquisition time by 16%. The addition of both SENSE and MAG to the NAV technique reduces average acquisition time by 59%. There was no difference in the length of proximal LAD (50 mm) visualized using all four techniques. Representative images are shown in Figure 1. Quantitative comparative results are summarized in Table 1.

Conclusion: It is feasible to combine SENSE and MAG to accelerate the acquisition of navigator-guided 3D free breathing CMRA techniques. Acquisition times can be reduced on average by nearly 60%, while maintaining the ability to visualize the proximal 50 mm of the LAD. Such a reduction in acquisition time may allow more routine incorporation of CMRA in clinical practice for non-invasive evaluation of proximal coronary arteries.

129. Coronary Magnetic Resonance Angiography in the Presence of Stents: Imaging of the Stentlumen

David Maintz,[1] Roman Fischbach,[2] Walter Heindel,[2] Warren Manning,[3] Matthias Stuber,[1] [1]*Beth Israel Deaconess Medical Center and Harvard Medical School, Boston, USA, and Dept. of Clinical Radiology, University of Münster, Münster, NRW, Germany;* [2]*Dept. of Clinical Radiology, University of Münster, Albert-Schweitzer-Str. 33, Münster, NRW Germany;* [3]*Beth Israel Deaconess Medical Center and Harvard Medical School, Cardiovascular Division, Boston, MA, United States*

Introduction: Coronary stenting is the predominant coronary revascularisation procedure with an estimated 70–90% of all coronary interventions (Ref. 1). Although stenting reduces the restenosis-rate, in-stent restenosis may occur in 17 to 60% of the patients. Given the disadvantages of conventional angiography (risk of complications, need of iodine contrast agent, radiation exposure), a non-invasive imaging modality for the assessment of the stent lumen would be desirable. While various coronary artery stents have been evaluated in vitro with regard to the total volume of their artifacts as a function of different imaging sequences, the visualization of the stent lumen has not previously been discussed. Therefore, we implemented an MR imaging methodology which allows for the quantification of in-stent signal attenuation. This technique has quantitatively been evaluated in 19 different coronary stents.

Purpose: To evaluate the possibility/feasibility to visualize coronary stentlumina using Magnetic Resonance Angiography (MRA) in vitro.

Methods: Nineteen different coronary artery stents were studied. Seventeen stents were made of stainless surgical steel (316L), one was made of nitinol (Radius) and one of tantalum (Wiktor). The stents were implanted in plastic tubes with an inner diameter of 3 mm. The tubes were positioned in a plastic container filled with gel and connected to a closed constant flow

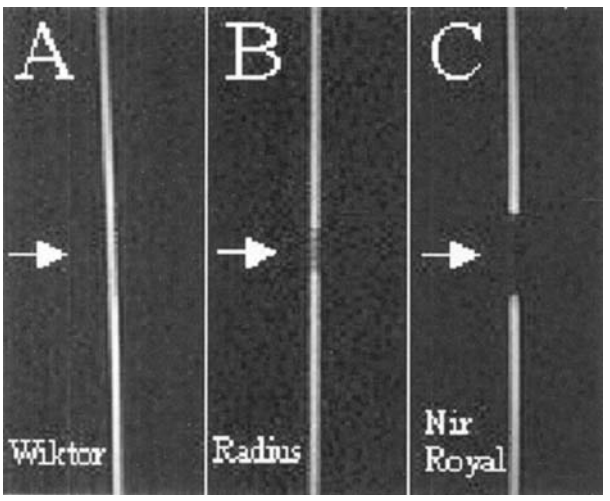

Figure 1 A,B,C. Example images (subtracted) of a tantalum stent (Wiktor), a nitinol stent (Radius) and a steel stent (Nir Royal).

circuit (18 cm/sec). MR Imaging was obtained on a 1.5 T whole-body MR system (Gyroscan ACS-NT, Philips Medical Systems, Best, The Netherlands) equipped with cardiac software (CPR6) and a PowerTrack 6000 gradient system (strength 23 mT/m; rise time 220 msec). A cardiac synergy coil (two anterior and three posterior elements) was used for signal reception. After localization of the stented "vessel" by a multislice, two-dimensional, segmented gradient echo scout sequence (TR = 11msec, TE = 2.4 msec, 256 × 128 matrix, 450 mm FOV, 10-mm slice thickness, 5-mm slice gap, ~1min acquisition time) coronary MRA was performed with a previously described (Ref. 2) dual inversion, ECG-triggered (artificial ECG), three-dimensional fast spin-echo sequence (parameters: linear k-space acquisition scheme, 28msec TE, TR of two RR intervals, 512 scan matrix, echo train length of 17 and interecho spacing of 7.6 msec, acquisition window of 130 msec per RR interval, half-Fourier sampling, FOV 360 mm with an resultant in-plane voxel size of 700 μm, two signal averages). A 16-mm thick 3D slab was imaged consisting of 8 adjacent slices of 2mm slice thickness each. Sixteen slices with a slice thickness of 1mm were reconstructed using zero-filling in kz direction. The same stents were imaged twice, with flow and without flow. Subsequently, both image data sets were subtracted and 4-mm thick multiplanar reformats (MPR) were obtained. Signal measurements (ROI-technique) were perfomed on the MPR images to get objective quantitative data on the intraluminal signal properties (CNR, SNR).

Results: The Wiktor stent (tantalum) showed the highest intraluminal signal of all evaluated stents. The intraluminal signal attenuation was minor when compared to the unstented vessel part and relatively homogeneous. Consistent with the low CNR the Wiktor stent can barely be distinguished from the unstented 'vessel' part (Figure1A). The Radius stent (nitinol) showed reduced intraluminal signal when compared to the Wiktor stent but an increased CNR when compared to the steel stents. The signal also appears less homogeneous with a stripe structure (Figure1B). Stents made of stainless steel caused the strongest artifacts, but the degree of intraluminal signal reduction varied among the stenttypes. The ACS Multilink and the Crossflex showed the lowest signal attenuation among the steel stents. In these cases, the lumen seemed to be artificially narrowed and the intraluminal signal was reduced when compared to the nonstented portion of the vessel while the main parts of the lumen still remain visible. In the Sirius, Tetra, Herculink, Tristar, V-Flex, be-Stent, Biodivisio, Flex AS, Jostent, Palmaz-Crown, NirPrimo and Palmaz stents, the intraluminal signal attenuation was more pronounced, the signal was more inhomogeneous (see stripe structure of the Sirius and Jostent), feigned lumen narrowing was more evident (e.g. be-Stent) and the lumen was not visible in its whole length (in the Herculink only in the middle). In the Nir Royal (Figure 1C), the Velocity and the Jograft, artifacts were most pronounced resulting in obscurity or even signal loss of the major parts of the stent lumen.

Conclusion: The present study includes a preliminary evaluation of intraluminal signal properties of coronary artery stents in an in vitro flow model. In summary, coronary artery stents are sources of artifacts in MRA that superimpose the stentlumen to various degrees. Nitinol and especially Tantalum stent lumina may be visualized. Future stent design needs to be focused not only on the mechanical but also the MR imaging characteristics of stents. The MR method used in this article may be also be helpful for the evaluation of future stent developments regarding their MR imaging suitability.

130. Submillimeter 3D Coronary MR Angiography with Real-Time Navigator Correction in 112 Patients with Suspected Coronary Artery Disease

Torsten Sommer,[1] Matthias Hackenbroch,[1] Ulrich Hofer,[1] Carsten Meyer,[1] Sebastian Flacke,[1] H. Schild,[1] [1]*University of Bonn, Sigmund-Freud-Strasse 25, Bonn, NRW, Germany*

Introduction: Three dimensional bright blood coronary magnetic resonance angiography techniques have been successfully applied to visualize proximal and mid portions of the native coronary arteries in healthy and diseased states. However the clinical value of this method has not yet been established in a large patient population.

Purpose: To evaluate high-resolution coronary MR angiography (coronary MRA) in a large group of patients with suspected coronary artery disease.

Methods: 112 patients (mean age 61 years, range 40 ? 79 years) with suspected coronary artery disease underwent free-breathing coronary MRA with real-time navigator correction (Intera, 1.5 T, Philips Medical Systems). An ECG-gated, fat-suppressed, 3D segmented-k-space gradient echo sequence (Turbo Field Echo, TR 7.4 ms, TE 2.2, 13 phase-encoding steps per cardiac cycle, flow-insensitive T2-prepulse for contrast enhancement, in plane resolution 0.79 × 0.70) and a five-element cardiac phased array coil were used. Two 3-cm-thick 3D volumes were planned along the major axis of the right and proximal/middle left coronary artery, respectively. Data acquisition was performed in mid-diastole. Cardiac catheterization with selective coronary angiography was performed in all patients within 14 days of the MR study. Only clinically stable patients with sinus rhythm were included. The evaluation included the analysis of the raw data set and reformatted images. Visualization of the coronary arteries (CA) was qualitatively assessed using a four point grading scale (1: CA with sharply defined borders, 2: CA with mildly blurred borders, 3: CA with markedly blurred borders, 4: CA not visible or obscured by severe artifacts).

Results: Image quality of grade 1 was achieved in 22%, grade 2 in 47%, grade 3 in 24% and grade 4 in 7% of patients. In coronary MRA's with good quality (grade 1 and 2, n = 77/112) sensitivity and specificity for detection of significant stenoses >50% in the proximal and middle main CA were 88% and 91%, respectively. In 31% of these patients (n = 24/77) there were clinically significant stenoses in side branches (diagonal branches, obtuse marginal branches) and/or distal parts of the CA (distal LAD, distal CX, posterior descending artery of RCA) which could all not be detected by coronary MRA (0/24).

Conclusion: Submillimeter 3D coronary MRA with real-time navigator correction allows high quality imaging of the proximal and middle main CA with good sensitivity and specificity for detection of stenoses > 50% in selected patients. However, stenoses of major side branches and the distal CA can not be reliably detected and in about 1/3 of patients image quality is non-diagnostic.

131. Potential Clinical Feasibility of Smash Accelerated Coronary Magnetic Resonance Angiography

Charles Mckenzie,[1] Peter Danias,[1] Kraig Kissinger, [1] Matthias Stuber, [1] René Botnar, [1] Warren Manning, [2] Daniel Sodickson.[1]
[1]*Beth Israel Deaconess Medical Center, Cardiovascular Division, Boston, Massachusetts United States;* [2]*Harvard University, Division of Cardiology\ES-406\330 Brookline Avenue, Boston, MA United States*

Introduction: T2-weighted, free breathing sub-millimeter 3D coronary magnetic resonance angiography (CMRA) with navigator diaphragmatic gating and correction (1,2) is capable of depicting the major proximal coronary segments. The major disadvantage of navigator CMRA is that required long data acquisition times (>10 min) are impractical for most cardiac patients. Previous work has shown that Parallel MRI (PMRI) techniques such as SiMultaneous Acquisition of Spatial Harmonics (SMASH) can be used to dramatically reduce the amount of time needed for data acquisition while still preserving the original image resolution and contrast (3). However, all PMRI techniques produce accelerated images with lower signal-to-noise ratios (SNRs), and possibly more artifacts, than the equivalent unaccelerated images.

Purpose: To examine the feasibility of SMASH CMRA in patients with known coronary artery disease (CAD) and to investigate whether the diagnostic information of CMRA is preserved.

Methods: We studied 8 adult subjects (7M, 1F; mean age 66 ± 10 years), all of whom had CAD of the right coronary artery (RCA) confirmed by recent X-ray angiography. The institutional Committee on Clinical Investigations approved the research protocol and written informed consent was obtained from all subjects.

We performed all scans on a Philips ACS NT 1.5T MR imaging system (Philips Medical Systems, Best, NL) using a custom surface coil array with six elements distributed in the right-left direction (4). After placement of electrocardiogram leads, subjects were positioned supine and the flexible coils were conformed to the chest wall and centered on the position of the heart. No breathholds or coached breathing were performed.

We performed CMRA with right hemi-diaphragm navigator gating and prospective slice correction (5) and a T2 prepared 3D turbo field echo sequence (TR 8.8 ms, TE 2.4 ms, 10 slices interpolated to 20, through plane resolution 3 mm interpolated to 1.5 mm, acquisition window 70 ms per cardiac cycle) (1, 2).

In each subject, we acquired three consecutive data sets from the volume containing the RCA: a low resolution volume for cil sensitivity calibration (in-plane spatial resolution 5.6 mm × 6.0 mm), followed by two high-resolution acquisitions (512 × 384, in-plane spatial resolution 0.7 mm × 1.0 mm), one unaccelerated reference volume and one 2 × SMASH accelerated volume. The use of SMASH accelerated imaging reduced data acquisition times from 15–20 min to 7–10 min. Only the RCA was imaged in this study since such imaging must be done in a double oblique plane that is particularly challenging for SMASH reconstructions.

The unaccelerated reference images were reconstructed using a sum-of-squares combination of component coil images (6). The accelerated data sets were reconstructed using Sum-of-Squares SMASH (7).

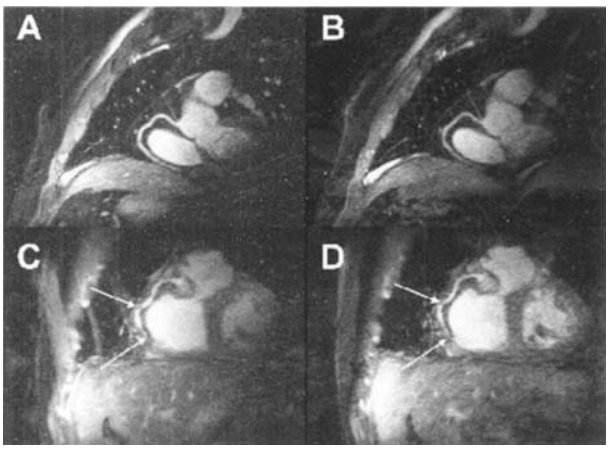

Figure 1.

Image evaluation was performed by consensus of two cardiologists in a random and blinded fashion. The presence of the RCA, the length of the vessel visualized, the overall image quality and the vessel sharpness were semiquantitatively scored. Image quality and vessel sharpness were rated on a 4 point scale (1 = poor, 2 = good, 3 = very good, 4 = excellent). The presence of CAD was also evaluated and its severity of disease was rated on a three point scale (0 = none (<50% stenosis), 1 = mild (50–75% stenosis), 2 = moderate/severe (>75% stenosis)). Confidence of interpretation of the images was also rated on a 3 point scale (1 = low, 2 = medium, 3 = high).

Results: Figure 1 shows examples of multiplanar reformats depicting the RCA. Fig. 1A is the unaccelerated image from a patient with non-significant CAD and Fig. 1B is the corresponding SMASH accelerated image. Figs. 1C and D are reference and accelerated images from a patient with moderate/severe disease of the proximal and mid-RCA. The arrows indicate >50% stenoses. Despite the reduction in SNR inherent in parallel imaging, the SMASH accelerated image depicts the RCA with clarity that is comparable to the unaccelerated image. The semiqualitative ratings of the images are summarized in Table 1. Only one of the SMASH accelerated scans was deemed to be uninterpretable (versus

Table 1

Summary of Image Analysis

RCA Visible	Unaccelerated 8/8	SMASH 8/8
Vessel length (mm)	57	55
Vessel sharpness (1–4)	2.3	2.3
Overall image quality (1–4)	3.0	2.4
Disease correctly identified	8/8	7/8
Confidence in interpretation (1–3)	2.6	2.0

no uninterpretable scans for the unaccelerated images). In all other cases the presence or absence of CAD was in agreement with the non-accelerated images and the X-ray angiography findings. However the reader's rated confidence in the interpretation of the SMASH images was lower than that for the unaccelerated images, largely due to the reduction in SNR in the SMASH images.

Conclusion: Despite a reduction in confidence in the interpretation of the SMASH accelerated images, this technique appears to provide similar information to conventional CMRA regarding the presence and severity of CAD. This suggests the potential feasibility of SMASH CMRA to reduce acquisition time by a factor of two. If this initial impression is confirmed by further, larger studies, the reduction in the time required to obtain CMRAs will make it much easier to routinely include such imaging in a comprehensive cardiac examination.

132. Three-Dimensional Black-Blood Magnetic Resonance Coronary Vessel Wall Imaging Detects Increased Vessel Wall Thickness in Patients with Non-Significant Coronary Artery Stenoses

Won Yong Kim,[1] Matthias Stuber,[2] Peter Börnert,[3] Kraig V Kissinger,[2] Warren Manning,[2] René Botnar.[2] [1]*Department of Cardiology, Brendstrupgaardsvej, Aarhus, Denmark;* [2]*Beth Israel Deaconess Medical Center, Cardiovascular Division, Boston, Massachusetts, United States;* [3]*Philips Research Laboratories, Hamburg, Germany*

Introduction: Subclinical disease may predate clinical disease by many years. In addition, acute coronary syndrome frequently results from the rupture of an atherosclerotic plaque in an area of only mild–moderate luminal narrowing (1). Intravascular ultrasound depicts high-resolution images of the coronary vessel wall and lumen and has provided novel pathophysiological insights to the diagnosis of and therapy for coronary artery disease. However, the invasiveness of the intravascular ultrasound technique prevents its application in routine screening of patients with suspected coronary artery disease. Thus, a non-invasive approach for direct visualization of the coronary vessel wall would be desirable to allow for assessment of subclinical disease. Recently, 2D black blood coronary magnetic resonance vessel wall and plaque imaging has been reported (2–3).To facilitate advancement of magnetic resonance coronary vessel wall imaging into a useful screening tool will require quantitative and reproducible evaluation of the entire proximal coronary artery wall. Therefore, three-dimensional approaches would be more favorable as they allow for a more extensive coverage of the coronary artery tree and improved signal-to-noise ratio with the potential for higher spatial image resolution.

Purpose: We sought to develop a high-resolution isotropic black-blood 3D magnetic resonance (MR) sequence with objective analysis to facilitate more extensive visualization and characterization of the proximal coronary vessel wall. We investigated the feasibility of this novel approach in adult healthy subjects and in patients referred for x-ray angiography.

Methods: Eleven adult subjects, six healthy subjects (2 males and 4 females; age 33 ± 12 years) and five patients (3 males and 2 females; age 69 ± 9 years) with non-significant (10–50% diameter reduction) coronary artery stenoses by x-ray angiography were studied using a commercial 1.5 Tesla Philips-NT MR scanner equipped with PowerTrak 6000 gradients (23 mT/m, 219 ms rise time). All subjects were in sinus rhythm and without contraindications to magnetic resonance exams. All subjects were examined in the supine position using a commercial 5-element cardiac synergy receiver coil. For cardiac synchronization and monitoring, four electrodes were placed on the left anterior hemithorax with the R-wave of the vector ECG used as a trigger for image acquisition. To further reduce cardiac motion artefacts, the image acquisition was placed at mid-diastole using a heart rate dependent trigger delay to predict the onset of mid-diastolic diastasis (4). All coronary MRA and vessel wall scans were performed during free breathing using a right hemidiaphragmatic navigator with a 5 mm gating window for respiratory motion compensation. Free-breathing 3D coronary vessel wall imaging was done along the major axis of the right coronary artery (RCA) with isotropic spatial resolution using black-blood spiral image acquisition (5). A modified dual inversion prepulse utilizing a non-selective 180° inversion pulse immediately followed by a local 2D selective 180° re-inversion pulse was applied to null signal from blood and surrounding tissue. The inversion time was adjusted for the zero crossing of the longitudinal magnetization of blood with an additional delay of 50–100 ms between the R-wave and the local inversion pulse to fulfill the mid-diastolic trigger delay condition. To suppress signal from epicardial fat a frequency selective fat suppression prepulse was applied. A 3D spiral imaging sequence was used for the vessel wall imaging (TR = 30 ms, 1 NSA, TE = 2 ms, acquisition window 60 ms, 26 slices with a thickness of 1–

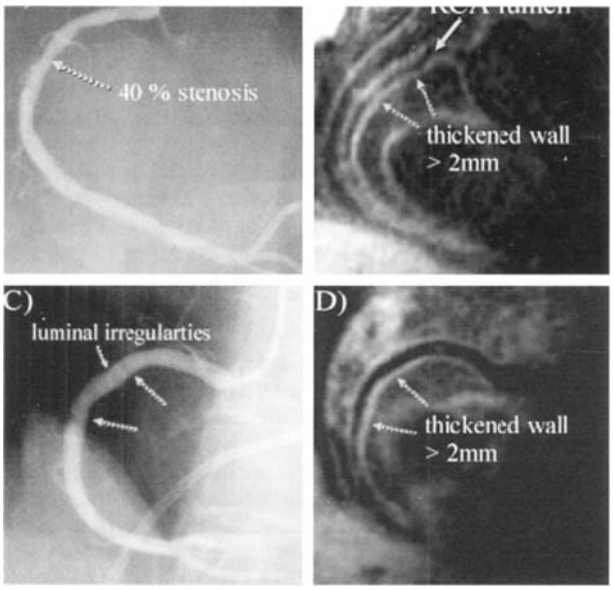

Figure 1. X-ray angiography in two patients with (A) a 40% stenosis and (C) luminal irregularities in the proximal RCA (dotted arrows). The corresponding MR vessel wall scans (B,D) demonstrate a thickened RCA wall (>2 mm) indicative of atherosclerotic plaque.

2 mm, FOV 400 mm, acquisition matrix 512 × 512, in-plane resolution 0.78 × 0.78 mm). To optimize signal-to-noise ratio with the shortest imaging time, data acquisition was performed every second heart beat. The imaging time for this scan was ~15 minutes during free breathing. An automated vessel wall detection tool was used to measure mean vessel wall thickness in the proximal coronary vessel. To visualize the whole circumference of the vessel wall, we also generated an animated sequence of cross-sectional views from the 3D dataset perpendicular to the major axis of the vessel.

Results: The 3D MR vessel wall scans allowed for visualization of the contiguous proximal RCA (63 ± 8 mm) in all subjects. The animated visualization of the cross-sectional views of the coronary artery lumen and wall allowed for evaluation of the entire vessel circumference to detect focal plaque burden. Mean vessel wall thickness was significantly increased in the patients with non-significant coronary artery stenosis ($p < 0.01$) compared to the healthy subjects. Thus, mean vessel wall thickness was 1.0 ± 0.2 mm in the healthy subjects vs. 1.8 ± 0.3 mm in the patients with non-significant coronary artery stenosis (Figure 1).

Conclusion: High-resolution black-blood 3D MR allows for in-vivo human coronary vessel wall imaging of the proximal coronary artery. This novel approach has the potential to reliably detect atherosclerotic plaque burden in patients with non-significant coronary artery stenoses.

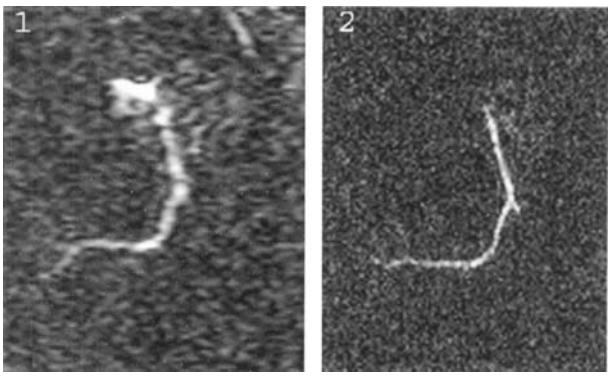

Figure 1. 1) 2D IA image of the LCX of a dog following injection of 3 mL of 9% Gd over 2 s. Images were non-triggered and collected at 3 frames/s. 2) A partition from a 3D image of the LCX of a dog following injection of 12 mL of 6% Gd over 20 s. One 3D data set was collected every 7 s.

133. MR Coronary Artery Imaging with Intraarterial Gadolinium Injections with an Inversion Recovery-Prepared Sequence in Canines

Jordin Green,[1] Reed Omary,[1] Syam Vasireddy,[1] Yiu-Cho Chung,[2] Richard Tang,[1] Yongzhong Li,[1] Paul Finn,[1] Debiao Li.[1] [1]*Northwestern University, 448 E. Ontario St., Chicago, Illinois, United States;* [2]*Siemens Medical Solutions, 448 E. Ontario St., Chicago, Illinois, United States*

Introduction: MR imaging with intraarterial (IA) injections of gadolinium (Gd) contrast agent may be useful for guiding interventional procedures on patients who have already undergone catheterization (1). The potential advantages of using MRI instead of X-rays in guiding interventional procedures include: No exposure to ionizing radiation and toxic contrast media, and MRI can obtain both vascular and physiological data in a single study.

Thick-slice projection imaging is required for guiding coronary interventions to cover the relevant anatomy with the necessary temporal resolution. Because of the partial volume effect in projection imaging, background signal must be supressed to prevent it from obscurring the coronaries. High flip angle steady-state methods have also been applied (2), but flip angle drop-offs at the edge of the slice can lead to poor vessel depiction.

Purpose: The purpose of this study was to demonstrate the feasibility of depicting coronary arteries using MR with IA Gd injections using an inversion recovery (IR) prepared sequence. This preparation scheme is designed to vastly reduce signal from all background tissues while preserving signal from the contrast-enhanced blood. This allows ready visualization of the coronary arteries in real-time.

Methods: Canines (n = 5) were prepared by surgically inserting a catheter into the left circumflex (LCX) coronary artery 10–15 mm from the origin. A power injector delivered diluted gadolinium-chelate directly into the LCX. Images were acquired at approximately 3 frames/s.

In the first experimental protocol, injection rate and Gd concentration was varied while total solution injected was fixed in order to determine optimal contrast injection settings. 3 mL of diluted contrast agent (3, 6 and 9% Gd by volume) was delivered through the catheter. Each dilute contrast agent was delivered at a rate of 0.5, 1.0, and 1.5 mL/s, corresponding to injection times of 6 s, 3 s, and 2 s respectively. In total, there were 9 different injection schemes. At the measurement onset, a non-selective inversion pulse was applied, followed by a wait time TI. This was then followed by the acquisition of 43 lines. This was immediately followed by another IR pulse, and the cycle was repeated. Two consecutive acquisition periods were used to form an image. A two-dimensional gradient-echo sequence was used for data acquisition with the following parameters: TR/TE/flip angle = 2.3 ms/1.3 ms/15°, FOV = 157 mm × 210 mm, matrix = 86 × 256, slice thickness = 20 mm and TI = 50 ms.

For the second experimental protocol, an ECG-triggered, 3D sequence was implemented. This sequence had a lower temporal resolution but higher spatial resolution compared to protocol 1. For this protocol, 12 mL of 6% Gd was injected over 24 s. At the detection of the trigger, a series of approximately 100 25° rf pulses were played out. This was followed by a 180° IR pulse and then acquisition. The acquisition parameters for this sequence were as follows: TR/TE/flip angle = 3.0 ms/1.5 ms/20°, FOV = 151 mm × 210 mm, matrix = 172 × 256, 43 lines/segment, 8 partitions interpolated to 16, with 32 mm coverage. TI was set to 50 ms.

Regions-of-interest were drawn in the vessel and outside the body in order to measure the signal-to-noise ratio (SNR).

Results: For both protocols, the IR-preparation completely suppressed the background. Increased signal intensity following injection was observed only in the LCX, permitting ready visualization of the first 45 mm of the LCX. A typical result for

protocol 1 is shown in Fig. 1. Preliminary results indicate that the optimal Gd concentration was 6%. Using the determined optimal injection parameters, mean peak post-contrast SNR in the LCX was measured at 4.43.

For the 3D protocol, the vessel is clearly depicted with excellent coverage. SNR was found to be 3.79. In the center image, approximately 57 mm of vessel is visible. No background subtraction or post-processing method was required to obtain this image. Note the excellent LCX definition because of the use of ECG-triggering and high image resolution.

Conclusion: This study showed the feasibility of coronary artery visualization at a temporal resolution of 3 frames/s with a small dose of IA contrast injection using an IR-prepared sequence. As well, using a 3D technique it is possible to obtain high-resolution images, though at a cost in temporal resolution. These images have the potential to serve as roadmaps for MR guided coronary interventions.

References
1. Omary RA et. al. *JVIR* 1999; 10: 1315–1321.
2. Serfaty J-M et. al. *Radiology* 2000; 217: 290–295.

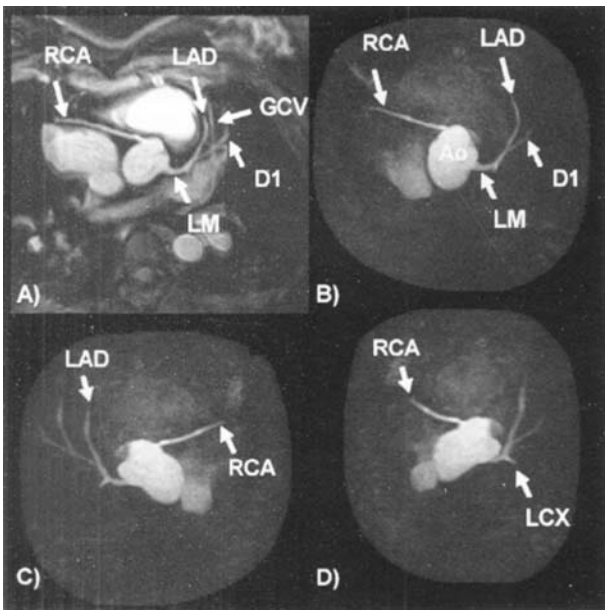

Figure 1. Proximal left and right coronary arterial system. A) Non-tagged anatomical acquisition. B...D) Projection coronary MRA displayed at 3 different viewing angles.

134. Aortic Spin Tagging for 3D Selective Visualization of the Coronary Arterial Lumen

Matthias Stuber,[1] Peter Börnert,[2] Elmar Spuentrup,[1] René Botnar,[1] Warren Manning.[1] [1]*Beth Israel Deaconess Medical Center, Cardiovascular Division, Boston, Massachusetts, United States;* [2]*Philips Research Laboratories, Technical Systems, Hamburg, Germany*

Introduction: Conventional coronary MRA techniques display the coronary blood-pool along with the surrounding structures including chest-wall, the myocardium, the ventricular and atrial blood-pool, and the great cardiac vessels. This representation of the coronary lumen is not directly analogous to the information provided by x-ray coronary angiography, in which the coronary lumen displaced by contrast agent is exclusively seen. Analogous "luminographic" data may be obtained using MR arterial spin tagging (1,2). Such an approach was implemented using a 2D selective 'pencil' excitation for aortic spin tagging in concert with 3D spiral imaging and real-time navigator technology for free-breathing data acquisition.

Purpose: To develop a coronary MRA technique which allows for free-breathing 3D selective visualization of the coronary artery lumen without user-assisted post-processing or segmentation.

Methods: Free-breathing 3D aortic spin tagging for coronary MRA was implemented on a commercial 1.5 T Philips Gyroscan ACS-NT system. Six healthy adult subjects were investigated. During the same scan, two 3D data sets with (tagged) and without (non-tagged) preceding aortic spin tagging were acquired. For volume targeted arterial spin labeling in the ascending aorta, a 2D selective pencil beam RF excitation with a diameter of 25 mm was used. The excitation angle of the 2D selective labeling pulse was alternated in run-time between 180° (tagged) and 0° (non-tagged). To allow for inflow of the labeled blood into the coronary arteries, the time delay (TL) between the spin-tagging and the diastolic imaging portion of the sequence was 200 ms. In one subject, an additional TL of 100 ms was applied for the right coronary artery. After completion of the scan, both tagged and non-tagged 3D data sets were subtracted (complex) for exclusive visualization of the coronary arterial blood-pool. For respiratory motion suppression, a diaphragmatic navigator was utilized for gating (5 mm gating window) and prospective 3D real-time motion correction of the imaged volume position. For signal read-out, an ECG triggered 3D interleaved segmented spiral imaging technique was used. Two spiral interleaves (variable angular speed, 20 ms read-out time per interleaf) were acquired per RR interval (TE = 2 ms; TR = 25 ms) using a ramped RF excitation angle scheme (45°, 90°). A field-of-view of 350 mm was sampled with a 512 × 512 matrix resulting in an in-plane voxel size of 0.7 × 0.7 mm. The slice thickness was 2 mm. Ten slices were acquired covering a volume of 20 mm. Fat signal was suppressed using a spectrally selective fat saturation pre-pulse. For visualization, maximum intensity projections of the

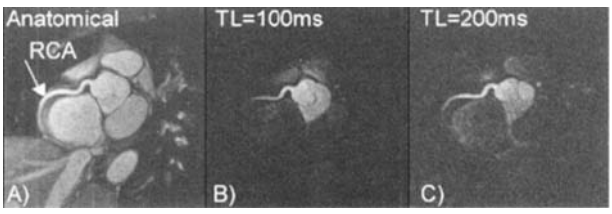

Figure 2. A) Non-tagged anatomical acquisition of a right coronary artery (RCA). Projection coronary MRA acquired with a TL of 100 ms (B) and 200 ms (C).

subtracted image data at multiple viewing angles (= projection coronary MRA) were subsequently performed.

Results: Three-dimensional projection coronary MRA were successfully obtained in all subjects. Average scanning duration during free-breathing was 12 min. Fig. 1 shows example image data (acquired during the same scan) including the non-tagged acquisition (A) and the 3D projection coronary MRA data displayed at different viewing angles (B–D). The left main (LM), a contiguous 6 cm segment of the left anterior descending (LAD), a 3 cm portion of the left circumflex (LCX), a diagonal branch (D1) and a 5 cm segment of the proximal right coronary artery (RCA) are visualized on the projection coronary MRA. When compared to the conventional images (Fig. 1A), the projection coronary MRA in Fig. 1B–D show a suppressed signal from the chest wall, the myocardium, the great vessels and epicardial fat, while the aortic root (Ao) and the coronary blood-pool appear signal-enhanced. This results in a high contrast between the coronary blood-pool and the surrounding tissue. Venous signal could also not be observed on the projection coronary MRA but a signal attenuated portion of the great cardiac vein (GCV) is seen on the conventional coronary MRA (Fig. 1A).

Using a labeling delay of 200 ms a longer right coronary artery segment (4 cm) could be observed when compared to the data acquired with a TL of 100 ms (2.5 cm) (Fig. 2).

Conclusion: The current implementation of spiral free-breathing aortic spin tagging allows for an exclusive, selective 3D visualization of the coronary artery lumen blood-pool while signal from the surrounding tissue is suppressed. Therefore, this technique is more analogous to x-ray coronary angiography but additionally affords the advantage of a flexible 3D visualization at any arbitrary viewing angle, which may especially be advantageous in the presence of non-concentric coronary stenoses. Hereby, straightforward maximum intensity projection algorithms can be used, and no user-assisted volume rendering or segmentation is needed. First results obtained with incremental labeling delays also suggest that this technique may be useful for the assessment of coronary flow.

135. Coronary Mra with 3D Undersampled Projection Reconstruction Truefisp

Andrew Larson,[1] Orlando Simonetti,[2] Steven Shea,[1] Debiao Li.[3] [1]*Northwestern University, Department of Radiology, Chicago, Illinois, United States;* [2]*Siemens Medical Systems, Ontario Center East Tower, Chicago, IL, United States;* [3]*Northwestern University, Department of Radiology, Chicago, IL, United States*

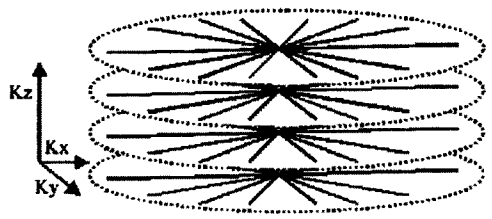

Figure 1. 3D PR TrueFISP K-Space Sampling Trajectory.

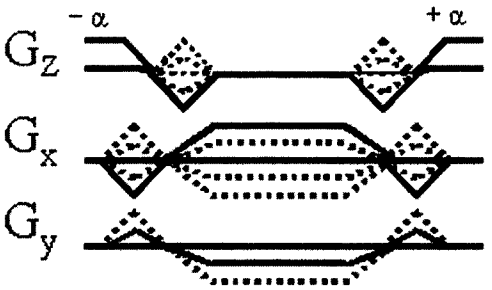

Figure 2. 3D PR TrueFISP Pulse Sequence.

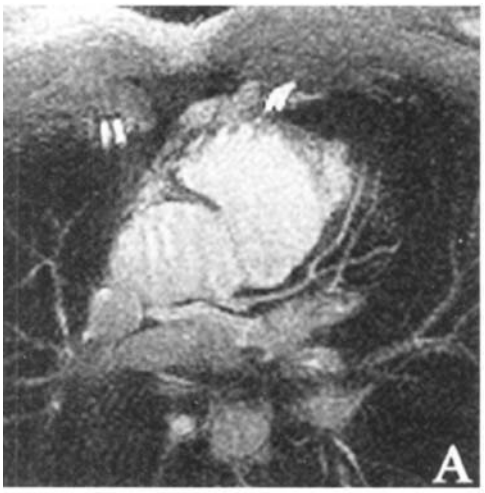

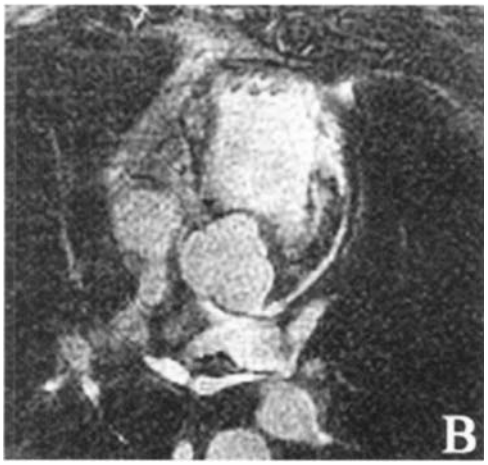

Figure 3. Images of the left coronary artery obtained using the 3D segmented PR TrueFISP sequence ($1.0 \times 1.0 \times 1.5\ mm^3$ resolution).

Introduction: Undersampled PR [1] offers improved imaging efficiency allowing a relative trade-off between SNR and number of acquired lines rather than the trade-off of resolution and number of acquired lines inherent to Fourier techniques. However, azimuthal k-space undersampling can result in radial streak artifact and decreased SNR. The intrinsically high SNR of 3D TrueFISP should compensate SNR deficits and allow the application of undersampled 3D PR TrueFISP to MR angiography. To our knowledge, this work represents the first attempt at combining 3D TrueFISP with undersampled projection reconstruction for coronary artery imaging.

Purpose: The purpose of this work was to investigate the feasibility of using the new 3D segmented PR TrueFISP technique for coronary artery imaging.

Methods: The 3D segmented PR TrueFISP sequence was implemented on a Siemens 1.5 T Sonata scanner with a high performance gradient system (40 mT/m amplitude, 200 mT/m/sec slew rate). The k_x–k_y plane for each partition was acquired using a radial sampling trajectory whereas the k_z dimension was encoded using conventional Fourier phase encoding techniques (Fig. 1). Sequence parameters included: TR/TE = 3.54/1.77 ms, flip angle = 65°, in-plane resolution = 1.0 × 1.0 mm^2, slice thickness = 1.5 mm (interpolated). Data acquisition matrix was 153 (radial k-space views) × 256. 51 views were acquired during each R–R interval following an RF fat-saturation pulse, $\alpha/2$ prepulse and 20 dummy RF cycles for magnetization preparation [2]. A total of 8 partitions were acquired during a 24 heart beat breath hold. A single repetition of the 3D PR TrueFISP sequence is depicted in Fig. 2. The raw data for each experiment was saved and exported off line to a PC with MATLAB software (The Mathworks, Inc., Natick, MA) for reconstruction using a regridding method.

The left coronary arteries of 8 healthy volunteers were studied after approval for participation by the Institutional Review Board of Northwestern University School of Medicine.

Results: MIP images from two of the volunteer studies using the 3D segmented PR TrueFISP technique are shown below in Fig. 3A & 3B.

Conclusion: The coronary arteries were successfully visualized in all volunteers with adequate SNR. Radial streak artifacts were present in some images but not found to impede the delineation of coronary arteries. 3D undersampled PR TrueFISP is a promising technique for coronary MRA and further evaluation of the technique is warranted.

References

1. Peters DC et al. MRM 2000: 43:91–101
2. Deshpande VS et al. MRM 2001: 46:494–502

136. Free-Breathing 3D Coronary Vessel Wall Imaging Utilizing a Local Inversion Technique and Spiral Image Acquisition

René M Botnar,[1] Won Y Kim,[2] Peter Börnert,[3] Matthias Stuber,[1] Elmar Spuentrup,[1] Warren J Manning.[1] [1]*Beth Israel Deaconess Medical Center, 330 Brookline Ave, Boston, Massachusetts, United States;* [2]*Institute of Experimental Clinical Research, Brendstrupgaardsvej, Aarhus, Denmark;* [3]*Philips Research Laboratories, Roentgenstaße 24–28, Hamburg, Germany*

Introduction: Bright blood coronary magnetic resonance angiography (MRA) has shown great potential for non-invasive assessment of intra luminal coronary artery disease (1), but angiography provides minimal information on the magnitude of underlying atherosclerotic plaque. Our current understanding is that luminal disease underestimates atherosclerotic plaque burden and that a majority of acute coronary syndromes occur at sites with non-flow limiting stenoses (2). Thus, a non-invasive approach for direct coronary plaque imaging would be desirable to allow for assessment of subclinical disease. Recently, two-dimensional (2D) black blood coronary MR vessel wall and plaque imaging using a dual inversion (Dual-IR) pre-pulse has been reported (3,4). However, for clinical use, three dimensional (3D) approaches would be advantageous as they allow for a more extensive coverage of the coronary artery tree, improved signal-to-noise (SNR), and thus the potential for higher spatial image resolution.

Purpose: Implementation of a navigator gated and corrected 3D coronary vessel wall sequence using a 2D selective local inversion pre-pulse and spiral image acquisition for visualization of the proximal portions of the coronary artery wall.

Methods: Free-breathing navigator gated and corrected 3D coronary vessel wall imaging using a local inversion technique and spiral image acquisition was implemented on a commercial Philips Gyroscan ACS-NT MR scanner (Philips Medical Systems, Best, NL) equipped with a PowerTrak 6000 gradient (23 mT/m, 220μs rise time) system. To null signal from blood and to minimize signal from tissues outside a circular region of

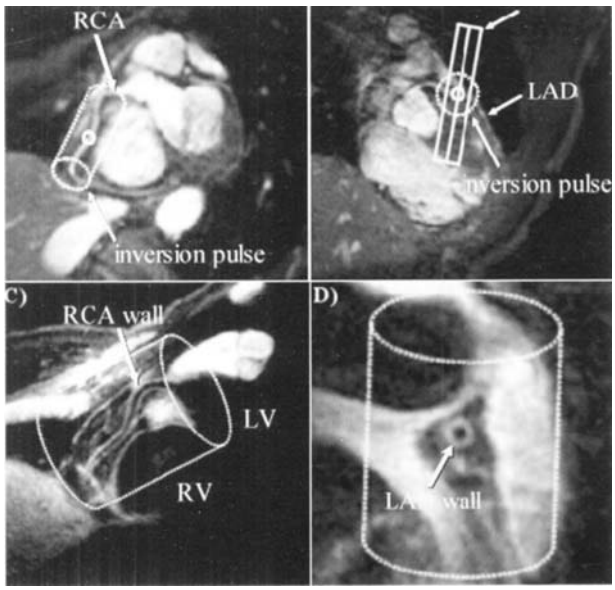

Figure 1. In-plane (C) and cross-sectional (D) coronary vessel wall images. The local inversion pre-pulse was either planned along (A) or perpendicular (B) to the coronary arteries.

interest, a modified Dual-IR technique was implemented. A non-selective 180° inversion pre-pulse is immediately followed by a 2D selective 180° RF pulse (local inversion). Thus, the magnetization of spins outside the pencil beam is inverted (−Mz) while it is selectively restored (+ Mz) only within the cylindrical area defined by the local inversion. At the inversion time [TI = T1*ln(2) − T1*ln(1 + exp(−TR/T1))], the longitudinal magnetization (Mz) of blood and tissues that encountered the first non-selective inversion pulse is near zero, whereas the magnetization of static tissue within the 2D locally re-inverted beam approaches the equilibrium magnetization. Signal from epicardial fat was minimized using a frequency selective saturation pre-pulse. Coronary vessel wall imaging was performed with a 3D stack (6–12 slices) of spirals approach (5). Thus, the kxky sub-planes of the 3D data set were sampled by 42 variable angular frequency spiral interleaves with 2 interleaves ($\alpha = 45°, 90°$) (6) per cardiac cycle. A spiral interleave duration of 23 ms, a TR of 30 ms, and a TE of 2 ms were chosen resulting in an acquisition window of 60 ms. To allow for mid-diastolic imaging, data acquisition was performed every second heart beat. In-plane spatial resolution varied from 0.58–0.78 mm and slice thickness from 1–4 mm. The local inversion pre-pulse was applied in early systole (50–100 ms after the R-wave), while imaging data were acquired in mid-diastole. An early systolic angiogram was used to position the graphical object (beam) of the local inversion pre-pulse on the RCA or LAD, whereas the mid-diastolic angiogram was used to position the 3D volume.

Results: All subjects completed scanning without incident. Coronary wall imaging time was inversely related to the heart rate and varied from approximately 6–9 minutes (cross-sectional) to 14–18 minutes (in-plane) with an average 50% navigator efficiency. Both, cross-sectional (Fig. 1d) and in-plane (Fig. 1c) vessel wall images were obtained.

In all subjects, the 2D selective local inversion pre-pulse (Fig. 1a–b) successfully suppressed unwanted signal outside of the locally inverted region of interest, while preserving the signal in the user selected cylindrical area (Fig. 1c–d) around the coronary vessel wall. Cardiac and respiratory motion artifacts were minimal due to the minimal signal ($SNR = 5 \pm 2$) from the non-cartilaginous chest wall and ventricular blood compared to myocardium in the region of interest.

Conclusion: We successfully implemented and demonstrated a novel local inversion technique for 3D coronary vessel wall imaging. This technique allows for localized imaging of the cross-sectional coronary vessel wall. Furthermore it enables in-plane visualization of the LM and the proximal RCA and LAD wall thereby providing a more comprehensive assessment of coronary wall anatomy. The major advantage of in-plane coronary vessel wall imaging is the relatively good coverage of the coronary artery tree, which allows for estimation of the coronary atherosclerotic plaque burden in the proximal and mid portion of the left and right coronary artery systems. At the present time, it is not certain if cross-sectional or in-plane plaque imaging will best fit the clinical needs for assessment of coronary plaque burden or plaque characterization. Continued studies in well-defined patient subsets will be necessary to investigate the clinical utility of these two approaches.

137. Dilatation of the Main Pulmonary Artery and Pulmonary Artery Branches Under Real-Time Magnetic Resonance Imaging

Carsten Rickers,[1] Michael Jerosch-Herold,[1] Xudong Hu,[1] Huafu Kong,[1] Myra Urness,[1] Cory Swingen,[1] Norbert Wilke.[1]
[1]*University of Minnesota, MMC#292, Mayo, 420, Delaware St SE, Minneapolis, Minnesota, United States*

Introduction: Drawbacks of conventional x-ray guided interventions include radiation exposure, a poor soft tissue contrast and the inability to aquire three-dimentional cross-sectional views.

Purpose We sought to investigate the feasibility of balloon dilatation of the pulmonary artery (PA) valve and pulmonary artery branches under real-time MRI guidance.

Methods: In five healthy animals (two dogs, three pigs) we placed a balloon-catheter (Scimed) with a diameter according to the valve or PA-branch size in the main pulmonay artery. For improved catheter tracking and high resolution intravascular imaging dedicated MRI guidewires (Surgi-Vision) were used. Under real-time MRI guidance (MR fluoroscopy with stead state free precession true FISP MR pulse sequence; 7 frames/sec) the balloon was partially filled with air or gadolinium solution and tracked towards the valve plane and than fully dilated. Balloonvalvuloplasty was monitored by high resolution real-time imaging (flip angle 60°; 128 read-out points × 100 phase encodings; 300 mm field of view) real-time imaging with a temporal resolution of 320 ms. Following the procedure gradient echo cine and spin-echo anatomical imaging was applied to rule out any vascular or cardiac damage.

Results: Real-time MRI made it possible to follow the position of an angioplasty balloon within the pulmonary artery and it's main branches. The catheter tracking as well as inflation and deflation of the balloon positioned in the valve or PA-bifurcation plane could be monitored. No vascular or

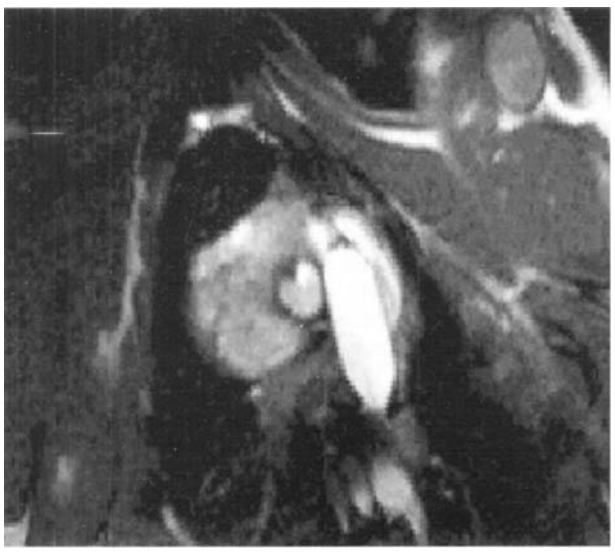

Figure 1. Dilatation of the pulmonary artery with a Gd filled balloon.

Table 1

Results

	Sensitivity	Specifity	Dist Anastomosis	IMA Grafts
HASTE	92%	97%	83%	75%
FISP	92%	94%	65%	92%

myocardial damage was detected. Current limitations are caused by a time delay between image acquisition and image display that will be overcome with faster computer hardware for image reconstruction.

Conclusion: These animal experiments suggest that balloonvalvuloplasty of the pulmonary valve and PA-branches can be performed under real-time and high resolution MRI. These results are the basis for ongoing experimental trials and developments for MRI-guided cardiovascular catheter interventions.

138. Methods and Clinical Importants of Magnetic Resonance Imaging in the Evaluation of Coronary Bypass Grafts

Thomas Wittlinger,[1] Thomas Voigtländer,[1] Karl Friedrich Kreitner,[2] Steffen Petersen,[1] Jürgen Meyer.[1] [1]*2nd Medical Clinic, University Hospital, Mainz, Rheinland-Pfalz, Germany;* [2]*Clinic for Radiology, university Hospital, Mainz, Rheinland-Pfalz Germany*

Introduction: The gold standard in the evaluation of coronary bypass grafts is the x-ray angiography. Being an invasive technique, coronary x-ray angiography has a complication rate of 3–4% and a mortality rate of 0.12–0.20%. The noninvasive imaging of bypass grafts is possible by using different MRI techniques.

Purpose: The aim of the study was to evaluate the reliability of the HASTE and the FISP 3-D sequences in the assessment of coronary bypass grafts.

Methods: We investigated 250 patients with a total of 785 grafts, 192 of them were arterial (IMA) and 593 venous grafts.

Target vessel was 259 cases the LAD, in 217 the RCA, in 120 cases the CX and in 189 cases sides branches of the LAD or CX. MRI (1.5 T, Magnetom Vision, Siemens AG) was performed using a multislice, ecg-gated breath-hold turbo spin echo sequence (HASTE) and a 3-D contrast agent enhanced angiograpy sequence (FISP).

In all patients coronary x-ray angiography was performed within 1 week.

Results: The HASTE squence showed a sensitivity of 92% and a specifity of 97%. The distal anastomosis could be detected in 83%. The FISP sequence showed a sensitivity of 92% and a specifity of 94%, the distal anstomosis could be detected in 65%. See Table above.

IMA grafts could be visualized in 92% with the FISP and 75% with the HASTE sequence.

Conclusion: These results shows that coronary bypass grafts can reliably be detected by using MRI. A total imaging of the vessel is possible in combining different imaging techniques. The proximal parts of the IMA grafts can be visualized best with the FISP, the distal parts of the grafts can be detected in 83% with the HASTE sequence.

139. Vascular Intervention Guided Solely by Real-Time MRI Using Intravascular Guidewire Coils

Alexander J Dick,[1] Michael A Guttman,[2] Venkatesh K Raman,[1] Dana C Peters,[1] Richard B Thompson,[1] Robert J Lederman.[1] [1]*National Heart Lung and Blood Institute, National Institutes of Health, 10 Center Drive, Bldg 10, B1 D219, Bethesda, MD, US;* [2]*National Heart Lung and Blood Institute, Bldg 10, B1D403, Bethesda, MD, US*

Introduction: Vascular intervention guided solely by real-time MRI (rtMRI) is an attractive alternative to X-ray fluoroscopy, but requires a compromise between spatial and temporal resolution. Prior approaches have involved superposition on previously acquired background images ("road-mapping"), which is limited by motion sensitivity.1 Intravascular guidewire coils (IVGC), which are sensitive to local RF signal, may allow for comprehensive real-time vascular intervention without

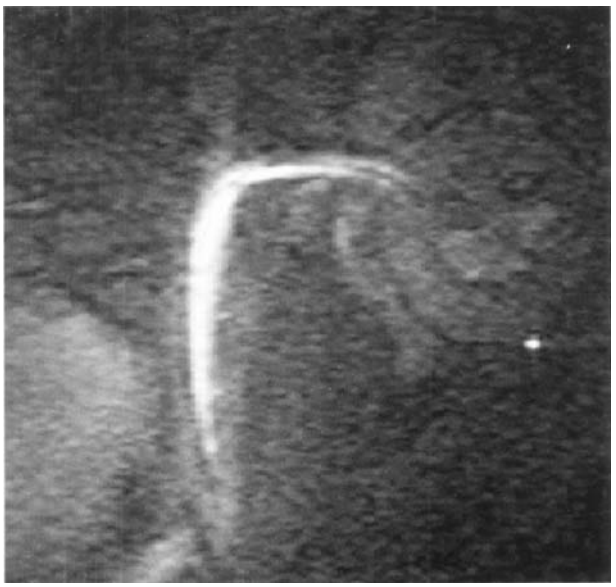

Figure 1. Left renal artery catheter engagement.

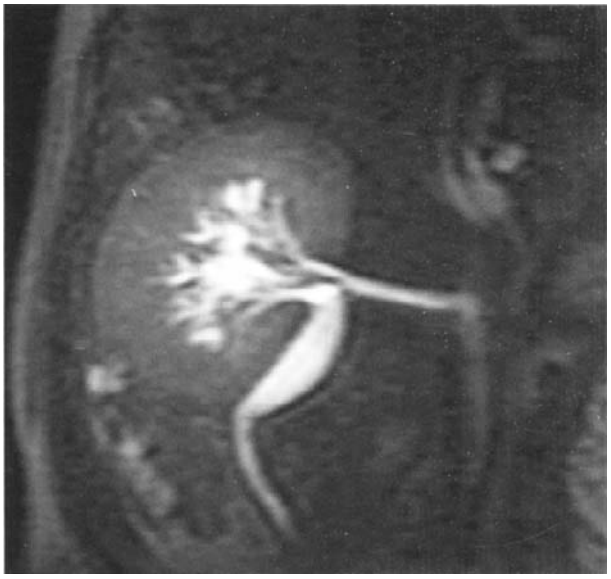

Figure 2. Right renal selective angiogram.

road-mapping. Enhanced visualization of the surrounding vessel or balloon may be obtained with an IVGC since its signal may be modified in amplitude or color separately from that of the surface coils. This may facilitate catheter and balloon tracking as well as permit high resolution endovascular arterial wall imaging.

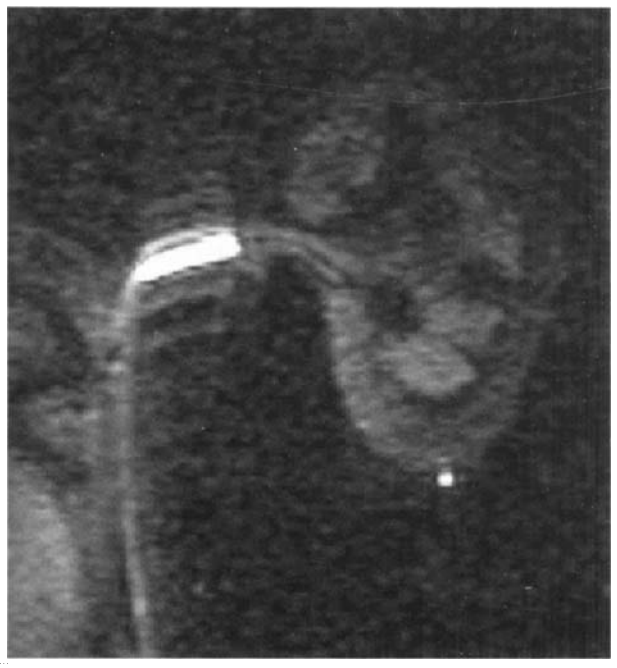

Figure 3. Left renal artery angioplasty.

Purpose: We report the feasibility of wholly rtMRI-guided intervention including catheter navigation, selective gadolinium (Gd–DTPA) MR angiography (rtSMRA) and balloon angioplasty, and high-resolution arterial wall imaging facilitated by an IVGC without roadmapping.

Methods: rtMRI was performed on a GE Signa 1.5T CV/i scanner (GE Medical Systems, Milwaukee, WI) with a custom data reconstruction engine, high-impedance phased-array surface coils (Nova Medical, Wakefield, MA) and in-room consoles (Aydin Displays, Horsham, PA). In 5 farm swine, a 0.030" loopless guidewire coil (Surgi-Vision, Gaithersburg, MD) was directed via percutaneous femoral or carotid arterial access using preformed non-metallic catheters into renal, mesenteric, coronary and contralateral iliac arteries solely using rtMRI guidance. Tandem IVGC/catheter movement permitted non-roadmapped navigation at 4–6 complete frames/s and 1.25 × 1.67 mm resolution using a fast gradient-recalled single-echo pulse sequence (FGRE). Navigation was assisted by the GE i-Drive interface with customizations for interactive control of saturation preparation, gating, channel scaling and coloring. Coronary, renal, mesenteric, and iliac arteries were engaged, and rtSMRA was conducted using 30 mM Gd–DTPA hand-injections and saturation-preparation, Cartesian and projection–reconstruction gradient echo sequences. Nonferrous 0.035" angioplasty balloons were positioned using the IVGC and inflated with 30 mM Gd–DTPA. In 3 pigs, iliac and femoral stenoses were created using vascular tape.

Results: IVGC enabled rtMRI navigation and selective engagement of the coronary, renal, mesenteric, and iliac arteries (Figure 1). rtSMRA delineated 2° and 3° branches and demonstrated parenchymal and venous phases (Figure 2). Proximal coronaries were engaged and visualized but mid- and distal vessels were not of diagnostic quality. IVGC-enhanced balloon positioning was achieved with 1.25 × 1.67 mm in-plane resolution. Balloon position, inflation profile, and caliber were visualized irrespective of vessels' alignment with Bo. Multiple aorto-ostial and proximal inflations were achieved. Gd–DTPA filled balloons were readily visualized during inflation (Figure 3). Stenoses were crossed with guidewire coils and angioplasty balloon using rtMRI, which visualized a balloon "waist" and even oversized balloon "melon seeding" during inflation. In 2 swine, balloon trauma to vessel wall was demonstrated using the guidewire coil to obtain high-resolution black blood vessel wall images using a fast spin-echo sequence before and after balloon inflation. The resolution achieved was 0.16 mm2 but image quality was dependent on perpendicular slice acquisition at the point of maximal signal along the IVGC and IVGC alignment to within approximately 30° of Bo.

Conclusion: An intravascular loopless guidewire coil permits wholly rtMRI-guided catheter tracking, selective arteriography, and percutaneous "angioplasty" of medium caliber arteries in swine. The high signal over a much longer length is an important improvement over previous passively or actively tracked MR imaging guide wires.2 Tandem catheter movement with an IVGC facilitates navigation and selective arteriography under rtMRI. Advantages of rtSMRA over non-invasive MRA include continuous scanning, time separation of venous and parenchymal enhancement, ability to visualize

more distal branches, motion insensitivity, and ability to perform multiple low-dose contrast injections. Vascular wall imaging is improved with this IVGC, but limited by the necessity to align with the magnetic field. Further development is necessary for satisfactory human rtMRI angioplasty.

140. MR-Venography Using High Resolution Balanced FFE

Elmar Spuentrup,[1] Arno Buecker,[2] Matthias Stuber,[1] Rolf W. Günther.[2] [1]*Beth Israel Deaconess Medical Center, 330 Brookline Avenue, Boston, Massachusetts United States;* [2]*Department of Diagnostic Radiology, Technical University of Aachen, Pauwelsstrasse 30, Aachen, NRW Germany*

Introduction: Improved gradient performance as now available on clinical MR-scanners enabled short TR and TE for high resolution Balanced-FFE (also referred to steady state free precession or True-FISP) sequences.

Purpose: We hypothesized that the high spatial resolution in conjunction with the intrinsic high signal of blood independent of flow makes Balanced FFE a potentially favorable imaging sequence for MR-venography. Furthermore, rapid data acquisition in Balanced- FFE sequences may allow for examination of the pelvis and lower extremities with continuous axial slices in a reasonable short data acquisition time.

Methods: High resolution Balanced-FFE MR-Venography was performed on a clinical 1.5T Philips ACS-NT MR unit equipped with a Powertrack 6000 gradient system (23 mT/m, 219 ms rise time). Sequence parameters included TR/TE = 5.0/2.5 ms, FA 85°, 512 × 512 matrix, 440 mm FoV. Six mm thick axial slices were acquired from the inferior vena cava to the proximal portion of the crus using a 4–5 element synergy or the body coil. Data were acquired during free-breathing and without cardiac triggering. Total MR data acquisition time was less than 10 min. 35 patients with in total 42 thromboses (vena cava (n = 10), iliac veins (n = 9), superficial/common femoral vein (n = 12) or popliteal/crus veins (n = 11)) were examined. Conventional x-ray phlebography, CT or ultrasound was available for comparison. Thrombus head localization was analyzed by 2 investigators and contrast-to-noise ratio between the thrombus and the blood pool was measured.

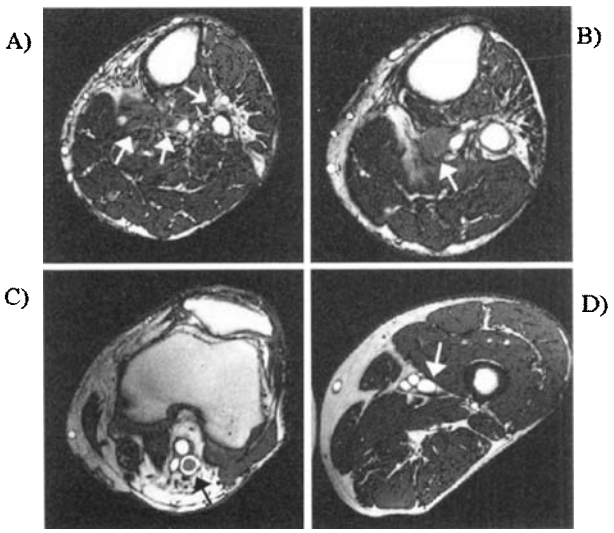

Figure 1. High solution Balanced-FFE MR-venography in a 75 y old male patient with a low signal free floating thrombus head in the popliteal vein (C) and occlusion more distally (A,B). Normal (bright) femoral vein (D).

Results: In 35 patients 42 thromboses were correctly detected and localized on the high resolution Balanced FFE MR-venography (figure) with a high contrast-to-noise ratio of >40.

Conclusion: The presented MR-venography using high resolution Balanced-FFE allows for fast high-resolution and high-contrast visualization of deep vein thrombosis.

141. A Morphological Classification Scheme for Atherosclerotic Lesions in Carotid Artery by MRI Using Histological Classification as Reference

Jianming Cai,[2] Marina Ferguson,[3] Thomas Hatsukami,[4] Chun Yuan.[4] [1]*PLA General Hospital, Department of Radiology, Beijing, China;* [2]*Dept. of Radiology, Box 357115, University of Washington, 1915 NE Pacific St, Seattle, WA 98195-7115, USA;* [3]*Marina Ferguson Inc, Seattle, 7032 14th Ave NW,, Seattle, Washington, USA;* [4]*University of Washington, Veterans Affairs Puget Sound Health Care System, Seattle Division, Seattle, Washington, United States*

Purpose: We have developed a high-resolution MRI technique that can identify the fine structure of the lesion in vivo of human carotid artery[1–3]. The aim of this study was to determine a morphological lesion type classification for atherosclerotic plaque by MRI using histological classification scheme developed based on AHA guidance [4].

Methods: Sixty subjects who were scheduled for carotid endarterectomy (CEA) underwent MRI with 2D black blood axial imaging of three contrast weightings (T1W, T2W and PDW), 3D Time-of-Flight protocol, and Gd-enhanced T1W imaging. Plaques were removed en bloc during the CEA and processed for histological evaluation. Lesion types from type I to VIII (AHA) were identified histologically and their corresponding MR images reviewed for tissue features independently. The k values were determined to measure the level of agreement between MRI and histology classification of the lesion type.

Results: There is a high level of agreement between MRI and histological findings for isolated extracellular lipid pools added (type III), confluent extracellular lipid core formed (lesion type IV), fibromuscular tissue layers produced (type V), surface defect, hematoma, thrombosis (type VI), calcification predominates (type VII) and fibrous tissue changed predominate (type VIII): 85% agreement, k (95%CI) = 0.80 (0.66 to 1.0), weighted k = 0.85. Lesion type I (isolated macrophage foam cells) and type II (multiple foam cell layers formed) usually showed normal wall thickness and signal intensity on MRI.

Conclusion: High-resolution MRI is capable of classifying intermediate to advanced atherosclerotic lesion types in carotid artery, and of distinguishing early lesions from intermediate and advanced lesions. MRI could noninvasively examine the regression and progression of carotid artery atherosclerotic plaque.

142. Magnetic Resonance Imaging of the Brain at 1.5 Tesla in Patients with Cardiac Pacemakers: Can It Be Done?

Alexandra Schmiedel,[1] Matthias Hackenbroch,[1] Marcus Reinke,[1] Alexander Yang,[1] Rainer Schimpf,[1] H. Schild,[1] Torsten Sommer.[1] [1]*University of Bonn, Germany, Sigmund Freud Strasse 25, Bonn, NRW Germany*

Introduction: Magnetic resonance (MR) imaging is probably the most important imaging modality for the diagnosis of cerebral diseases. Most MR scanners in the Western World operate at a field strength of 1.5 T. The potential effects of magnetic resonance imaging on cardiac pacemakers (PM) are multiple. Especially at a field strength of 1.5 T, the presence of a PM is considered to be a strict contraindication to MR imaging in the vast majority of medical centers. The main concerns of MR imaging at 1.5 T compared to 0.5 T are 1. heating of the PM leads since the power absorption in a linear antenna is proportional to the square of the frequency of the radio-frequency (RF) field, and 2. inhibition or triggered stimulation of PM output due to pulsed gradient magnetic fields mimicing intrinsic cardiac activity.

Purpose: To evaluate safety and feasibility of MR imaging of the brain at 1.5 Tesla in patients with implanted PM.

Methods: In vitro testing of electrodes and pacemakers:

25 PM models and 48 PM electrodes were exposed in vitro to MR imaging (Intera, Philips Medical Systems, Best, The Netherlands, 1.5 Tesla, maximum magnetic field gradient 30 mT m-1, maximum slew rate 120 T m-1 s-1) with continuous registration of PM output and temperature at the lead tip by using a fibro-optic temperature probe. MR imaging sequences producing a whole-body-averaged Specific Absorption Rate (SAR) of 3.9 W/kg (worst case scenario) and 1.2 W/kg (upper limit for most standard sequences used at routine examinations at our MR unit), respectively, were applied. All measurements were performed in the expected position of the PM and PM leads within the magnetic bore during an MR exam of the brain.

Patient examinations:

48 patients with implanted PM and strong clinical need for diagnostic information underwent a total of 57 MRI exams of the brain. Patients, who were dependent on PM were excluded. MRI was performed under cardiological surveillance, continuous ECG, pulse oximetry, and capnography monitoring using a MR-compatible monitoring device (Maglife C, Bruker, Wissembourg, France). Prior to the MR exam PMs were programmed to an asynchronous mode (A00, V00 or D00) to prevent artificial inhibition and/or triggering. Evaluation of all programmed and measured pacemaker parameters, including assessment of lead impedance, battery voltage and pacing threshold was performed immediately before and after MR imaging and at 3-months follow-up.

To reduce the risks of thermal injuries during MR imaging the RF exposure was restricted to the whole-body-averaged maximum SAR of 1.2 W/kg, the imaging time of each sequence was restricted to 10 minutes, and a pause of 5 minutes was established between each sequence to allow the lead tips to cool.

Results: In vitro testing of electrodes and pacemakers:

The maximum temperature rise at a SAR level of 3.9 W/kg varied depending on the electrode type between 0.1°C and 3.5°C (mean 0.4° C). At lower radio frequency (RF) exposure with SAR levels of 1.2 W/kg the electrode specific maximum temperature rise was between 0°C and 0.9 °C (mean 0.1°C).

Reed switch activation due to the static magnetic field resulting in fixed pacing in the asynchronous mode at the PM specific magnet rate was observed in all cases when PMs were approached to the MR scanner. However, there was a deactivation of the reed switch in 18 out of 25 PM within the center of the magnetic resulting in inhibition and/or triggered stimulation of PM. No changes occurred to the programmed parameters of all devices tested. The ability to fully interrogate each device remained preserved. At the conclusion of MRI all PMs continued to operate normally.

Patient examinations:

No patient reported a torque or heating sensation or other unusual symptoms during MR imaging. In all PMs the reed switch was activated by the static magnetic field in the surroundings of the MR scanner. In 28 MRI exams (51%) the reed switch remained closed during the complete MR exam resulting in asynchronous stimulation at the PM model specific magnet rate. In 29 MRI exams (49%) the reed switch was again deactivated when the patient was positioned in the magnet bore resulting in asynchronous pacing (A00, V00 or D00) at the programmed intervention rate. Thorough analysis of ECG did not reveal any rhythm perturbation. Particularly, no rapid pacing occurred. MRI affected neither programmed data of PM, nor the feasibility of interrogating, programming, or telemetry. Comparing the results of the PM inquiries obtained prior to MRI, immediately after completion of MRI and at 3-months follow-up, battery voltage (2.84 ± 0.06 V vs 2.83 ± 0.07 V vs 2.84 ± 0.07 V), pacing thresholds (0.21 ± 0.14 ms vs 0.20 ± 0.16 ms vs 0.20 ± 0.16 ms), and lead impedance (648 ± 200 Ω vs 635 ± 190 Ω vs 643 ± 229 Ω) did not change significantly ($p > 0.05$).

Conclusion: MR imaging of the brain at 1.5 T may pose a potential serious risk due to gradient field induced inhibition or triggered stimulation of pacemaker output which may occur as the Reed switch is not necessarily deactivated within the center of the static magnetic field. This problem can be avoided by programming the PM to an asynchronous mode prior to the MR imaging examination.

Increases in temperatures at the lead tips that are large enough to raise concerns about safety are unlikely to occur during MR imaging of the brain at 1.5 T, as only a small part of the transmitted RF power is transmitted into the pacemaker leads.

In summary, we conclude that MR imaging of the brain at 1.5 T in patients with implanted cardiac pacemakers can be safely performed in carefully selected clinical circumstances

when appropriate strategies (programming to asynchronous mode, adequate monitoring techniques, limited RF exposure) are used.

143. Effects of Magnetic Resonance Imaging on Cardiac Pacemakers: In Vitro Evaluation and Safe Performance on 62 Patients at 0.5 Tesla

Alexandra Schmiedel,[1] Marcus Reinke,[1] Matthias Hackenbroch,[1] Christian Vahlhaus,[1] Rainer Schimpf,[1] H. Schild,[1] Torsten Sommer.[1] [1]*University of Bonn, Germany, Sigmund Freud Strasse 25, Bonn, NRW, Germany*

Introduction: In the last years there has been a number of publications (1–5) - reporting safe performance of magnetic resonance imaging (MRI) studies at field strengths between 0.35 and 1.5 T on patients with more advanced cardiac pacemakers (PM). However, these studies were small, mostly case reports or collectives up to five patients and no consistent strategy was evaluated.

Purpose: In this prospective study safety and feasibility of MRI in patients with implanted PMs was evaluated in vitro and in vivo.

Methods: In vitro testing of electrodes and pacemakers:

21 PM models and 44 PM electrodes were exposed in vitro to MRI (Gyroscan T5II, Philips Medical Systems, Best, The Netherlands, 0.5 Tesla, maximum magnetic field gradient 10 mT m-1 with a maximum slew rate of 6.8 T m-1 s-1) with continuous registration of PM output and temperature at the lead tip by using a fibro-optic temperature probe. MR imaging sequences producing a whole-body-averaged Specific Absorption Rate (SAR) of 1.3 W/kg and 0.6 W/kg, respectively, were applied. All measurements were performed in the center and at the edge of the gradient and RF fields.

Patient examinations:

53 Patients with implanted PM underwent a total of 62 MRI exams under cardiological surveillance, continuous ECG, pulse oximetry, and capnography monitoring using a MR-compatible monitoring device (Maglife C, Bruker, Wissembourg, France). Patients who were dependent on PM were excluded from MR imaging. Prior to the MR exam PMs were programmed to an asynchronous mode A00, V00 or D00). Evaluation of all programmed and measured pacemaker parameters, including assessment of lead impedance, battery voltage and pacing threshold was performed immediateley before and after MR imaging and at 3-months follow-up. To evaluate reed switch function within the static magnetic field prior to MR imaging, patients unterwent continuous electrocardiography (ECG) in the position for subsequent MR imaging in the magnet bore.

To reduce the risks of thermal injuries during MR imaging the RF exposure was restricted to the whole-body-averaged maximum SAR of 0.6 W/kg, the imaging time of each sequence was restricted to 10 minutes, and a pause of 5 minutes was established between each sequence to allow the lead tips to cool.

Results: In vitro testing of electrodes and pacemakers:

In all tested electrodes the highest temperature rise in dependence on lead loop position in the magnet bore during MRI exposure was measured when the loop was placed at or near the center of the body coil. The maximum temperature rise in the worst case position at a SAR of 1.3 W/kg varied considerably dependent on the electrode type between 0.1°C and 23.5°C (mean 4.68°C). Proceeding farther away from the center and towards the ends of the body coil there was a distinct decline of heating effects with electrode specific maximum values between 0°C and 1.55°C at the edge of the coil.

At lower radio frequency (RF) exposure with SAR levels of 0.6 W/kg the electrode specific maximum temperature rise in the worst case position was between 0°C and 8.95°C (mean 1.79°C).

Reed switch activation due to the static magnetic field resulting in fixed pacing in the asynchronous mode at the PM specific magnet rate was observed in all cases when PMs were approached to the MR scanner. However, there was a deactivation of the reed switch within the center of the magnetic bore in 8 out of 21 PM resulting in inhibition and/or triggering of PM output during MR imaging. No changes occurred to the programmed parameters of all devices tested. The ability to fully interrogate each device remained preserved. At the conclusion of MRI all PMs continued to operate normally.

Patient examinations:

No patient reported a torque or heating sensation or other unusual symptoms during MR imaging. In all PMs the reed switch was activated by the static magnetic field in the surroundings of the MR scanner. In 42 MRI exams (68%) the reed switch remained closed during the complete MR exam resulting in asynchronous stimulation at the PM model specific magnet rate. In 20 MRI exams (32%) the reed switch was again deactivated when the patient was positioned in the magnet bore resulting in asynchronous pacing at the programmed intervention rate.

Thorough analysis of ECG did not reveal any rhythm perturbation Particularly, no rapid pacing occurred. MRI affected neither programmed data of PM, nor the feasibility of interrogating, programming, or telemetry. Comparing the results of the PM inquiries obtained prior to MRI, immediately after completion of MRI and at 3-months follow-up, battery voltage (2.76 ± 0.05 V vs 2.76 ± 0.05 V vs 2.76 ± 0.05 V), pacing thresholds (0.19 ± 0.14 ms vs 0.19 ± 0.14 ms vs 0.18 ± 0.14 ms), and lead impedance ($638 \pm 202\,\Omega$ vs $631 \pm 199\,\Omega$ vs $641 \pm 211\,\Omega$) did not change significantly ($p > 0.05$).

Conclusion: Our data indicate that MR imaging at 0.5 T may pose a potential serious risk due to

1. RF induced thermal injury at the lead tips, depending of a) the specific model of the lead, b) the SAR level of the MR imaging sequence and c) the position of the lead loop in the RF coil, and
2. gradient field induced inhibition or triggered stimulation of pacemaker output which may occur as the Reed switch is not necessarily deactivated within the center of the static magnetic field.

However, we conclude that MR imaging at 0.5 T in patients with implanted cardiac pacemakers can be safely performed in carefully selected clinical circumstances when appropriate strategies (programming to asynchronous mode, adequate monitoring techniques, limited RF exposure) are used.

144. Percutaneous Endomyocardial Injection Using Real-Time Magnetic Resonance Imaging

Robert Lederman,[1] Michael Guttman,[1] Dana Peters,[1] Richard Thompson,[1] Jonathan Sorger,[1] Alexander Dick,[1] Venkatesh Raman,[1] Elliot Mcveigh.[1] [1]*National Institutes of Health, Building 10, Room B1 D219, Bethesda, Maryland, United States*

Introduction: Real-time MRI (rtMRI) is an attractive alternative to fluoroscopic X-ray to guide novel cardiovascular therapeutic procedures. The ability to image both blood and soft-tissue spaces well might enable targeted intramural delivery of cellular and pharmacologic agents

Purpose: We explore the feasibility of in vivo spatially-targeted trans-catheter left ventricular wall injection guided by real-time MRI.

Methods: We used a GE Signa CV/i 1.5 T MRI scanner with a fast reconstruction engine capturing raw scanner data to an external workstation previously described [1]. The GE real-time slice navigation interface was customized with real-time interactive controls including optional individual channel gain, individual channel coloring, non-selective saturation preparation, ECG gating, multi-slice acquisition, and volume rendering. Monitors and keyboards were located in the scanner room for image-guidance of the procedures.

Coaxial trans-femoral guiding catheters were custom modified as an intravascular receiver coil (Boston Scientific, Plymouth, Minnesota) and a spring-loaded needle device was customized for MRI compatibility (Stiletto™, Boston Scientific).

Imaging parameters were SSFP which generated 4 completely refreshed frames/s using a 128 × 96 matrix, FOV 32 × 24 cm, partial Fourier, and slice thickness 7 mm. Injections used Gd–DTPA 30 mM diluted with saline to be iso-osmolar. Experiments were conducted in 5 farm swine. X-ray fluoroscopy was readily available but was not used.

Results: Figure 1 below shows a typical pair of injections. [A] The cardiac chambers and LV myocardium are outlined. The LV guiding catheter is outlined in grey. [B] The guiding catheter is pointed at the interventricular septum. [C] The Stilletto is extended beyond the guiding catheter and makes contact with the apical septum. [D] Saturation preparation darkens the background to enhance visualization of injected Gd–DTPA. The first injection is shown in white and indicated by the arrow. [E] The guide is withdrawn proximally and the Stilletto is extended a second time, injecting a second time in the same imaging plane more proximally along the interventricular septum. Arrows indicated the first and second injection sites. [F] Even after saturation preparation is stopped, injectate persists and is readily visualized as focal intramural depositions.

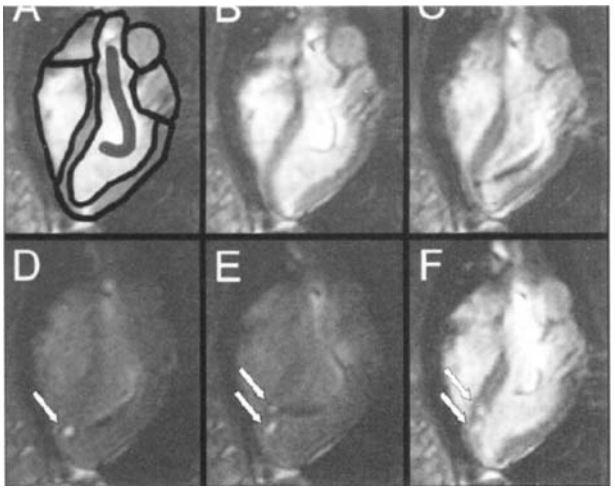

Figure 1.

The "active" GCC and "passive" Stilletto were readily visualized, and all 16 myocardial segments were easily accessed. 78% of 51 injections were successful using this 1st generation device. Orthogonal views showed injectate dispersion was often non-spherical, possibly reflecting fiber orientation.

Conclusion: Percutaneous transcatheter endomyocardial drug delivery is readily feasible using rtMRI, and permits precise 3-dimensional localization of injection within the LV wall. rtMRI may soon prove a useful addition to the therapeutic cardiovascular armamentarium.

145. Transcatheter Closure of an Atrial Septal Defect Under Real Time MRI Guidance

Carsten Rickers,[1] Michael Jerosch-Herold,[1] Sudong Hu,[1] Huafu Kong,[1] Myra Urness,[1] Norbert Wilke.[1] [1]*University of Minnesota, MMC#292, Mayo, 420, Delaware St SE, Minneapolis, Minnesota, United States*

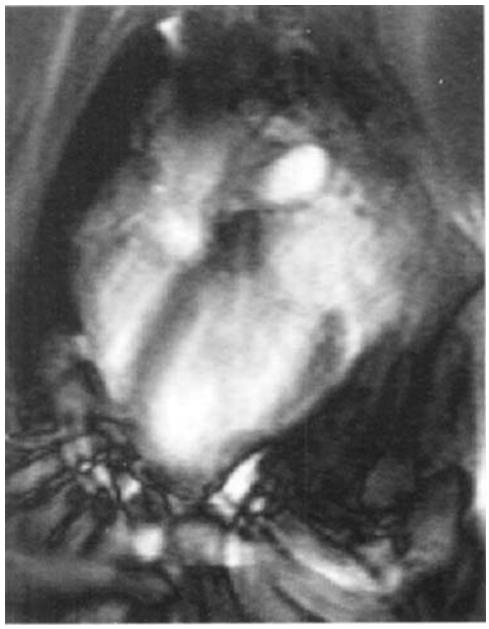

Figure 1. Correct position of an amplatzer ASD occluder.

Introduction: Drawbacks of conventional x-ray guided catheter interventions in pediatric cardiology include radiation exposure, a poor soft tissue contrast and the inability to aquire three-dimentional cross-sectional views.

Purpose: For the first time we assessed the feasibility and safety of MRI guided transcatheter closure of an artificially created secundum atrial septal defect (ASD) with the Amplatzer device (AGA medical) using an intravascular antenna guidewire (Surgi-vision) in a porcine model.

Methods: In two healthy farm pigs a 14 mm ASD was created by percutaneous balloon dilatation of the fossa ovalis. The animals were transported under general anaesthesia to a dedicated cardiac MR-scanner (SIEMENS, Sonata). Anatomical imaging was performed to determine the exact location and diameter of the ASD. The device was selected according to the ASD diameter. For improved catheter tracking and high resolution intravascular imaging, miniature antenna guidewires (Surgi-Vision) were used. Under real-time MRI guidance (MR fluoroscopy with steady state free precession true FISP MR pulse sequence; 2–5 frames/sec) the introducer sheath was tracked towards the left atrium. Deployment of the device was monitored by high resolution real-time imaging (flip angle 60 degrees; 128 read-out points × 100 phase encodings; 300 mm field of view) with a temporal resolution of 320 ms. Following the procedure gradient echo cine and spin-echo anatomical imaging was applied to rule out any vascular or cardiac damage.

Results: Real-time MRI can be used to follow the position of an antenna guiding catheter within the inferior vena cava and the heart. The catheter tracking as well as the deployment of the left and the right atrial disc of the device could be monitored. No vascular or valvular damage was detected. Necropsy showed an excellent placement of the device in the area of the fossa ovalis. Current limitations of this method are caused by a time delay between image acquisition and image display that will be overcome with faster computer hardware and software for image reconstruction, steering of the catheter,and readjustment of the slice position and orientation to track the catheter.

Conclusion: These preliminary data suggest that a novel MR guided transcatheter ASD closure is feasible under real-time and high resolution MRI. The results of this ongoing study are the basis for further experimental trials and developments of devices for MRI-guided cardiovascular catheter interventions.

146. Phenotypic Characterization of Occult Myocardial Dysfunction in *mdx* Mice with Muscular Dystrophy by MRI Tagging

Xin Yu,[1] Wei Liu,[1] Junjie Chen,[1] R. Mark Grady,[2] Samuel A. Wickline.[1] [1]*Cardiovascular MR Laboratories, Washington University School of Medicine, St. Louis, MO, USA;* [2]*Department of Pediatrics, Washington University School of Medicine, St. Louis, MO, USA*

Introduction: Duchenne muscular dystrophy (DMD) is one of the most common neuromuscular disease in humans. It results from the failure to express dystrophin, a cytoskeletal protein that is part of a complex that links the cytoskeleton to the extracellular matrix. The *mdx* mouse, in which a nonsense mutation in the dystrophin gene eliminates expression of the dystrophin, is a model of this disorder. However, overt heart failure from cardiomyopathy is virtually absent in *mdx* mice whereas nearly all DMD patients have clinical evidence of a cardiomyopathy by 18 years of age.

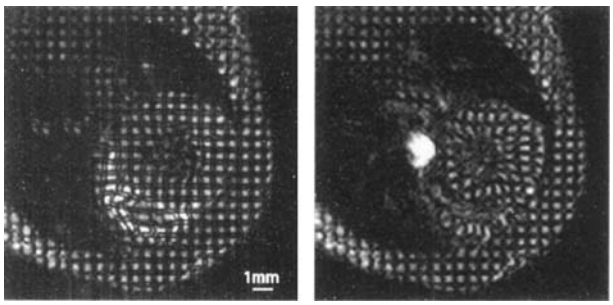

Figure 1. Diastolic and systolic tagged images of a mouse heart.

Purpose: Although no clinically detectable defects in cardiac function are present in *mdx* mice, whether other signs of myocardial dysfunction exist that preclude the manifestation of cardiomyopathy is unknown. In this study, ventricular function of *mdx* mice was characterized by MRI tagging to provide a more sensitive indicator of myocardial dysfunction.

Methods: Adult *mdx* mice (n = 4) and C57/BL6 mice (wild type, n = 4) were imaged on a Varian Inova 4.7 T scanner with a custom-made surface coil. Mice were sedated with isofluorine by a nose cone. Tagged images of three short-axis slices were acquired at basal, midventricular, and apical levels. The tagging sequence used a SPAMM1331 sequence applied twice immediately after ECG trigger, yielding a grid tagging pattern.

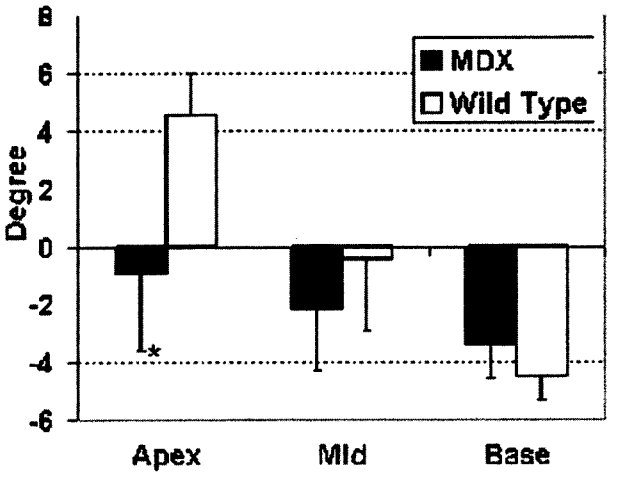

Figure 2. Net ventricular twist in *mdx* mouse and control. (*P < 0.05 compared to control)

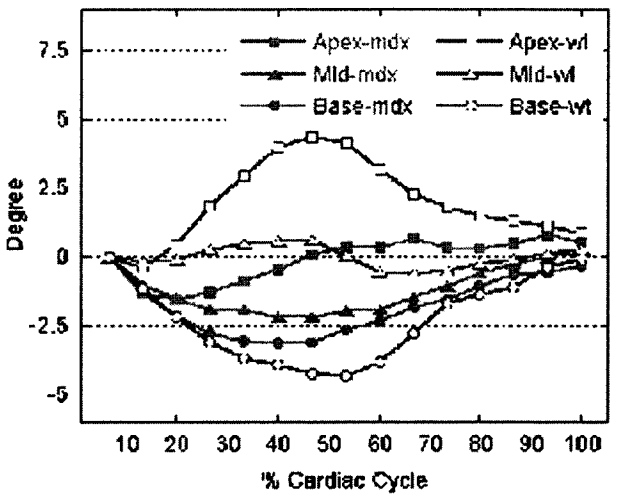

Figure 3. Time course of ventricular twist.

The tag pulse flip angle was 140 degrees and tagging resolution was 0.6 mm (Figure 1). The tagging sequence was followed by gradient-echo cine sequence with the following imaging parameters: TR/TE,10.7 ms/3 ms; FOV, $4 \times 4\,cm^2$; matrix size, 256×256; slice thickness, 1 mm. A total of 15 frames were acquired in one cardiac cycle.

Images were analyzed with MATLAB based software developed in our laboratory. Epicardial and endocardial boders, intersecting tag points were traced interactively. Subsequently, LV wall thickness, stroke volume, and ejection fraction were calculated. Finite element analysis method was employed to calculate ventricular twist and radial shortening. Myocardium was divided into non-overlapping triangular elements using sets of adjacent tag points as the vertices. LV twist was calculated as the rotation angle of the centroid of triangular element around the center of LV cavity. Positive twist value indicated clockwise twist viewed from base. Radial shortening was calculated as the displacement of the centroid of triangular element relative to the center of LV cavity. Positive radial shortening indicated inward motion.

Results: LV ejection fraction was equivalent in *mdx* and C57/BL6 mice: (66.9 ± 10.3)% for *mdx* mice and (68.3 ± 8.4)% for C57/BL6 mice (p = NS). Diastolic wall thickness was also similar. In *mdx* mice, radial shortening at apex, midventricle and base was similar: (0.42 ± 0.06) mm at apex, (0.38 ± 0.02) mm at midventricle, and (0.37 ± 0.06) mm at base. In C57/BL6 mice, maximal shortening occured at midventricle: (0.44 ± 0.09) mm at apex, (0.51 ± 0.04) mm at midventricle, and (0.32 ± 0.04) mm at base ($p < 0.05$ compared to midventricle). At midventricle, radial shortening in *mdx* mice was significantly smaller than that of C57/BL6 mice.

Compared to wild type mice, *mdx* mice exhibited a significantly altered pattern of ventricular twist (see Figure 2 and 3). In wild type mice, apex twisted clockwise while base twisted counterclockwise. The net twist at apex and base was of the same magnitude: 4.5° ± 1.4° at apex and −4.5° ± 0.8° at base. Twist at midventricular level was minimal (−0.4° ± 2.5°). However, in *mdx* mice, such heterogeneity in ventricular twist was not present. Instead, all three slices exhibited counterclockwise twist with the twist at apex being the smallest.

The time course of twist also was different for *mdx* mice (Figure 3). Early counterclockwise twist was maximal within the first third of the cycle, followed by slow recovery throughout the remainder of the cardiac cycle as compared to a more gradual development and resolution of twist in wild type mice.

Conclusion: Significant differences were observed in ventricular twist patterns in *mdx* mice despite lack of differences in traditional clinical indices of global cardiac function and anatomy. This study suggests that ventricular twist might be a sensitive marker for detecting myocardial dysfunction that could be applied clinically to define early and subtle defects in cardiac function in patients with muscular dystrophy. Such indices can only be obtained with MRI, which could render it a useful tool for phenotypic characterization of genetic diseases of the heart.

147. MR-Guided Coronary Artery Stent Placement in a Pig Model Using Interactive Real-Time Radial Balanced FFE

Elmar Spuentrup,[1] Alexander Ruebben,[1] Tobias Schaeffter,[2] Rolf W. Günther,[1] Arno Buecker.[1] [1]*Department of Diagnostic Radiology, Technical University of Aachen, Pauwelsstrasse 30, Aachen, NRW, Germany;* [2]*Philips Research Laboratories, Hamburg, Germany*

Introduction: While peripheral artery stent placement has been successfully performed under MR-guidance, MR-guided coronary artery stent placement is a much more challenging vascular intervention. The main hindrance toward MR-guided coronary artery stent placement is the small size of the coronary arteries and the inherent motion due to the respiratory and the cardiac cycle. This requires substantially faster and higher spatial resolution real-time MR-imaging techniques when compared to peripheral interventional MRA.

Purpose: The purpose of this study was to investigate the potential of interactive real-time MR-imaging for MR-guided coronary artery stent placement.

Methods: A new ultra fast interactive real-time MR-imaging technique (radial Balanced FFE (1), also referred to radial steady state free precession or radial True-FISP) which combines steady state free precession for high signal-to-noise ratio and radial k-space sampling for motion artifact suppression was implemented on a 1.5 T clinical whole body interventional MR-scanner. Sequence parameter were TR = 2.5 ms, TE = 1.2 ms, FA45°, 80 radials, 128×128 matrix, reconstructed to 256×256 pixel, 300 mm field-of-view, 2–5 elements of a cardiac synergy coil. Data were acquired without respiratory or cardiac triggering. Using a dedicated ultra fast reconstruction hardware (2) in conjunction with the sliding window reconstruction technique images were displayed online with a frame rate of 15 images/sec. Ten balloon-expandable stainless steel coronary stents were placed in 6 pigs (40–70 kg body weight) in both coronaries using a nitinol guidewire, passive device visualization and interactive

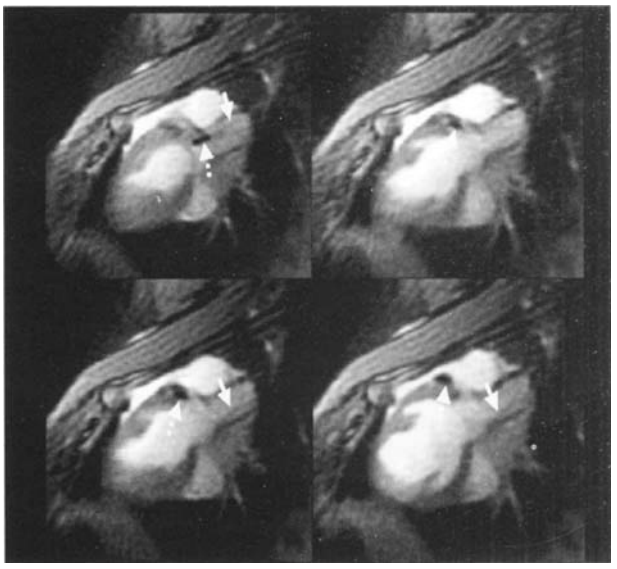

Figure 1. Real-time radial Balanced FFE images during coronary artery stent placement in the proximal LAD. The mounted stent is displayed with an artifact (dashed arrow) exceeding the that of the nitinol guidewire (arrows) allowing for stent visualization.

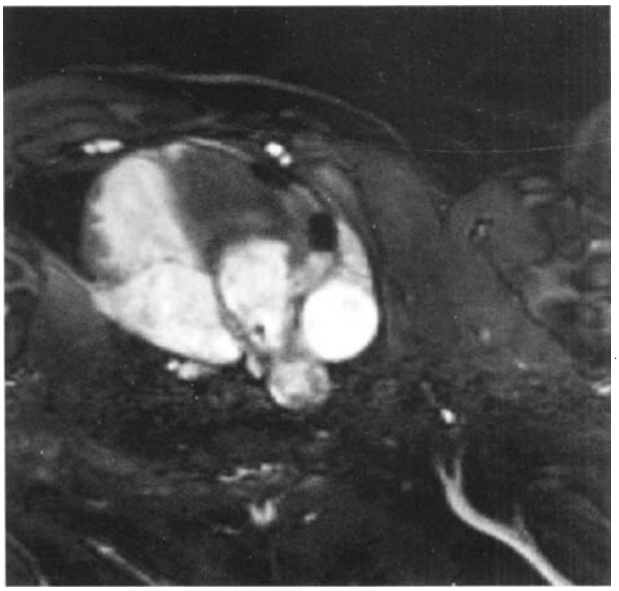

Figure 2. Double oblique fast 3D Balanced FFE coronary MRA scan in parallel to the left coronary artery after MR-guided placement of two stainless steel stents in the left coronary artery (arrows). Measurement time including navigator gating was < 2 min.

slice positioning. Positions of the employed coronary stents were proven by a fast navigator gated free-breathing double-oblique cardiac triggered 3D Balanced FFE coronary MRA sequence (3) and macroscopically on the ex-vivo heart.

Results: The presented real-time MR-imaging sequence reliably allowed for high quality coronary MR-fluroscopy without motion artifacts in all pigs. Nine of 10 coronary stents were correctly placed under MR-guidance (fig. 1 and 2). One stent dislodged backwards from the left coronary artery because of a too small balloon size. The stent dislocation was correctly predicted by real-time MR imaging.

Conclusion: The presented ultrafast interactive real-time MR-imaging technique allows for MR-guided coronary artery stent placement in a pig model.

148. Ischemic NHE Blockade Reduces Post-ischemic Calcium Overload

Michiel Ten Hove,[1] Jan Van Emous,[1] Cees Van Echteld.[2]
[1]*Interuniversity Cardiology Institute of the Netherlands, CardioNMR laboratory, Room G02.523, Utrecht, Netherlands;*
[2]*University Medical Center Utrecht, CardioNMR laboratory, Room G02.523, Utrecht, Netherlands*

Introduction: Blocking the cardiac Na^+/H^+-exchanger (NHE) during ischemia has been shown to be cardioprotective. The cardioprotective effect is thought to be achieved via reduced ischemic Na^+ overload leading to less reversed Na^+/Ca^{2+}-exchange upon reperfusion resulting in reduced post-ischemic Ca^{2+} overload. In this study we tested the effect of ischemic inhibition of the NHE on $[Na^+]_i$, pH_i, $[Ca^{2+}]_i$ and post-ischemic contractile recovery in isolated rat hearts, using two different NHE-blockers: cariporide and eniporide.

Purpose:

Methods: Isolated rat hearts were perfused according to Langendorff at a constant pressure of 73.5 mmHg at 37°C with a modified Krebs–Henseleit buffer (pH 7.4) with glucose as substrate and paced at 5 Hz. Left ventricular developped pressure (LVDP) and end diastolic pressure (EDP) were measured with a left ventricular balloon. EDP was set to 6.4 mmHg. $[Na^+]_i$ and pHi were measured using simultaneous ^{23}Na and ^{31}P NMR spectroscopy. $TmDOTP^{5-}$ (3.5 mM) was

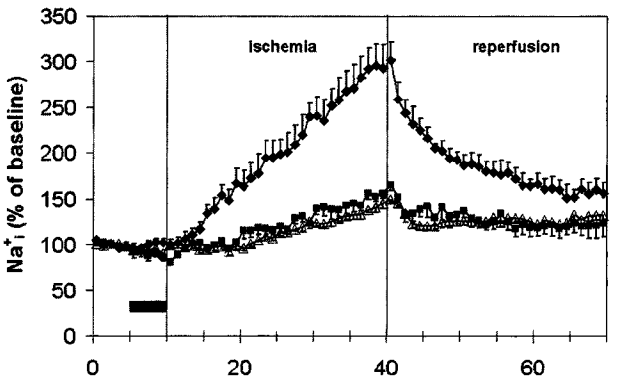

Figure 1. $[Na^+]_i$ during ischemia and reperfusion.

used to discriminate between intra- and extracellular Na^+, necessatating a lower free $[Ca^{2+}]$ (0.85 mM). $[Ca2^+]_i$ was measured in a different set of experiments using indo-1 surface fluorometry with λ_{exc}. 359 nm and λ_{em}. 385 & 456 nm. Cells were loaded by perfusing the hearts with indo-1 AM added to the perfusate. An optic fiber was placed against the left ventricle. The ratio of the intensity of the emmited light at 385 nm and at 456 nm is proportional to the $[Ca^{2+}]_i$. Since changes in pH_i alter spectral characteristics of Indo-1 the ratio as % of baseline values is used as an indication of the $[Ca^{2+}]_i$ and data on ischemia are not shown. NHE-blockers (3 μM) were administered 5 minutes prior to 30 minutes of global ischemia followed by 30 minutes of drug-free reperfusion.

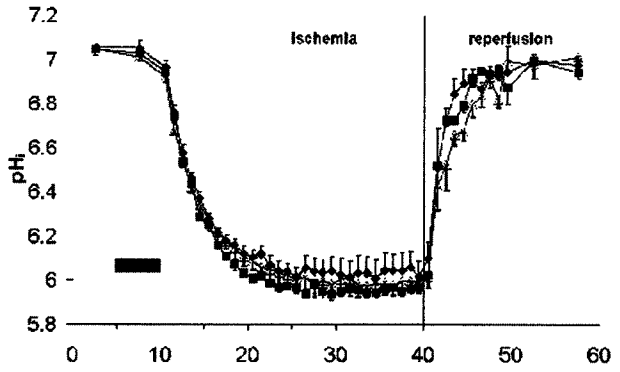

Figure 2. pH_i during ischemia and reperfusion.

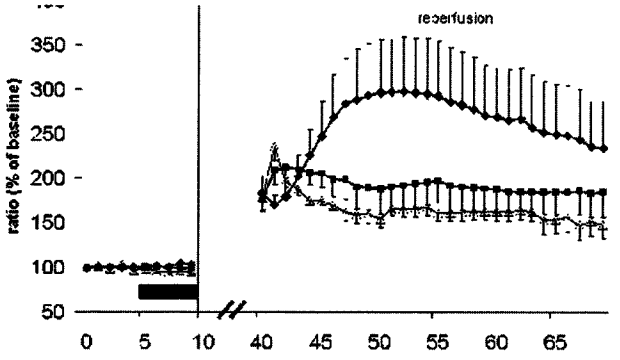

Figure 3. End-diastolic $[Ca^{2+}]_i$ presented as ratios; pre-ischemic and during reperfusion.

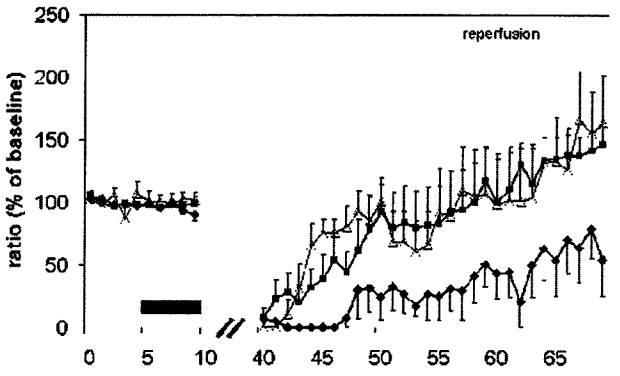

Figure 4. $[Ca^{2+}]_i$ transients presented as ratios; pre-ischemic and during reperfusion.

Results: NHE blockade reduced ischemic Na^+ overload, delayed the recovery of pH_i during reperfusion, resulted in a better recovery of $[Ca^{2+}]_i$ transients and reduced post-ischemic Ca_i^{2+} overload, reflected in lower diastolic $[Ca^{2+}]_i$. Results on $[Na^+]_i$, pH_i and $[Ca^{2+}]_i$ are shown in figures 1–4. After 30 minutes of reperfusion RPP amounted to 73 ± 10, 118 ± 14 ($p < 0.05$) and 142 ± 31 % of baseline values ($p < 0.05$) in untreated, cariporide and eniporide treated hearts, respectively, and EDP was 36.4 ± 4.1, 30.0 ± 5.7 ($p < 0.05$) and 21.3 ± 3.6 ($p < 0.05$) mmHg in untreated and cariporide and eniporide treated hearts, respectively.

Conclusion: Both, cariporide and eniporide, effectively reduced ischemic Na^+ overload and post-ischemic $Ca2^+$ overload and improved post-ischemic contractile recovery. The delayed recovery of pHi upon reperfusion indicates that the NHE is still (partly) inhibited by that time, probably via incomplete washout. This idea is supported by the fact that eniporide, reportedly the most potent blocker, showed the most pronounced delay. The reduction in $Ca2^+$ overload can be explained by reduced reversed Na^+/Ca^{2+}-exchange, due to 1. reduced ischemic Na^+ overload, 2. diminished NHE-mediated Na^+ influx upon reperfusion, 3 direct inhibition of the Na^+/Ca^{2+}-exchanger protein by the prolonged acidosis.

149. Combined Blockade of the Sodium Channel and the NHE Virtually Prevents Ischemic Sodium Overload

Michiel Ten Hove,[1] Cees Van Echteld.[2] [1]*Interuniversity Cardiology Institute of the Netherlands, CardioNMR Laboratory, Room G02.523, Utrecht, Netherlands;* [2]*University Medical Center Utrecht, CardioNMR Laboratory, Room G02.523, Utrecht, Netherlands*

Introduction: Either, blocking the Na^+-channel or blocking the Na^+/H^+-exchanger (NHE) has been shown to reduce Na^+ and Ca^{2+} overload during ischemia and reperfusion and to improve post-ischemic contractile recovery.[1,2] The effect of combined blockade of both Na^+ influx routes on ionic homeostasis is unknown.

Purpose: In this study the effect of combined blockade of the Na^+-channel and the NHE using lidocaine and eniporide, respectively, during ischemia on $[Na^+]_i$, pH_i and contractile recovery was studied in isolated rat hearts.

Methods: Isolated rat hearts were perfused according to Langendorff at a constant pressure of 73.5 mmHg at 37°C with a modified Krebs–Henseleit buffer (pH 7.4) with glucose as substrate and were paced at 5 Hz. Left ventricular developed pressure (LVDP) and end diastolic pressure (EDP) were measured with an intraventricular balloon. $[Na^+]_i$ and pH_i were measured using ^{23}Na and ^{31}P NMR spectroscopy, respectively. ^{23}Na and ^{31}P were measured simultaneously at frequencies of

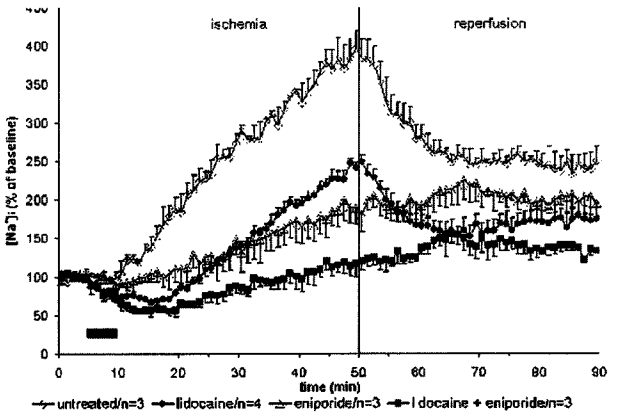

Figure 1. $[Na^+]_i$ during ischemia and reperfusion

105.9 and 162.0 MHz, respectively, on a Bruker Avance DRX400 spectrometer. ^{23}Na spectra were acquired by adding 144 FID's using 90° pulses and a 208 ms interpulse delay. ^{31}P spectra were acquired by adding 12 FID's using 90° pulses and a 2.5 s interpulse delay. ^{31}P and ^{23}Na spectra were both collected with a time resolution of 30 s and processed with a time resolution of 1 min. To discriminate between intra- and extracellular Na^+, the shift reagent TmDOTP5 − (3.5 mM) was added to the perfusate, necessitating a lower free Ca^{2+} concentration (0.85 mM). To block the NHE and the Na^+-channel, eniporide (3 μM) and lidocaine (200 μM), respectively, were administered during 5 minutes immediately prior to 40 minutes of global ischemia and 40 minutes of drug-free reperfusion. Data are presented as mean ± SEM. Hearts were divided in 4 experimental groups: untreated hearts, hearts treated with eniporide, hearts treated with lidocaine and hearts treated with both eniporide and lidocaine.

Results: During ischemia untreated hearts showed a rise in $[Na^+]_i$ to 397 ± 22 % of baseline values. During perfusion with lidocaine the $[Na^+]_i$ and the rate pressure product (RPP) decreased. During ischemia the decrease in $[Na^+]_i$ persisted for about 10 minutes followed by a rise in $[Na^+]_i$ to 241 ± 6 % of baseline values. Eniporide reduced ischemic $[Na^+]_i$ overload, end-ischemic $[Na^+]_i$ was 188 ± 21 % of baseline values. Combined administration of both drugs resulted in a summation of the effects found in the lidocaine and eniporide group, respectively; during drug perfusion $[Na^+]_i$ decreased, persisting for about 10 minutes during ischemia, followed by a reduced rise in $[Na^+]_i$ compared to the lidocaine group. End ischemic $[Na^+]_i$ was 117 ± 17 % of baseline values. During reperfusion the $[Na^+]_i$ decreased rapidly in untreated and lidocaine treated hearts. Hearts treated with eniporide did not show a decrease in $[Na^+]_i$ during reperfusion. Hearts treated with both eniporide and lidocaine showed a rise in $[Na^+]_i$ during reperfusion. Results are shown in figure 1. Administration of lidocaine, alone and in combination with eniporide, resulted in a slower development of acidosis. End ischemic pH_i and realkalanization did not show significant differences, probably due to limmited numbers of experiments. In general, recovery of RPP and EDP inversely correlates with end-ischemic $[Na^+]_i$.

Conclusion: Combined blockade of the Na^+-channel and the NHE results in a summation of the effects on $[Na^+]_i$ of blocking either the Na^+-channel or the NHE. The Na^+-channel mediates Na^+ influx mainly during the first minutes of ischemia, whereas the NHE starts to contribute substantially to ischemic Na^+ influx after 5 − 10 minutes of ischemia. The slower development of acidosis in lidocaine treated hearts has been reported before[1] and can be explained by reduced ATP consumption by the Na^+/K^+-ATPase during the first 10 minutes of ischemia.

150. Cardiac Overexpression of the A_1-Adenosine Receptor Protects Intact Mice Against Myocardial Infarction and Improves Global LV Function on Day 1 Post-MI as Demonstrated by Cardiac MRI

Zequan Yang,[1] Rachael J. Cerniway,[1] Stuart S. Berr,[1] Anne M. Byford,[1] G. Paul Matherne,[1] Brent A. French.[1]
[1] *University of Virginia, Departments of Biomedical Engineering, Pediatrics and Radiology, Charlottesville, Virginia, United States*

Introduction: We have previously shown that cardiac-specific, 300-fold overexpression of A1-adenosine receptors (A1-ARs) in transgenic mice protects isolated hearts against ischemia / reperfusion injury (1). However, this line of transgenic mice exhibits bradycardia (HR of 620 ± 14 vs. 713 ± 8 bpm in wild-type) and an increased incidence of arrhythmia during ischemia, making it unsuitable for the in vivo study of myocardial infarction (MI). To study the effects of cardiac-specific A1-AR overexpression on MI, we chose a different line of transgenic mice (30 × A1-AR) that expresses the A1-AR at more moderate levels (approximately 30-fold over wild-type). The 30 × A1-AR line exhibits minimal bradycardia

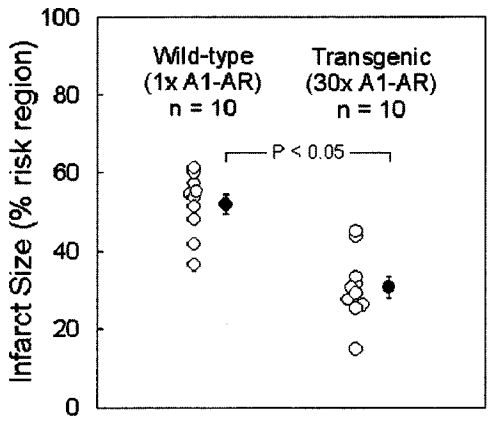

Figure 1. Cardiac-specific overexpression of the A1-adenosine receptor (A1-AR) protects intact mice against myocardial infarction. Ten wild-type and ten transgenic mice with30-fold level of A1-AR over expression (30 × A1-AR) were subjected to a 45 min LAD occlusion followed by 24 hr of reperfusion. Infarct size in 30 × A1-AR mice was reduced by >40% in comparison with littermate control mice ($P < 0.05$).

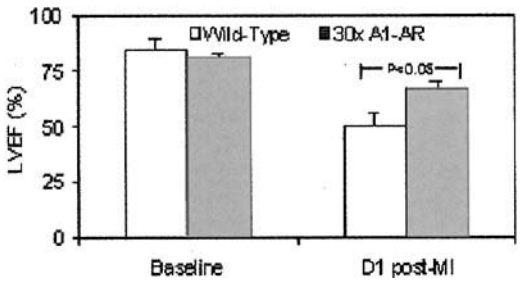

Figure 2. Cardiac overexpression of the A1-adenosine receptor (A1-Ar) improves global LV function on Day 1 post MI. Baseline left ventricular ejection fraction (LVEF) was determined by cardiac MRI 2d before MI. A 45 min coronary occlusion was imposed on Day 0, and cardiac MRI was performed again on day 1 post MI to determine LV volumes and LVEF. Global LV function was improved by 34% in transgenio vs. wild-type control mice ($P < 0.05$).

(681 ± 11 bpm) and is no more prone to arrhythmia during coronary occlusion than wild-type mice.

Purpose: The purpose of this study was to determine whether cardiac-specific overexpression of the A1-AR protects intact mice against MI, and whether such cardioprotection might have an impact on global left ventricular (LV) function as assessed by cardiac MRI on Day 1 post-MI. This question is significant because previous reports indicate that infarct size does not correlate well with LV dysfunction when these endpoints are assessed shortly after MI in wild-type animals (2–3).

Methods: To investigate the role of the A1-AR in the setting of MI, 30 × A1-AR transgenic (n = 10) and wild-type, littermate control (n = 10) mice underwent 45 min of LAD occlusion followed by 24 hr of reperfusion. Two days before and 1 day after MI, LV ejection fraction (LVEF) was assessed by cardiac MRI in 5 mice from each group. Cardiac MRI was performed using a Helmholtz coil (RF Design Consulting, Newberry, FL) on a Varian INOVA 4.7T scanner equipped with Magnex gradients. Mice were anesthetized with pentobarbital for ECG-triggered, 2D cine FLASH imaging using a TE of 3.9 ms and a flip angle of 20°. During each imaging session, the entire LV was assessed using 7 to 8 contiguous short-axis slices. The images were then scaled and converted to the appropriate format for analysis using ARGUS (Siemens Medical Systems) to yield LV end-systolic volumes, end-diastolic volumes and ejection fractions (LVEF). Hearts from euthanized animals were stained with triphenyltetrazolium chloride and phthalo blue to determine infarct size and region at risk (respectively).

Results: Infarct size (expressed as % risk region) in wild-type mice was 52 ± 3% (Fig. 1). In contrast, moderate overexpression of the A1-AR in the 30 × A1-AR line of transgenic mice markedly reduced infarct size to 31 ± 3% ($P < 0.05$). As shown in Fig. 2, LVEF (mean ± SEM) at baseline was no different between wild-type (85 ± 5%) and 30x A1-AR mice (81 ± 2%). However, LVEF was significantly better preserved in 30 × A1-AR mice one day post-MI (67 ± 3%) than in littermate controls (50 ± 6%, $P < 0.05$). In parallel studies, neutrophil infiltration in the LV was assessed by myeloperoxidase (MPO) assay. One day after a sham operation, myocardial MPO levels were no different between wild-type and 30 × A1-AR mice. However, one day after MI, myocardial MPO levels in wild-type mice (158 ± 18 U/g) were 2.7-fold higher than in 30 × A1-AR mice (63 ± 16 U/g, $P < 0.05$).

Conclusion: In summary, cardiac overexpression of the A1-AR has minimal effects on heart rate and yet reduces infarct size by 40% in intact mice. This cardioprotective effect is associated with reduced neutrophil infiltration and improved LV function post-MI. The finding that LVEF is markedly improved on Day 1 post-MI in 30 × A1-AR mice is noteworthy because our laboratory (2) and others (3) have previously noted that infarct size does not correlate tightly with cardiac dysfunction early after MI in wild-type animals. Thus factors other than infarct size may contribute to the marked improvement in LVEF observed on Day 1 post-MI in 30 × A1-AR versus wild-type mice.

151. MRI Guided Deployment and Postinterventional Assessment of Endovascular Stents in the Pulmonary Position in Swine

Titus Kuehne,[1] Maythem Saeed,[2] Philip Moore,[3] Oliver Weber,[2] Kelly Gleason,[2] Gabriela Krombach,[3] Charles Higgins.[2] [1]*University of California, San Francisco, University Hamburg, Germany;* [2]*University of California, San Francisco, Department of Radiology, San Francisco, California, United States;* [3]*University of California San Francisco, Department of Pediatric Cardiology, San Francisco, California, United States*

Introduction: In recent years, placement of endovascular stents and valved stent for treatment of pulmonary obstruction and insufficiency has been rapidly gaining acceptance. However patients are often left with residual pulmonary insufficiency and the risk of restenosis. Close monitoring of such patients is essential in order to prevent heart failure. To minimize radiation exposure and avoid the need for multiple imaging studies a one-stop and non ionzing technique would be desirable to evaluate and monitor during a single session: (1) cardiac and pulmonary anatomy; (2) ventricular function; (3) quantitative blood flow volumes in native and stented pulmonary arteries, and (4) interventional procedures.

Purpose: To assess the ability of MRI to (1) guide stent deployment in the pulmonary position using real time MR imaging and (2) evaluate stent morphology after deployment and pulmonary blood flow through the stent.

Methods: The study was performed in a dual imaging facility consisting of a x-ray angiography (Integris V5000) and 1.5 T short bore MRI unit (Philips Intera I/T, Philips Medical System, Netherlands). The arrangement of the labaratory allowed for performance of interventional procedures under x-ray and MR imaging control without changing the position of the animal.

In 5 pigs (20–27 kg) selfexpanding nitinol stents (Memotherm, Angiomed, Germany) were placed across and distal to

the pulmonary valve using MRI guidance. The stent material is MR non-ferromagnetic. Stent dimensions were 18 mm in diameter and 25 mm in length when fully expanded.

For interactive real time MR imaging of catheters and stent delivery a balanced Fast Field Echo (bFFE) and a T1 weighted Turbo Field Echo sequence (T1-TFE) were employed. Visualization of catheters and guidewires, including a (1) balloon tipped wedge catheter, (2) long sheath with the stent loaded at its tip, and (3) 0.035-inch nitinol guidewires, was based on $T2^*$ (susceptibility) or T1 for catheters doped with 1% solution of Gd–DPTA.

After stent deployment the position and morphology of the stent were verified using multiphase multislice bFFE. Pulmonary blood flow volumes were measured using velocity encoded cine (VEC) MRI. Flow volumes were measured within the lumen of the stents and compared to measurements next to the stent. Flow measurements next to the stent were performed beyond any visible susceptibility artifacts derived from the stent. Pulmonary and right ventricular blood pressures were measured using the wedge catheter.

At the conclusion of MRI guided interventional procedures the animals were brought back into the x-ray angiography unit to confirm stent position and to assess the possibility of complication during MRI. Measurements of blood pressures were repeated in the pulmonary artery and right ventricle. After euthanasia, the hearts were excised and examined for the position and morphology of the stent and pulmonary artery.

Results: Stent deployment was successful in all five animals. In three animals the stent was placed 1–3 mm distal to the pulmonary valve, in one animal across the pulmonary valve and in the fifth animal 4 mm distal from the desired position. Image quality of the heart and great arteries was optimized when acquired with ECG gated bFFE-sequence at a slice thickness of 10 mm. Important anatomical details of the right ventricle, pulmonary artery and pulmonary valve were clearly visualized. The curvature of long segments of the shaft of catheters and guidwires were visualized on T1-TFE images. Thereby, thick slices of 30 mm were required due to the torturous anatomy of the right ventricle and pulmonary artery. Definition of the tip of catheters and guidwires was reasonable on (1) T1-TFE images using the balloon catheter filled with 1% solution of Gd–DPTA and (2) bFFE images using thin slices of 5–10 mm. It should be noted that fast and reliable catheter tip detection was not feasible within the cardiac chambers using bFFE with thin slices.

All nitinol stents were visualized after deployment using bFFE. SNR was reduced within the stent lumen due to radiofrequency shielding effects of the stent. The SNR measured on bFFE images in the center of the stent ($SNR = 3.9 \pm 0.5$) was significantly smaller when compared to the measurements acquired at the center of the pulmonary artery distal to the stent ($SNR = 8.1 \pm 1.9$, $p < 0.01$). A circumscribed total signal void was noted at the stent wall due to susceptibility artifacts. The width of susceptibility artifacts was 2.4 ± 0.9 pixels on bFFE images.

VEC MRI flow measurements within the lumen of the stent correlated well with measurements acquired next to the stent ($r = 0.96$). There was no significant difference between flow volumes measured at these two sites. Retrograde pulmonary blood flow was measured within the stent placed across the pulmonary valve. A pulmonary regurgitant fraction of $37 \pm 2\%$ was determined form the ratio of pulmonary antegrade flow (5.1 ± 0.5 L/min/m2) to pulmonary retrograde flow (1.9 ± 0.4 L/min/m2). X-ray pulmonary angiography revealed severe pulmonary regurgitation in this animal. In the other 3 animals with a stent placed distal to the pulmonary valve pulmonary antegrade (4.9 ± 1.2 L/min/m2) but no retrograde blood flow was measured. Similarly no pulmonary regurgitation was noted on x-ray angiography.

MRI guided pressure measurements within the right ventricle and pulmonary artery were identical to pressure measurements under x-ray angiography control. No complication were noted during and after stent placement, such as (1) vascular perforation due to catheter manipulation, (2) stent migration, or (3) intramural injury using MRI, x-ray angiography and at autopsy.

Conclusion: MRI has the potential to guide stent placement in the cardio-pulmonary system. In addition, it provides immediate postinterventional evaluation of stent position, morphology and physiologic flow measurements within and next to the stent lumen.

152. Myocardial Perfusion MR Imaging with Sense in Clinical Routine

Sven Plein,[1] John Ridgway,[2] Timothy Bloomer,[1] Tim Jones,[3] Gavin Bainbridge,[4] Mohan Sivananthan.[1] [1]*Leeds General Infirmary, Gt. George Street, Leeds, West Yorkshire, United Kingdom;* [2]*Leeds Teaching Hospitals, Department of Medical Physics, Leeds, West Yorkshire, United Kingdom;* [3]*University of Leeds, BHF Heart Research Centre, Leeds, W Yorks, United Kingdom;* [4]*The Leeds General Infirmary, The Cardiac MRI Unit, B Floor, Leeds, West Yorkshire, United Kingdom*

Introduction: Magnetic Resonance Imaging (MRI) during the first pass of paramagnetic contrast agents can be used to assess myocardial perfusion. MRI may offer advantages over the currently used nuclear perfusion techniques, namely a better

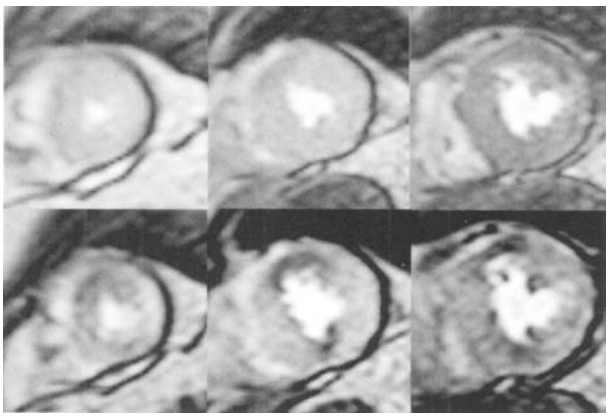

Figure 1. 3 Slices shown from apex to mid ventricle. Top row: rest images, bottom row: stress images.

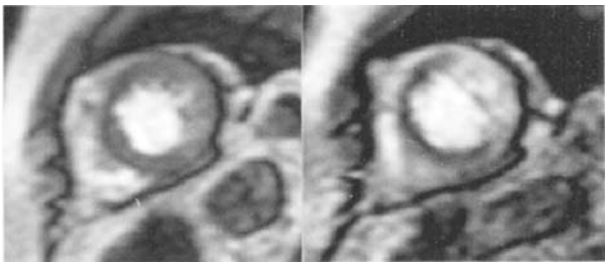

Figure 2. Single slice shown (apex). Left: rest image, right: stress image.

spatial resolution and freedom from attenuation artefacts. In order to provide high sensitivity and to allow quantitative data analysis, MRI perfusion imaging should be performed with multislice coverage and high temporal resolution. This requires very short acquisition times, which are not necessarily achievable with conventional acquisition sequences. The use of hybrid sequences such as turbo gradient echo–echo planar imaging has therefore been proposed. However, these provide lower SNR than non-EPI techniques and can be limited by susceptibility ($T2^*$) and water/fat shift artefacts. A recently developed alternative method to shorten acquisition times in MRI is sensitivity encoding (SENSE). It can reduce acquisition times by a factor of 2 or more. This is achieved at the expense of lower SNR (by approximately the square root of the SENSE factor) and larger fields of view (FOV), because image aliasing has to be avoided. Applied to perfusion imaging, SENSE may allow multi-slice acquisition in every heart beat with non-EPI techniques.

Purpose: It was the purpose of this study to evaluate myocardial perfusion MRI with SENSE in a clinical setting.

Methods: 52 patients with a history of myocardial infarction or angina were studied on a Philips 1.5T INTERA CV system with Master gradients (30 mT/m amplitude and 150 m/T/sec slew rate) and using a 5 element cardiac synergy coil and a Vectorcardiogram. The perfusion sequence was a dynamic segmented k-space gradient echo pulse sequence combined with SENSE (Saturation recovery T1 TFE, TR 3.1 ms, TE 1.6 ms, flip angle 15°, FOV as required to avoid image aliasing, matrix 160 × 112, reconstructed to 256 × 256, SENSE-factor 2). 4 slices can be acquired every heart beat up to a heart rate of 100 bpm.

Before the contrast perfusion scan, a "dummy" scan over 4 heart beats was acquired without contrast in the same orientation as the planned perfusion scan to select the appropriate FOV and to ensure that no image aliasing was present. Perfusion imaging was then performed at rest and after 20 minutes delay during Adenosine stress (140 mcg/kg/min for 5 minutes). A bolus of 0.05 mmol/kg Dimeglumin gadopentate (Magnevist, Schering AG, Berlin, Germany) was rapidly injected by hand followed by a flush of 10 ml Normal Saline. A SENSE reference scan was acquired, which is used to reconstruct SENSE scans.

Analysis was performed qualitatively by visual comparison of resting and stress images. The image quality and the presence of artefacts was assessed. The presence of fixed and inducible perfusion defects were reported for 4 segments (anterior, lateral, inferior, septal) of each slice. So far, 26 patients had an x-ray angiogram and these results were used to calculate the sensitivity and specificity of MRI perfusion to detect significant (>70%) coronary stenoses. For this, ventricular segments were assigned to coronary territories as follows: anterior and septal segments to the left anterior descending artery; lateral segment to the left circumflex artery; inferior segment to the right coronary artery.

Results: One patient did not tolerate the Adenosine infusion (chest pain) and stress imaging could not be performed. In three patients artefacts caused by:residual fold-over were observed. In one patient the interpretation of one slice was not possible due to these artefacts. Image quality allowed analysis of all slices in the remaining 50 patients. Full thickness and subendocardial defects could be identified. The FOV ranged from 350 mm to 450 mm, resulting in a spatial resolution of 2.2–2.8 mm × 3.1–4 mm. The sensitivity to detect significant CAD in individual coronary vessels was 85.7% with a specificity of 81.8%. Figure 1 shows an example of mainly subendocardial inducible defects in the LAD and RCA territories. In Figure 2, a transmural defect in the LAD territory is seen.

Conclusion: Myocardial perfusion imaging with SENSE is feasible in a clinical setting. Multi-slice coverage of the LV can be achieved with high temporal resolution. Image quality in this study was good and the diagnostic accuracy of the protocol was comparable with data reported in previous studies of MRI perfusion imaging.

153. Simultaneous Evaluation of Exercise–Stress Wall Motion and Myocardial Perfusion Using Real-Time Interactive Multislice MRI—Clinical Validation

Phillip Yang,[1] Krishna Nayak,[1] Shuichiro Kaji,[1] Masahiro Terashima,[1] Erasmo Delapena,[1] Jan Engvall,[1] Michael Mcconnell,[1] John Pauly,[1] Dwight Nishimura,[1] Bob Hu.[1]
[1]*Stanford University, Falk CVRB, Stanford, California, United States*

Introduction: Echocardiographic evaluation of stress-induced wall motion and radionuclide study of myocardial perfusion are current gold standard in non-invasive assessment of ischemia. While MR techniques have been shown to evaluate stress-induced wall-motion or myocardial perfusion separately, a comprehensive method to assess both functions was previously not possible. In order to address these issues, a real-time interactive multislice (RT-MS) imaging sequence has been developed. This technique enables simultaneous imaging of three dynamically adjustable short-axis slices in apical, mid, and base regions at 16 images/second/slice or 48 complete images/second with spatial resolution of 3.12 mm over 20 cm field of view.

Purpose: Clinical study consisting of 8 healthy subjects was conducted to validate this imaging technique. Systematic evaluation of regional myocardial perfusion and wall motion was performed at rest and stress conditions.

Methods: Real-time imaging: The RT-MS was developed within the framework of Stanford RTI system enabling real-time reconstruction and interactive control of the imaging parameters. A conventional 1.5T GE Signa scanner equipped with high-performance gradient capable of 40 mT/m amplitude and 150 mT/m/ms slew rate was used. A read-out trajectory

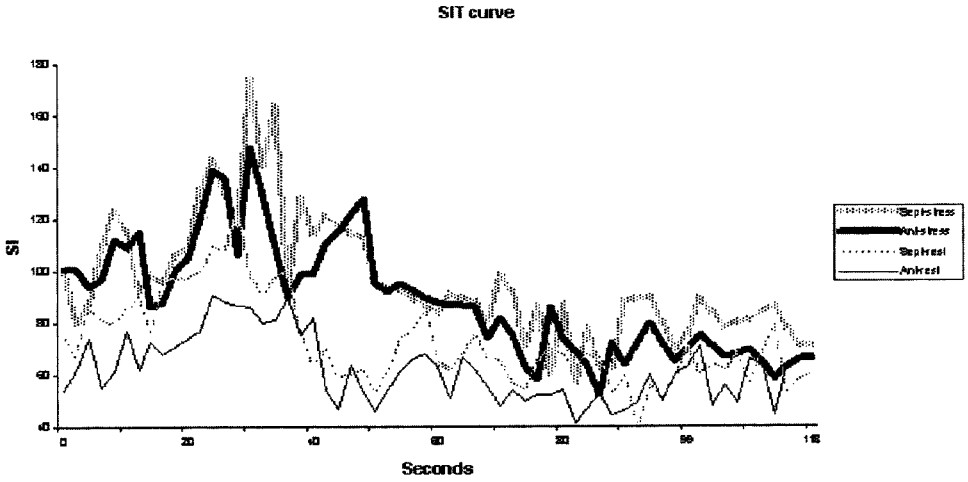

Figure 1.

utilizing partial k-space circular EPI (duration 7.6 ms) and a pulse sequence consisting of slice-selective excitation (excitation duration 0.64 ms, slice thickness 5 mm, flip angle 70°, and TR 10 ms) were implemented. Protocol: Eight healthy subjects underwent stationary bicycle exercise followed by aerobic exercise in the scanner to maintain the heart rate in tachycardia range. The desired short axis views were selected dynamically followed by an intravenous bolus of Gd–DTPA (0.03–0.05 mmol/kg) injected manually through the antebrachial vein at 3 ml/sec followed by normal saline flush. Following a 15-minute interval, resting scan was performed with an identical concentration of Gd–DTPA injection. Two-minute video of stress and rest images were acquired and saved for analysis. Data analysis: For perfusion analysis, an image consisting of three slices at end-diastole were obtained at 2-second interval for a total of 2 minutes at both stress and rest conditions generating a total of 120 images/patient. The short axis views were divided into anterior, septal, lateral, and inferior regions for semi-quantitative analysis using signal-intensity time (SIT) curve in each region. For wall motion analysis, the saved video was evaluated for image quality at rest and stress conditions using the standard 16-wall segment model. Image quality was based on the following grading scale: 1—no visualization of endocardium, 2—inadequate visualization (<50%), and 3—adequate visualization (>50%).

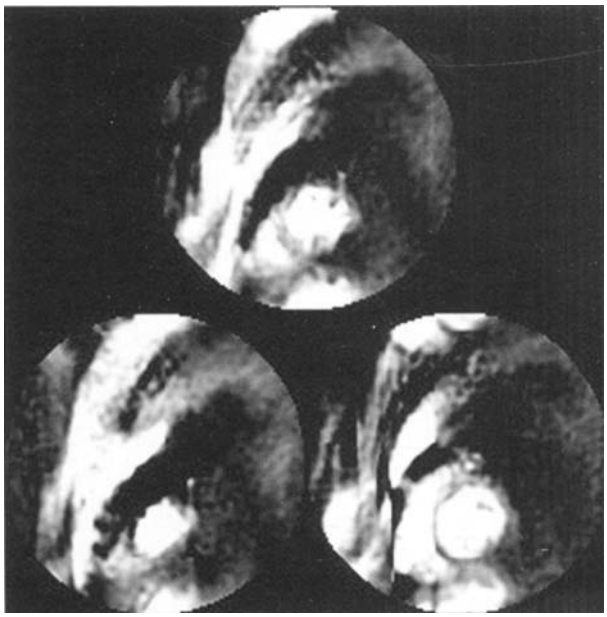

Figure 2.

Results: The total scan time for both rest and stress conditions did not exceed 10 minutes. Including the exercise time and the 15-minute interval between the two scans, the total study was completed in less than 30 minutes.Myocardial perfusion based on SIT curve demonstrated the following signal enhancement (mean ± standard deviation) at rest and stress, respectively: LV 107 ± 4%, 126 ± 10%; anterior 139 ± 15%, 157 ± 25%; septal 138 ± 16%, 154 ± 17%; lateral 110 ± 21%, 168 ± 30%; and inferior 116 ± 21%, 162 ± 31%. There was a statistically significant increase in signal enhancement from rest to stress conditions ($p < 0.01$). A representative SIT curve for the septal and anterior regions at rest and stress are illustrated in Figure 1 demonstrating peak enhancement at both rest and stress conditions. Wall motion analysis based on the visualization of the endocardium demonstrated adequate image quality in 93% of the wall segments at rest and stress with heart rate ranging from 60 to 140 beats/minute. The least optimal image quality was observed in the inferior and lateral regions. The image quality (mean ± standard deviation) in the inferior and lateral regions were 2.9 ± 0.3 and 2.9 ± 0.3, respectively. A representative 3 short axis views taken at a heart rate of 120 beats/minute are shown in Figure 2.

Conclusion: A real-time interactive multislice imaging capable of simultaneous imaging of wall motion and myocardial perfusion at both rest and exercise-induced stress

conditions has been developed. This study validates potential clinical utility for this imaging sequence by demonstrating reduced scan time, complete volumetric coverage, optimal temporal resolution, real-time display and interactivity, and elimination of both cardiac and respiratory gating.

154. Do Missing Dynamics Affect Myocardial Perfusion Reserve Index Calculation? A Comparison Between Every Heart Beat and Every Second Heart Beat Image Acquisition

Holger Thiele,[1] Sven Plein,[2] Marcel Breeuwer,[3] John Ridgway,[2] David Higgins,[4] Gerhard Schuler,[1] Mohan Sivananthan.[2] [1]*University of Leipzig, Department of Cardiology, Leipzig, Sachsen, Germany;* [2]*Leeds General Infirmary, Great George Street, Leeds, West Yorkshire, United Kingdom;* [3]*Philips Medical Systems—Building QV 162, P.O. Box 10.000, Best, Netherlands;* [4]*University of Leeds, Great George Street, Leeds, West Yorkshire, United Kingdom*

Introduction: First pass myocardial perfusion imaging can be successfully used for diagnosing myocardial ischemia. It is commonly accepted practice to analyze the upslopes of the myocardial signal as contrast passes through and to calculate the myocardial perfusion reserve index (MPRI) by dividing the stress upslope by the rest upslope after correction for the left ventricular input function. Thresholds have been defined to allow differentiation between normal myocardial segments and those with perfusion defects. However, many different sequences with every heart beat or every 2nd heart beat image acquisition have been used, which affect the number of points used for calculating the upslope. In particular under stress conditions dynamics can be missed due to ventricular or supraventricular extra beats.

Purpose: The effects of missing data points on the MPRI calculation and the number of points used for the calculation have not been systematically evaluated so far.

Methods: Fifteen patients underwent first-pass magnetic resonance perfusion imaging under rest and stress using adenosine at standard dose (140 microg/kg/min). MR images were acquired on a 1.5 Tesla MR scanner (Intera CV, Philips, The Netherlands). Four short axis slices of the heart were acquired every heart beat using an ECG-gated T1-weighted inversion recovery turbo gradient echo sequence with sensitivity encoding (TR 3.1 ms, TE 1.6 ms, flip angle 15°, FOV 350–450 mm, matrix 160 × 112, reconstructed to 256 × 256, SENSE-factor 2). At end expiratory breath hold a bolus of 0.05 mmol/kg bodyweight gadolinium–DTPA (Magnevist, Schering AG, Berlin, Germany) was rapidly injected into a peripheral vein under rest and stress conditions. In all patients no dynamics were missed during the first pass of the contrast.

Off-line image analysis was performed on a dedicated workstation using prototype software (EasyScil, Medical Imaging Information Technologies—Advanced Development Department, Philips Medical Systems, The Netherlands). The endocardial and epicardial borders were drawn manually. The maximal upslopes of the myocardium and the left ventricle were calculated from the average time-signal intensity (SI) profiles using 3 dynamics for the upslope calculation with the formula (SI dynamic n − SI dynamic n-2)/(time dynamic n − time dynamic n-2), where n is the number in the dynamic series. The upslopes were calculated for the original image series, for image series from which the dynamics of every 2nd heart beat were removed (to simulate acquisition in every 2nd heart beat), and for image series resulting from removing 1 or 2 dynamics during the maximal upslope (to simulate the occurrence of missing dynamics). The MPRI was calculated for all possible constellations as (upslope myocardium stress/upslope left ventricle stress)/(upslope myocardium rest/upslope left ventricle rest).

Results: All images obtained were appropriate for image analysis. Images acquired every 2nd heart beat yielded a lower upslope for the myocardium and the left ventricle. Missing dynamics during the first pass of the contrast agent resulted in lower calculated upslopes, which was more pronounced in every 2nd heart beat acquisition sequences. The results are shown in the Table (*$p < 0.01$ versus every heart beat; #$p < 0.01$ versus every 2nd heart beat; dyn = dynamic; MC = myocardium; LV = left ventricle).

Conclusion: Missing dynamics during first pass myocardial perfusion imaging may affect the resulting MPRI and hinder the definition of thresholds or lead to false positive or negative perfusion defects after the previous definition of a threshold, in particular during acquisition every 2nd heart beat. Sequences, which acquire data every heart beat should be recommended. However, they should still be carefully checked for missing dynamics during the upslope. In cases where data points are missing for the upslope calculation, caution should be applied to the interpretation of the results.

Table 1

	MC Rest	LV Rest	MC Stress	LV Stress	MPRI
Every heart beat	12 ± 4	127 ± 29	18 ± 8	115 ± 31	1.7 ± 0.9
1 dyn missed	12 ± 4	114 ± 28*	18 ± 8	104 ± 25*	1.7 ± 0.8
2 dyn missed	12 ± 4	98 ± 25*	18 ± 8	96 ± 24*	1.6 ± 0.8
Every 2nd heart beat	10 ± 3*	95 ± 24*	15 ± 6*	89 ± 19*	1.6 ± 0.6
1 dyn missed	10 ± 3	72 ± 20#	14 ± 6	70 ± 17#	1.5 ± 0.6#
2 dyn missed	10 ± 3	55 ± 16#	14 ± 5	56 ± 15#	1.4 ± 0.4#

155. Magnetic Resonance Imaging (MR) Demonstrates Improved Myocardial Perfusion Reserve After Angiogenic Implant Therapy

Prasad Panse,[1] Andrey Zenovich,[1] Xudong Hu,[1] Carsten Rickers,[1] Myra Urness,[1] Neeta Panse,[1] Huafa Kong,[1] Naveen Murthy,[1] Jon Wegner,[1] Michael Jerosch-Herold,[1] Serjan Nikolic,[2] Norbert Wilke.[1] [1]*University of Minnesota, Mayo Mail Code 292, Minneapolis, Minnesota, United States;* [2]*RIPAMF, Stanford University, 26102 Eden Landing Rd, Suite 6, Hayward, CA, United States*

Introduction: Different methods such as Transmyocardial laser revascularisation(1), and gene therapy have been tried to induce angiogenesis with varying degrees of sucess. Angiogenic implant therapy is a novel method of inducing angiogenesis in ischemic myocardium based on bioresorbable polymer micro-implants.

Purpose: The purpose of the present study is to evaluate the effects of Angiogenic implant therapy by Magnetic resonance first pass perfusion imaging (MRFPP).

Methods:

An Ameroid occluder was placed in 9 pigs to gradually occlude the left circumflex artery and create a model of chronic ischemia. After 4 weeks, post ameroid, all the animals had a baseline rest/adenosine (250 micrograms/kg/min) MRFPP imaging and were then randomised into sham operated group (n = 4) and the AIT treated group (n = 5). The AIT group was treated with 15 microimplants in the ischemic region.

6 weeks after the sham/AIT procedure a repeat rest/adenosine MRFPP was performed. Perfusion was quantified by dividing the myocardium in 8 segments with customised software to generate the signal intensity over time curves. A fermi model of constrained deconvolution was used to fit the curves and yield the rest and stress flows. Myocardial perfusion reserve was determined as the ratio of stress over resting blood flow. Cine analysis was done to determine the Ejection fraction (EF%).

Results: See table (*$p < 0.05$ (AIT vs.sham).

Rest cine showed EF% in AIT (52% + / − 7%) was greater than in sham (32% + / − 3%). Dobutamine cine also revealed EF in AIT (65% + / − 6%) to be greater than in sham (40% + / − 4%).

Conclusion: For the first time, MRFPP showed that AIT improves myocardial perfusion reserve and global ventricular function in chronic ischemia. These promising results warrant upcoming Clinical trials.

Table 1

Perfusion Reserve

	MPR, BL	MPR, 6 wks
Ischemic region, AIT	1.78 ± 0.63	3.8 ± 1.76*
Ischemic region, sham	1.57 ± 1.18	1.57 ± 0.38

156. Blood Pool Contrast Enhanced MRI Detects Suppression of Microvascular Permeability in Early Post-Infarction Reperfusion: Value of Nicorandil Therapy

Gabriele A. Krombach,[1] Charles B. Higgins,[1] Mitsuaki Chujo,[2] Maythem Saeed.[1] [1]*Department of Radiology, Universtity of California San Francisco, Parnassus Avenue 505, San Francisco, CA, USA;* [2]*Chugai-Pharmaceutical Co, Kyobashi 2, Tokyo, Japan*

Introduction: Using contrast echocardiography, Ito et al (1) found in patients after reperfusion that acute intravenous administration of nicorandil, an adenosine triphosphate (ATP) sensitive potassium (K +) channel opener with a nitrate-like effect, preserves microvascular integrity and myocardial viability. This therapy is clinically approved as an anti-anginal drug in Japan and Europe. In another study Lund et al (2) showed in rats the beneficial effect of this therapy in reducing myocardial infarction using extracellular nonspecific and necrosis specific MR contrast media. Unlike blood pool MR contrast media, both extracellular nonspecific and necrosis specific MR contrast media are not suitable for assessment of microvascular integrity in reperfused infarction (3).

Purpose: 1) to determine the effect of nicorandil therapy on microvascular integrity (permeability) in early post-infarction reperfusion using the blood pool MR contrast medium Clariscan; 2) to compare the size of Clariscan enhanced region on MRI with the true infarction and area at risk at postmortem in control and nicorandil treated animals, and 3) to determine the acute effect of continuos infusion of nicorandil therapy during reperfusion on LV function using functional MRI.

Methods: Twenty-four rats were enrolled in this acute study. Left thoracotomy was performed and the left anterior coronary artery was occluded by placing a snare loop around the artery. Animals were subjected to 45 min of coronary artery occlusion followed by 3 hrs of reperfusion. Two groups of rats were randomly assigned to receive either saline or nicorandil infusion. At 15 min after occlusion, group 1 animals (n = 12) received a bolus of 100 μg/kg nicorandil followed by continuos infusion of 25 μg/kg/min nicorandil during the 3 hrs reperfusion. Group 2 animals (n = 12) received saline infusion and served as control. Accumulation of the contrast media in the ischemically injured region was monitored for 45 min after injection using serial T1-weighted spin-echo imaging at a single midventricular level. At 45 min, multi-slice images were acquired to measure the extent of microvascular injury, end diastolic volume and wall thickness in the heart. Acquisition parameters were: TR/TE = 300/12 ms, matrix 256 × 128 data points interpolated to 256 × 256 during Fourier transformation, FOV 50 × 50 mm, slice thickness 2 mm, four acquisitions, scan time 2.5 min. Signal intensities were obtained from remote normal and ischemically injured myocardium. After imaging, the left coronary artery was re-occluded and phthalocyanine blue dye was injected intravenously to define the area at risk. Slices were then incubated in triphenyltetrazolium chloride (TTC) solution to define infarcted myocardium. Area at risk and infarction were determined at postmortem and compared to Clariscan enhanced region.

Results: On signal-intensity-time curve, accumulation of Clariscan in the injured region was attenuated in nicorandil treated animals, suggesting that nicorandil therapy reduced the permeability and severity of microvascular injury. The profile

of enhancement was shifted to the right and associated with a significant reduction in peak regional signal intensity values (90 ± 16% in control and 65 ± 8% in nicorandil treated rats, $p < 0.05$). Furthermore, Clariscan enhanced region was smaller in nicorandil treated animals (18 ± 2% of LV) than that in control (44 ± 2% of LV) in early post-infarction reperfusion. On functional MR imaging, nicorandil treated animals showed reduction in LV end diastolic volume (0.75 ± 0.05 ml/kg body weight) compared to control animals (1.22 ± 0.1 ml/kg). Nicorandil infusion during late occlusion and reperfusion preserved remote normal wall thickness (2.7 ± 0.1 mm in nicorandil and 2.4 ± 0.1 mm in control, $p < 0.05$), both parameters are markers of acute LV dilatation (remodeling).

At postmortem, animals treated with nicorandil showed smaller size of infarction in nicorandil (12 ± 1% of LV, $p < 0.01$) than in control (29 ± 2% of LV), but identical area at risk in nicorandil and control (48 ± 2% versus 50 ± 2%). Inter-observer variability in the measurements of the extent of microvascular injury, area at risk and infarction was 4.2 ± 2.9%.

Conclusion: Blood pool contrast enhanced MRI detects suppression of microvascular permeability in early post-infarction reperfusion after nicorandil therapy. Furthermore, nicorandil therapy reduced the extent of microvascular injury in reperfused infarction.

Aknowledgement: This study was in part supported by a gift from Chugai-Pharmaceutical Co. Tokyo, Japan.

157. Concordance Between 'Delayed Enhancement' and 'Constant Infusion' Approaches for the Evaluation of Myocardial Viability

Rebecca Thornhill,[1] Frank Prato,[1] Gerald Moran,[2] Gerald Wisenberg,[1] Jane Sykes.[1] [1]*University of Western Ontario, Department of Nuclear Medicine & Magnetic Resonance, London, Ontario, Canada;* [2]*McMaster University, Dept. Medical Physics and Applied Radiation Sciences, Hamilton, Ontario, Canada*

Introduction: In canine [Pereira 1999] and human [Pereira 2001, Flacke 2001] studies of myocardial infarction, MRI during a constant infusion of Gd–DTPA has been used to distinguish infarcted from normal myocardium. It has been shown that the distribution volume of Gd–DTPA (λ) in infarcted myocardium is increased by approximately 2–3 fold. In such constant-infusion studies (CI), maintaining the infusion until blood and tissue concentrations of Gd–DTPA have reached equilibrium allows for the direct quantification of λ and, hence, myocardial viability. In each of the CI studies performed to date, the infusion was maintained for at least 30 min. CI studies are widely considered too cumbersome and lengthy for routine clinical cardiac MR exams. 'Delayed enhancement imaging' (DE), performed 10–20 min after a bolus is a faster alternative to CI. No direct quantification of λ is possible with this technique, however, as both perfusion *and* λ contribute to the enhancement patterns observed. Furthermore, it has been suggested that the permeability of necrotic myocytes may be highly variable [Moran 2001]; this could manifest in variable delays in delivery of Gd–DTPA to infarcted myocardium.

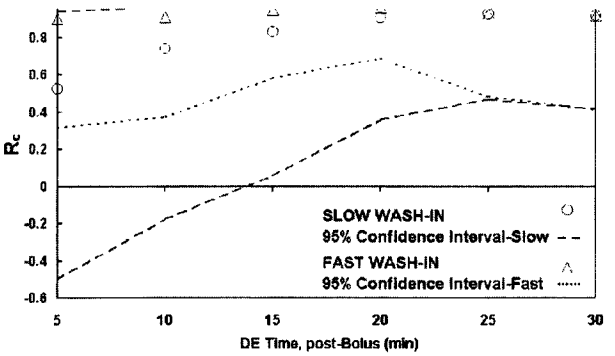

Figure 1. Rc as a function of DE time for 'slow' (circles) and 'fast' (triangles) wash-in groups.

Purpose: Given these concerns, a direct comparison of the patterns of contrast enhancement between the DE and CI approaches seemed prudent. Concordance was assessed in a validated canine model of reperfused AMI. Both approaches were applied in the same animals and the estimates of λ obtained with DE (λ_{DE}) were compared with those made with the CI technique (λ_{CI}).

Methods: Four research-bred mongrel dogs were studied as follows: a snare was placed around a branch of the LAD, the snare was tightened for 2 h and then released. Imaging began after 2 h reperfusion (Siemens Vision 1.5T). A bolus (0.2 mmol/kg) of Gd–DTPA was administered and the evolution of contrast enhancement was followed using a saturation recovery TurboFLASH sequence (srTFL, TR/TE 2.4/1.2 ms, recovery period 20 ms). Images were acquired prior to Gd–DTPA and then repeated at a rate of once per minute for 30 min post-bolus. Regions of interest (ROI) were located in the infarct territory, in normal myocardium and in the LV blood pool. Estimates of λ_{DE} were obtained by calculating the ratio of the change in signal-intensity (SI) in the myocardium (pre-post contrast) to the change in SI in the blood. To assess CI, a second bolus (0.1 mmol/kg) was then injected and followed immediately by a 60 min constant infusion (0.004 mmol/min/kg). Imaging continued throughout the infusion. The images acquired at 60 min were used to calculate λ_{CI}. Imaging was repeated at 3–4 days post-infarction and then once/week, for

Table 1

Rc for each DE time

DE time (min)	Rc (95%CI)
5	0.821 (0.028 – 0.980)
10	0.889 (0.281 – 0.988)
15*	0.932 (0.496 – 0.993)
20*	0.937 (0.525 – 0.993)
25*	0.931 (0.488 – 0.993)
30	0.915 (0.402 – 0.991)

* indicates a significant difference from Rc at DE = 5 min.

four weeks. For each imaging session, λ_{DE} calculated at 5, 10, 15, 20, 25 and 30 min post bolus injection was compared with the λ_{CI} for that day and a concordance coefficient, Rc, was calculated for each comparison (i.e. a total of six Rc for each day of imaging). Using the SI vs. time curves, all λ_{DE} and λ_{CI} data were then divided into two groups: one for infarcted ROIs which demonstrated 'slow wash-in' kinetics and a second, 'fast wash-in' group for those in which the delivery of Gd–DTPA was the same as it was for normal regions. New sets of Rc were then calculated for the slow and fast wash-in groups. Regional myocardial blood flow (RMBF) was determined using radiolabeled microsphere injections at baseline, occlusion, 2 h reperfusion, and at 30 days.

Results: Microsphere measurements confirmed that RMBF was reduced during occlusion and restored to normal following reperfusion. The λ_{CI} for the infarct ROIs was always significantly greater than that which was calculated for the normal ROIs, regardless of the day of imaging (mean +/− SD: λ_{CI} for the infarct ROIs = 0.78 +/− 0.14 ml/g; λ_{CI} for the normal ROIs = 0.40 +/− 0.06 ml/g, $p < 0.05$). Examining the data for all imaging sessions (day 0 to day 30) failed to reveal any significant differences in Rc among the follow-up sessions ($p = 0.09$). Rc data were then pooled to arrive at one set of six Rc coefficients, i.e. λ_{CI} vs. each of the λ_{CI} calculated at 5–30 min post-bolus (Table 1). Rc was best when a DE time of 20 min post-bolus was used. Post hoc testing revealed that Rc for the 15–25 min DE times were significantly better than that which was found for the 5min time ($p < 0.05$), but no other comparisons reached significance. When the λ data were divided into 'slow' and 'fast' groups, it can be seen from Fig. 1 that the Rc for slow wash-in were worse than those for fast wash-in: when for DE times <20 min post-bolus were employed, Rc for the slow group became significantly less than those for the fast group ($p < 0.05$ for Rc values calculated at DE = 5, 10, and 15 min).

Conclusion: Although the concordance between the CI and DE techniques was reasonable for DE times >15 min post-bolus, the work presented here serves to highlight the effect of variable wash-in kinetics. When tracer delivery to the infarct is normal, then the contrast enhancement observed by the DE technique is a good reflection of λ. If delivery is delayed, however, then the accumulated contrast in the infarct territory may result in enhancement that is indistinguishable from that of normal tissue at the time of imaging. Since there is no means of prospectively identifying regions of slow wash-in, institutions opting for the simplicity of the DE technique would be well advised to select a DE imaging time of approximately 20 min post-bolus.

158. In Vivo MR Imaging of Catheter-Based Vascular Gene Delivery

Xiaoming Yang,[1] Ergin Atalar,[1] Jean-Michel Serfaty,[1] Danming Wang,[1] Ananda Kumar.[1] [1]*Johns Hopkins University School of Medicine, Department of Radiology, Baltimore, Maryland, United States*

Introduction: Gene therapy is an exciting frontier in modern medicine [1]. To date, most investigations about imaging of gene therapy have primarily focused on non-cardiovascular systems [2]. The reasons for this are due to the anatomic and physiologic characteristics of the cardiovascular system, including: (i) thin vessel wall, which requires high-resolution imaging modalities; (ii) cardiac bits/vessel pulse, which requires specific methods to reduce motion artifacts; (iii) blood flow, which requires strategies to enhance the interaction between genes and the target vessel wall; and (iv) complicated endovascular interventional procedures.

Purpose: The purpose of this study was to develop an in vivo imaging tool to monitor a catheter-based vascular gene delivery procedure using high-resolution MR imaging.

Methods: We produced gadolinium/blue-dye and gadolinium/gene-vector media by mixing Magnevist with a trypan-blue or a lentiviral vector carrying a green fluorescent protein (GFP) gene. The gadolinium was used as an imaging marker for magnetic resonance (MR) imaging to visualize vessel wall enhancement, while the blue-dye/GFP was used as a tissue stain marker for histology/immunohistochemistry to confirm the success of the transfer [3]. Using 12 Remedy gene delivery catheters (Fig. 1), we transferred the gadolinium/blue-dye ($n = 8$) or gadolinium/GFP-lentivirus ($n = 4$) into the arteries of 12 pigs, monitored under high-resolution MR imaging.

All experiments were performed on a 1.5 Tesla MR unit. To image deeply-located iliac arteries, we used an MR imaging-guidewire operated at a receive-only mode [4], while to image the superficially-located femoral arteries, we used a custom-made, 3-cm surface coil. We first inflated the dilation balloon with 3% Magnevist and obtained a coronal scout MR image of the pelvis using a fast spoiled-gradient (FSPGR) pulse sequence with 500/2.1-msec repetition time (TR)/echo time (TE), 31.2-kHz bandwidth (BW), 24 × 24-cm field of view (FOV), 256 × 256 matrix, and 3 mm thickness. We then acquired an axial high-resolution MR image of the target arterial wall across the inflated balloon, using: (i) a spin-echo (SE) sequence with 150/10-msec TR/TE, 16-kHz BW, 6 × 6-cm FOV, 128 × 256 matrix, 1–3 number of excitations (NEX), and 3 mm thickness; and (ii) an FSPGR sequence with 14.8/4.9-msec TR/TE, 15.6-kHz BW, 4 × 4 FOV, 256 × 256 matrix, 8 NEX, and

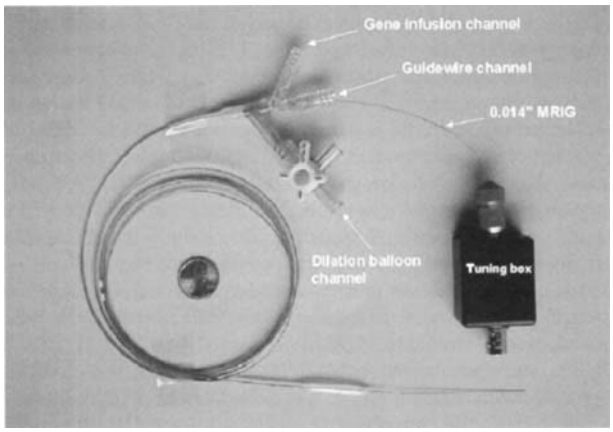

Figure 1. A remedy gene delivery balloon catheter with an MR imaging-guidewire (MRIG) placed in the guidewire channel.

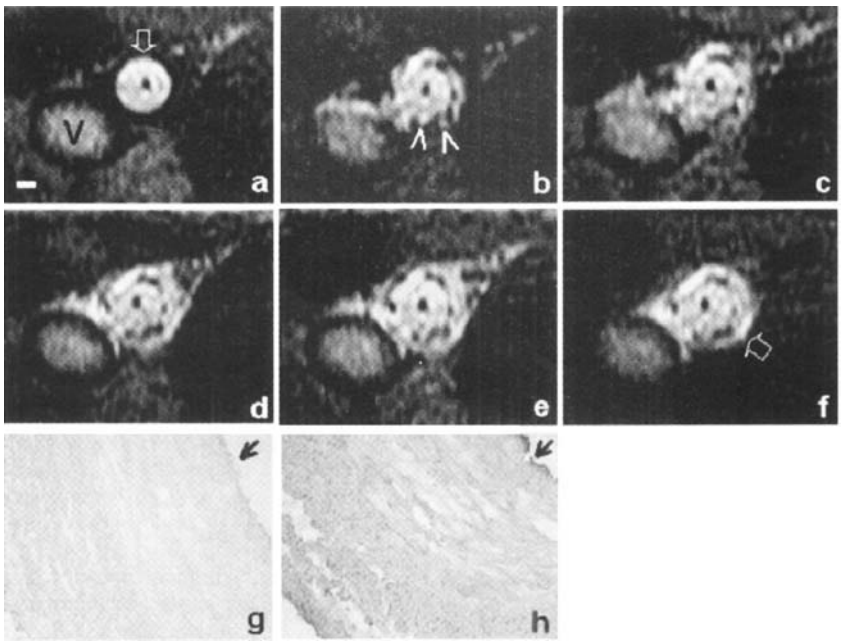

Figure 2. MR images of the gadolinium/GFP-lentivirus delivery. a, Before delivery. B–f, During delivery, the arterial wall is enhanced as a ring (arrow in f). Corresponding immunohistochemistry in control (g) and GFP-targeted (h) arteries.

3 mm thickness. The total scan time for each image was 1 minute. During the infusion of the gadolinium/blue-dye/GFP-lentivirus medium, the dilation balloon was inflated at 4 atm support pressure, and the medium infusion was constantly maintained using a pump.

Results: The results showed, in all 12 pigs, the gadolinium enhancement of the target vessel walls on MR imaging and the blue/GFP staining of the target vessel tissues with histology/immunohistochemistry (Fig. 2). The average time period for the target vessel walls to maintain peak signal intensity was from minute 6 ± 2 (standard deviation (SD)) to minute 20 ± 3 (SD) after initiation of the gadolinium/GFP-lentivirus infusion, and the signal intensity dropped to the pre-infusion level within 40–50 minutes. This study shows the potential of using MR imaging to dynamically visualize: (i) where the gadolinium/-genes are delivered; (ii) how the target portion is marked; and (iii) whether the gene transfer procedure causes complications, such as perforation of the target vessel wall.

Conclusion: We present a technical development using high-resolution MR imaging as an in vivo imaging tool to monitor catheter-based primary vascular gene delivery. We believe that this work opens up an exciting avenue for the future efficient management of cardiovascular ischemic disorders using MR imaging-based vascular gene/drug therapy.

159. Direct Imaging of Left Ventricular Regional Dysfunction Using SENC MRI

Nael Osman,[1] Jerome Garot,[2] Smita Sampath,[1] Bernhard Gerber,[1] Catherine Wu,[1] Ergin Atalar,[1] Joao Lima,[1] Jerry Prince.[1] [1]*Johns Hopkins University, Baltimore, Maryland, United States;* [2]*Hopital Universitaire Henri Mondor, 51 Avenue du Marechal De Lattre de Tassigny, 94010 Creteil, France*

Introduction: Regional function of the heart is currently assessed by observing myocardial wall motion throughout systole, and, more specifically, endocardial excursion, using echocardiography or cine-MRI. This qualitative assessment of regional cardiac function is observer-dependent and often fails to detect subtle changes in segmental contractility. More recently, several MRI methods have been developed, including MR tagging, stimulated echo, and phase contrast, to quantify regional left ventricular function by providing quantitative parameters of segmental contractility. However, these methods do not provide direct measurements from the scanner, but produce intermediate images that require labor-intensive processing. With MR tagging, for example, the systolic deformation of the heart causes the bending of tag lines that, while clearly visible, are not adequate to quantify local contraction.

Purpose: We propose what we call strain-encoded (SENC) imaging for *direct* imaging of segmental contractility.

Methods: A 1-1 SPAMM pulse sequence is applied at end-diastole to encode the tissue with a sinusoidal pattern (spatial frequency is $0.5\,mm^{-1}$, i.e., 2 mm tag separation). The sinusoidal pattern modulates the longitudinal magnetization orthogonal to the imaging plane. Deformations of tissue during systole change the local frequency of the pattern in proportion to the through-plane strain component. Imaging is acquired using an SPGR imaging sequence with an additional gradient in the through-plane direction, which we call the *tuning* pulse. The

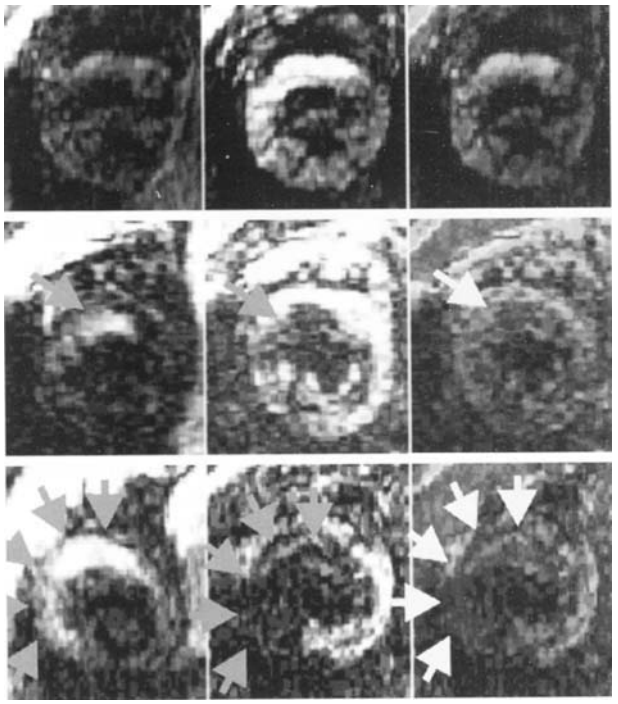

Figure 1.

tuning pulse produces strain-encoded images, whose intensity distribution reflects local frequency; hence, the through-plane strain component. The SENC images depict the longitudinal compression of the heart on short-axis planes, or its circumferential shortening on long-axis planes. Three cases (a normal and two post-infarct human subjects) have been done. Late-enhancement images were acquired in order to verify the location and extent of infarction in patients.

Results: The SENC pulse sequence has been demonstrated on human normal and post-infarction hearts. Figure 1 shows SENC images for three cases, each in a row. The first row depicts a normal heart and the others show two postinfarct cases. The first column shows SENC images with a low tuning frequency, which enhances regions with no deformation. The second column shows the SENC images for a high tuning frequency, which enhances the contracting regions. The last column shows longitudinal strain measured from the first two columns as described in [1], where the blue color indicates contraction. The red regions in the wall mark dysfunctional regions. The figure shows that the low tuning frequency can detect the dysfunctional region (marked with the arrows) as bright spots in the wall without the need for computed strains.

Conclusion: Using SENC, it is possible to visualize infarcted regions without the need for postprocessing, as demonstrated on two patients. Depending on the value of the tuning pulse, the SENC images display regional hyperintensity (or hypointensity) that indicates regional abnormal wall motion. This makes SENC a promising tool for future clinical applications.

160. Cardiac Imaging with Undersampled 3D Projection Reconstruction (VIPR) in a Single Breath-Hold

Oliver Wieben,[1] Walter Block,[1] Andrew Barger,[1] Thomas Grist,[1] Charles Mistretta.[1] [1]*University of Wisconsin-Madison, E3/311 Clinical Science Center, Madison, Wisconsin, United States*

Introduction: Undersampled projection reconstruction (PR) has been recently introduced to MR Angiography [1] and cardiac imaging [2,3]. These PR techniques allow for faster image acquisition than spin-warp imaging with tolerable artifacts in selected applications. Reduced SNR and streak artifacts are the limiting factors in undersampled radial trajectories while replication artifacts prohibit undersampling in Fourier encoding.

Block et al. [4] demonstrated a 3D projection trajectory, VIPR (Vastly undersampled Isotropic Projection Imaging), that isotropically images high resolution 3D volumes by undersampling in all three k-space dimensions.

Purpose: Here we investigate the use of VIPR with retrospective ECG gating for cardiac imaging. This technique can provide a multiphase dataset with isotropic resolution over a large volume from data acquired during a single breath-hold. Potential advantages of this approach include the reformatting capabilities from isotropic resolution and the simplified scan prescription without the need for any localizers.

Methods: In VIPR, each projection passes through the center of k-space. The projections are aligned so that their endpoints are evenly distributed over the surface of a sphere. The data are acquired in an interleaved fashion as shown in Figure 1.

A half echo acquisition was used to improve acquisition speed. Each left half of the echo samples an even projection. Once the center of k-space is acquired the amplitude of the gradient is changed so that the right half of the echo samples the adjacent odd projection [5]. The missing data are synthesized using a homodyne reconstruction. This method allows to acquire twice as many projections in approximately the same scan time to reduce the artifact level.

The sequence was implemented on a 1.5 T Signa Horizon CardioVascular scanner (GE Medical Systems, Waukesha, WI) with peak gradient amplitudes of 40 mT/m and a maximum slew rate of 150 mT/m/s. Healthy human volunteers were imaged using a cardiac phased array coil with 4 elements during the injection of a Gd-based contrast agent with a dose of 0.3 mmol/kg. The bolus was venously administered at an injection rate taylored to deliver the dose over the duration of the scan.

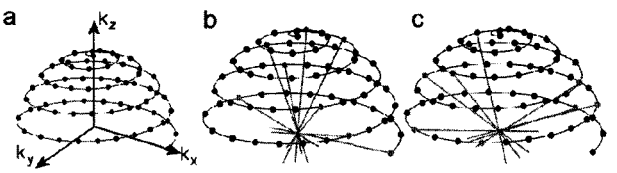

Figure 1. (a) The endpoints of the projections in VIPR sample the surface of a sphere. The projections can be subdivided into interleaved subsets as shown in (b) and (c).

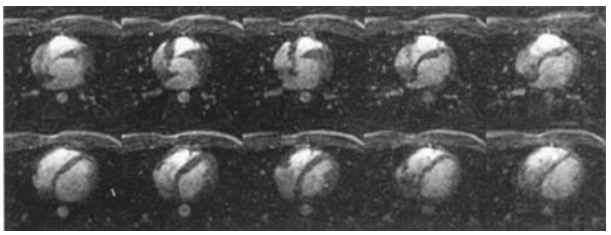

Figure 2. Two axial slices throughout the cardiac cycle. Each image represents a 150 ms period.

The number of samples in each readout was $N_r = 128$, which requires $\pi/2 \times N_r 2 \sim 26{,}000$ projections to fullfill the Nyquist theorem. A total of 15,000 projections (30,000 half echoes) were acquired over a $40 \times 40 \times 40\,cm^3$ cubic image volume with a spoiled gradient echo sequence (TR/TE = 3.1/1.2 ms) and a bandwidth of 62.5 kHz. The total scan time was 48 s and the 128 images were zero-filled to a 256×256 in-plane matrix size.

The location of the R-waves in respect to the projection numbers were detected by the internal ECG unit of the scanner and stored for retrospective gating with an offline reconstruction.

Results: Figure 2 shows 2 slices throughout the cardiac cycle reconstructed in the axial plane. Each image volume represents a 150 ms interval of the cardiac cycle. The blood pool is enhanced from the contrast agent and can be well differentiated from the myocardium, e.g. for volume measurements.

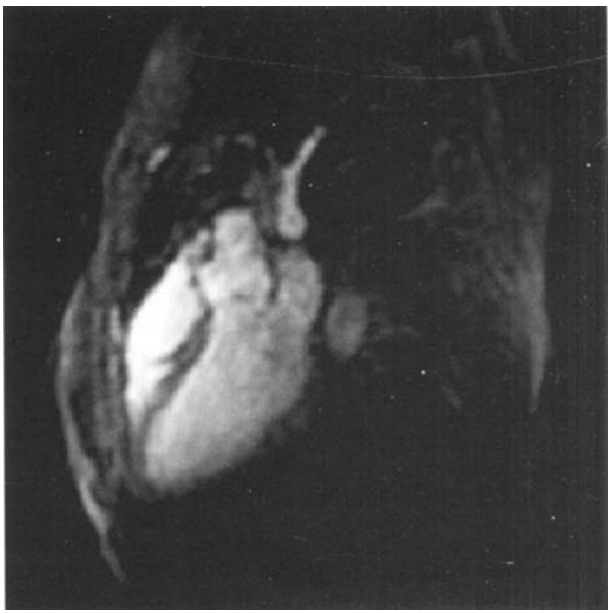

Figure 3. Reformatted images provide isotropic resolution in arbitrary directions.

An example of a reformatted view is shown in Figure 3. This view demonstrates good spatial resolution in the z-direction also. Note the large volume coverage in all dimensions.

Conclusion: In this preliminary work we have demonstrated a novel technique for 3D single breath-hold cardiac MR which provides isotropic resolution. With VIPR, the reconstructed images can be reformatted in arbitary orientations without loss in resolution. Therefore, for example, both ventricles can be equally well analyzed contrary to more conventional scans where the orientation of thick slices is optimized for one of the ventricles. In addition, the prescription process is shortened and greatly simplified compared to 2D techniques with double oblique scan orientations.

The in-plane resolution of $3.1 \times 3.1\,mm^2$ is rather large compared to other approaches. However, the resolution in the third dimension is also 3.1 mm, which is much smaller than with most other techniques and might be advantageous for measurements such as volumes and ejection fraction. We are investigating methods to limit the FOV in PR imaging to improve the spatial resolution without introducing artifacts from objects outside the samller FOV.

The temporal resolution of the technique is currently limited by the streaking artifacts from high signal structures such as fat. This is particularly problematic for the VIPR sequence with True-FISP (fast imaging with steady precession). Fat supression techniques can potentially reduce these artifacts.

We have also shown in a previous study [6] that 3D PR acquisitions are well suited for motion detection and correction as they intrinsically provide information similar to navigator echoes. These capabilities may allow for longer acquisition times during free breathing. The additional projections could provide higher temporal resolution within the cardiac cycle or less streaking artifacts.

161. Single Shot Black Blood Imaging Using Steady-State Free Precession

Jason A. Polzin,[1] David Stanley,[2] Qun Chen.[3]
[1]*GE Medical Systems, P. O. Box 414, W875, Milwaukee, Wisconsin, United States;* [2]*GE Medical Systems, 1601 Lavaque Road, Proctor, Minnesota, United States;* [3]*Northwestern University, 2650 Ridge Avenue, Evanston, Illinois, United States*

Introduction: Black Blood imaging is a technique to visualize cardiac morphology where blood in the ventricle appears dark and myocardium appears bright. One commonly used technique employs a double-inversion recovery (IR) preparation pulse consisting of a non-selective inversion followed by a selective inversion the result of which effectively inverts everything outside of the imaging slice. The inversion time (TI) is set to null the blood signal that has flowed from outside of the slice. The preparation is then followed by a fast-spin echo (FSE) readout. Each echo-train of the FSE readout is acquired across two R–R intervals with the entire acquisition divided into 8–12 echo-trains. Because of the long breath-hold time required for this application, it is not feasible to use this technique in patients with compromised cardiac function.

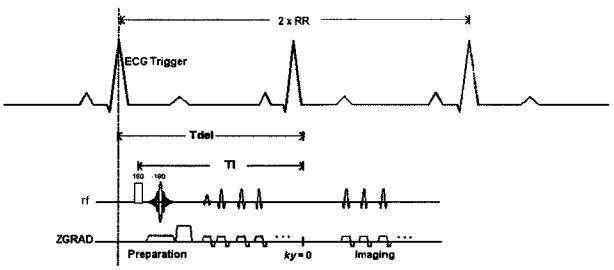

Figure 1. Double IR FIESTA Pulse Sequence Diagram.

Purpose: A new technique where the patient does not need to hold their breath or can hold their breath for very short periods of time is needed.

Methods: A double-inversion pulse was used in conjunction with a single-shot Fast Imaging Employing Steady-State Acquisition (FIESTA) readout to generate images with bright myocardium and dark ventricular cavities. The acquisition was cardiac gated with the trigger delay set to acquire the center of *k*-space during diastole. The inversion time was set to minimize the blood pool signal. During the inversion time a half-α/half-TR preparation sequence followed by dummy acquisitions were played to reach steady state. The pulse sequence diagram is shown in the figure below.

Images using this pulse sequence were acquired on a 1.5 T scanner (Signa CVi, GE Medical Systems, Milwaukee, WI). Data were collected for both double-IR FSE and the single-shot FIESTA acquisition. FIESTA data was acquired with the following imaging parameters; 256 frequency × 128–256 phase matrix, ±125 kHz receiver bandwidth (RBW), fractional and full NEX, 5–10 mm slice thickness, 3.5–4.2 ms TR, 1.6–1.9 ms TE, 3/4 to full Phase FOV, and 35–40 cm FOV. Flip angle was set to 30–40° to maximize the myocardium signal (in conventional CINE FIESTA larger flip angles are used to maximize the myocardium–ventricle contrast). Double-IR FSE data was acquired with an ETL of 32, 256 × 256 matrix, ±31.25 kHz RBW, Minimum TE, TR = 2R − R, 36–40 cm FOV, 3/4 to full Phase FOV, and 8 mm slice thickness.

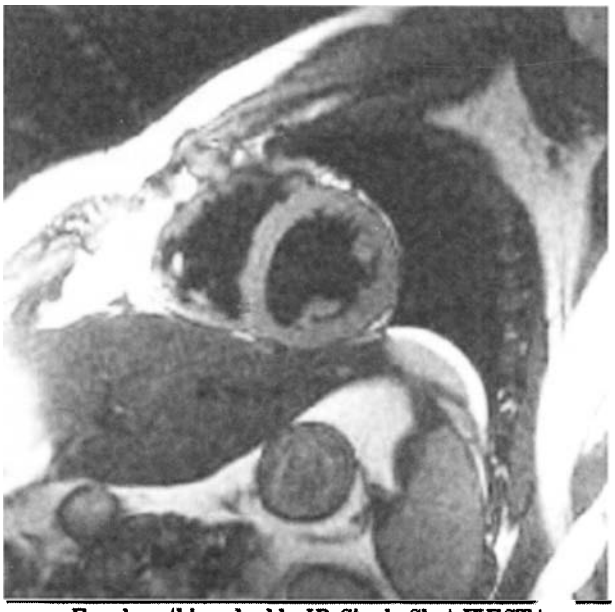

Figure 2. Free breathing double-IR Single Shot FIESTA.

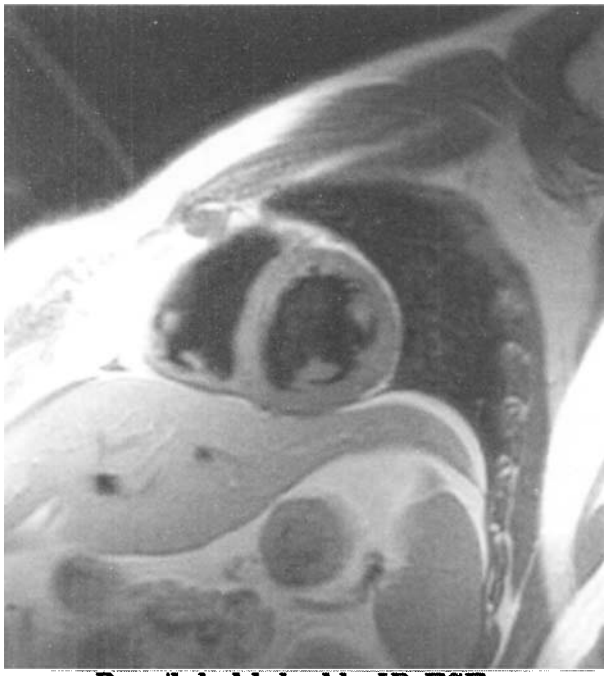

Figure 3. Breath hold double-IR FSE.

Results: Two representative images are shown; one using a single-shot FIESTA based acquisition and the other using a multiple R–R FSE acquisition. Black blood images using the single-shot FIESTA acquisition were similar in quality to the FSE images. While the SNR was slightly lower, the FIESTA acquisition did not suffer from the T2 blurring inherent in FSE based acquisitions. The boundary between the left ventricle and the myocardium was clearly visualized even without suspending respiration.

*Conclusion:*The black-blood FIESTA technique described here is a robust fast acquisition that can be used to image cardiac morphology without requiring a breath-hold. This technique can be used in patients for whom a breath-hold double-IR FSE acquisition is not feasible. For some cases, this technique is superior to a single-shot FSE based acquisition because of the absence of T2 blurring and the short acquisition time.

162. 3D Magnetization-Prepared True-FISP Using a Linear Flip Angle Series

Vibhas Deshpande,[1] Yiu-Cho Chung,[2] Al Zhang,[2] Steven Shea,[1] Paul Finn,[1] Debiao Li.[1] [1]*Northwestern University, Department of Radiology, Chicago, Illinois, United States;* [2]*Siemens Medical Systems, 448 E. Ontario St., Chicago, IL, USA*

Introduction: Volume targeted breath-hold imaging using a true-FISP (fast imaging with steady precession) sequence has been described for MR coronary angiography (1). Substantial improvements in SNR and CNR were shown as compared to FLASH (fast low angle shot). A fat saturation pulse followed by an $\alpha/2$ preparation (2) and 20 dummy cycles was used to suppress the fat signal and image artifacts due to transient signal oscillations while approaching steady-state. However, severe oscillations may still occur if large resonance offsets are present. Recently, Nishimura et al. (3) showed a variable flip angle approach to eliminate these oscillations. This series has to be recalculated if T1, T2, flip angle, or number of dummy cycles are perturbed. We propose that linearizing a flip angle series in the dummy cycles could reduce magnetization oscillations as well.

Purpose: The goal was to validate a linearized flip angle magnetization preparation (20 dummy cycles with linearly increasing flip angles-LFP) to reduce signal oscillations in the approach to steady-state in true-FISP as compared to the $\alpha/2$ and 20 dummy cycles using constant flip angles.

Methods: The sequence was a 3D segmented data acquisition with 'n' centrically reordered phase-encoding lines per cardiac cycle. All gradients were balanced in each TR. Alternating rf pulses were used to maintain a relatively uniform signal in the presence of field inhomogeneities. A fat saturation pulse (120 deg.) was applied, followed by LFP in the dummy cycles e.g. imaging flip angle was 70 deg. and number of dummy cycles was 20, therefore the flip angles were linearly ramped as -3.5, $+7$, -10.5,. $+70$ deg. in the dummies and then maintained at $+/-$ 70 deg. during data acquisition.

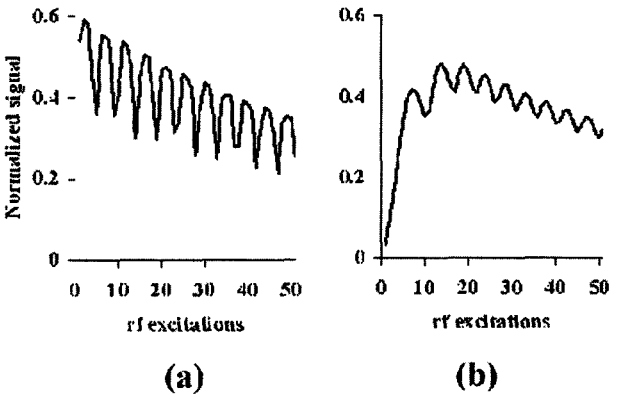

Figure 1. Simulation results showing blood signal trajectories at 100 Hz resonance offset with (a) $\alpha/2$ and 20 dummy cycles preparation and (b) LFP. Notice the reduced signal oscillations in (b).

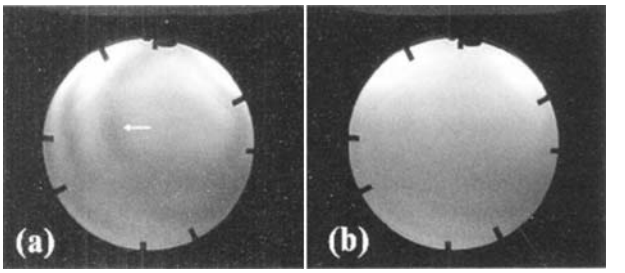

Figure 2. Phantom imaging performed with (a) $\alpha/2$ and 20 dummy cycles preparation and (b) LFP. Note that the banding artifact seen in (a) (arrow) is minimized in (b).

Simulations and Phantom Studies

Simulations were performed to determine whether signal oscillations were reduced by LFP if large resonance offsets existed. Blood signal trajectories were compared with the sequence in ref. 1 ($\alpha/2$ and 20 dummy cycle preparation, constant flip angles). Simulation paramters included: T2/T1 = 250/1200 ms, $\alpha = 70$ deg., R–R interval = 1 s, lines per segment = 31. Phantom imaging was used to validate the simulation results. A bottle of water doped with gadolinium was used as a phantom and imaging was performed using both sequences. The parameters were as follows: TR/TE = 3.54/1.77 ms, $\alpha = 70$ deg., lines per segment = 31, FOV = 218 × 250 sq. mm, matrix size = 248 × 256, number of partitions = 12, slab thickness = 18 mm, readout bandwidth = 980 Hz/pixel.

Volunteer Imaging

Healthy volunteers were studied (n = 12) to evaluate improvements in image quality and SNR using LFP. Imaging parameters include: TR/TE = 4.06/2.03 ms, $\alpha = 70$ deg., (25–39) lines per heartbeat, matrix size = (100–156) × 512, number of partitions = 6, slab thickness = 18 mm, imaging time = 24 heartbeats, readout bandwidth = 810 Hz/pixel. Image quality was evaluated by a blinded reviewer.

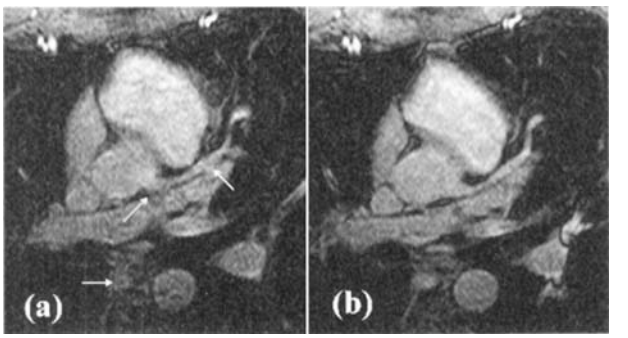

Figure 3. Original images of the LAD acquired using (a) $\alpha/2$ and 20 dummy cycles preparation and (b) LFP. Apparent off-resonance artifacts like ghosting and blurring (arrows) observed in (a) are reduced in (b).

Results: Simulations demonstrate that if frequency offsets exist, LFP is better at suppressing signal oscillations (Fig. 1). Phantom studies show that image artifacts caused due to frequency offsets are reduced with LFP (Fig. 2). Volunteer studies show improved image quality and the signal is more uniform in the LFP images (Fig. 3). A 10% increase in the SNR ($p < 0.001$) over the constant flip angle preparation was observed. Eight out of 12 images acquired using LFP were rated as improved image quality while 4 sets were estimated to be equal.

Conclusion: Results show that LFP substantially reduces signal oscillations in true-FISP at large resonance offsets. Coronary artery imaging demonstrated reduction in image artifacts and a small increase in SNR. The increase may be due to reduced ghosting artifacts, which prevents distribution of the energy. LFP can be seen as a first order approximation to the series in ref. 3. In conclusion, LFP is a simple and robust method to reduce magnetization oscillations in true-FISP.

References

1. Deshpande VS et al. MRM 2001; 46:494–502.
2. Deimling M et al. Proc. SMRM 1994; p 495.
3. Nishimura DG et al. Proc. ISMRM 2000; p 301.

163. Using Unfold to Remove Radial Streak Artifact in Undersampled Projection Reconstruction Cine Imaging

Andrew Larson,[1] Orlando Simonetti.[2] [1]*Northwestern University, Department of Radiology, Chicago, Illinois, United States;* [2]*Siemens Medical Systems, Ontario Center East Tower, Chicago, IL, United States*

Introduction: In order to improve imaging efficiency, the recently introduced UNFOLD technique [1] uses the temporal dimension of cine k-t space as an additional axis upon which to encode spatial information. UNFOLD achieves a temporally periodic modulation of the aliased component of each voxel's complex signal intensity by periodically shifting a k-space sampling function which in effect modulates a point spread function (PSF) governing spatial aliasing properties. Shifting of an undersampled rectilinear Fourier k-space sampling trajectory (Dirichlet-shaped PSF) results in a corresponding phase modulation of aliased voxel signal components. This aliased portion can then be removed with bandpass temporal filtering techniques. Azimuthal rotation of an undersampled radial k-space sampling trajectory results in a corresponding rotation of the associated starlike PSF [2] (Fig. 1). Periodic rotation of this PSF results in a periodic spatial modulation of the streak artifact due to azimuthal k-space undersampling. Bandpass temporal filtering techniques can subsequently be used for radial streak artifact removal.

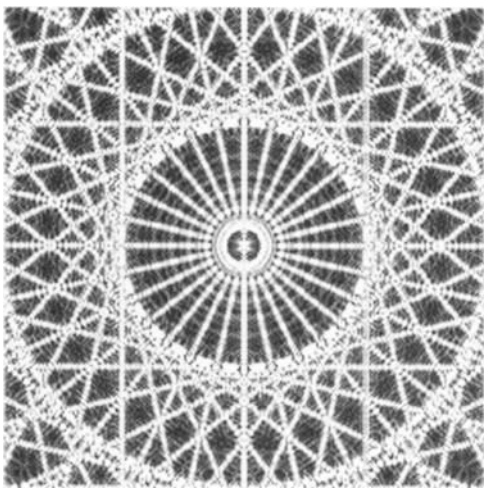

Figure 1. PSF for discrete polar k-space sampling.

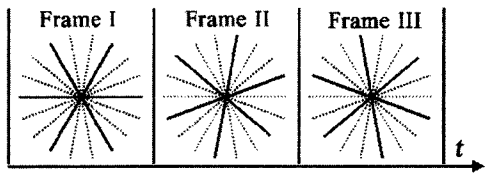

Figure 2. Incrementally rotated PR k-space sampling trajectory.

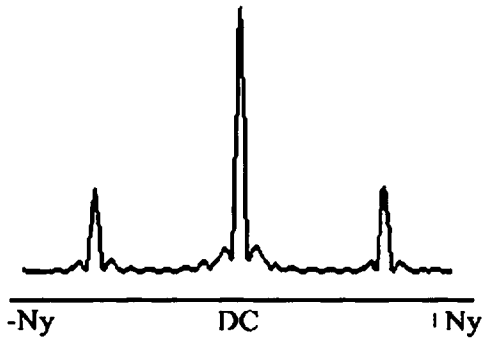

Figure 3. Central 1/3 FOV Aggregate Temporal Frequency Spectrum.

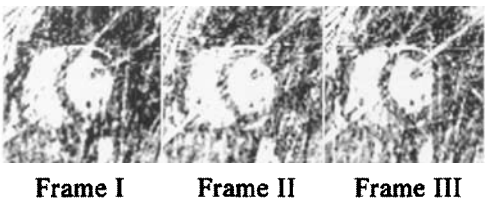

Figure 4. Subset of consecutive reconstructed cine images (during a static portion of the cardiac cycle) prior to temporal filtering. Image intensities were adjusted to accentuate the dynamic spatial orientation of the resultant radial streak artifact.

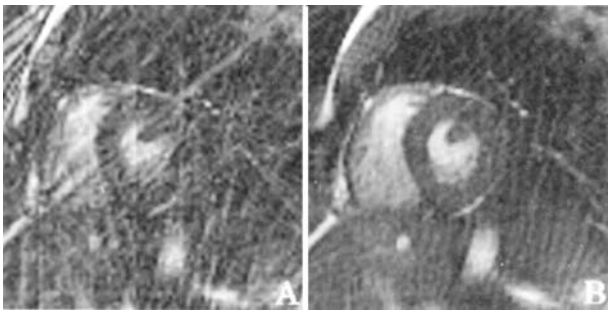

Figure 5. Short axis cine image at end diastole (a) obtained using a real-time 14 view radial TrueFISP acquisition scheme. Identical image reconstructed using a factor of 3 radial UNFOLD method (30 f.p.s.).

Purpose: The purpose of this work was to investigate the feasibility of using the UNFOLD technique to suppress radial streak artifact in radically undersampled PR cine imaging.

Methods: For this study, a real-time radial TrueFISP sequence was implemented on a Siemens 1.5T Magnetom Sonata scanner (Siemens Medical Systems, Iselin NJ) with a high performance gradient system (40 mT/m amplitude, 200 mT/m/sec slew rate). The sequence parameters were 1.4 kHz/pixel BW, TR/TE of 2.4/1.2 ms, flip angle of 70°, 300 mm FOV, and 128 RO. Fourteen views (radial k-space lines) were acquired for each cine frame. The overall k-space sampling trajectory was azimuthally rotated between frames such that an identical trajectory was sampled every third frame Fig. 2. Sixty cine frames were acquired at a temporal resolution of 33.6 ms (~30 f.p.s.).

The raw data was exported off line to a PC with MATLAB software (Mathworks, Inc., Natick, MA) for reconstruction using a regridding method and a factor of 3 UNFOLD algorithm incorporating a Fermi filter [1].

Results: An aggregate temporal frequency spectrum from the central 1/3 portion of the FOV is shown in Fig. 3. A subset of reconstructed cine images prior to temporal filtering is displayed in Fig. 4. The aliased components, resulting in the radial streak artifacts present within Fig. 5A were suppressed using the UNFOLD technique to produce a cine series exhibiting substantially less streak artifact, an image of which is displayed in Fig. 5B.

Conclusion: In this work, the UNFOLD method was successfully integrated with a real-time PR TrueFISP acquisition scheme for suppression of radial streak artifact. In vivo experiments demonstrated the feasibility of using this acquisition technique for achieving a temporal resolution of 33.6 ms (~30 f.p.s.) for rapid cardiac cine imaging.

References

1. Madore B et al. MRM 1999; 42:813–828.
2. Scheffler K et al. MRM 1998; 40:474–480.